ABSTRACT

Title of Document:	**MICROFLUIDIC PLANAR PHOSPHOLIPIDS MEMBRANE SYSTEM ADVANCING DYNAMIC STUDIES OF ION CHANNELS AND MEMBRANE PHYSICS**
	Chenren Shao, 2012
Directed By:	Professor, Donald L. DeVoe, Department of Mechanical Engineering

The interrogation of lipid membrane and biological ion channels supported within bilayer phospholipid membranes has greatly expanded our understanding of the roles membrane and ion channels play in a host of biological functions. Several key drawbacks of traditional electrophysiology systems used in these studies have long limited our effort to study the ion channels. Firstly, the large volume buffer in this system typically only allows single or multiple additions of reagents, while complete removal either is impossible or requires tedious effort to ensure the stability of membrane. Thus, it has been highly desirable to be able to rapidly and dynamically modulate the (bio)chemical conditions at the membrane site. Second, it is difficult to change temperature effectively with large thermal mass in macro device. Third, traditional PPM device host vertical membranes, therefore incompatible with confocal microscopy techniques. The miniaturization of bilayer phospholipid membrane has shown potential solution to the drawbacks stated above.

A simple microfluidic design is developed to enable effective and robust dynamic perfusion of reagents directly to an on-chip planar phospholipid membrane (PPM). It allows ion channel conductance to be readily monitored under different dynamic reagent conditions, with perfusion rates up to 20 µL/min feasible without compromising the membrane integrity. It is estimated that the lower limit of time constant of kinetics that can be resolved by our system is 1 minute. Using this platform, the time-dependent responses of membrane-bound ceramide ion channels to treatments with La^{3+} and a Bcl-x_L mutant were studied and the results were interpreted with a novel elastic biconcave distortion model.

Another engineering challenge this dissertation takes on is the integration of fluorescence studies to micro-PPM system. The resulting novel microfluidic system enables high resolution, high magnification and real-time confocal microscope imaging with precise top and bottom (bio)chemical boundary conditions defined by perfusion, by integrating *in situ* PPM formation method, perfusion capability and microscopy compatibility. To demonstrate such electro-optical chip, lipid micro domains were imaged and quantitatively studied for their movements and responses to different physical parameters. As an extension to this platform, a double PPM system has been developed with the aim to study interactions between two membranes. Potential application in biophysics and biochemistry using those two platforms were discussed.

Another important advantage of microfluidics is its lower thermal mass and compatibility with various microfabrication methods which enables potential integration of local temperature controller and sensor. A prototype thermal PPM chip

is also discussed together with some preliminary results and their implication on ceramide channel assembly and disassembly mechanism.

MICROFLUIDIC PLANAR PHOSPHOLIPID MEMBRANE PLATFORM
ADVANCING DYNAMIC STUDIES OF ION CHANNELS AND MEMBRANE
PHYSICS

By

Chenren Shao.

Dissertation submitted to the Faculty of the Graduate School of the
University of Maryland, College Park, in partial fulfillment
of the requirements for the degree of
Doctor of Philosophy
2012

Advisory Committee:
Professor Donald L. DeVoe, Chair
Associate Professor, Srinivasa R. Raghavan, Dean's Representative
Professor Marco Colombini
Assistant Professor Sarah Bergbreiter
Professor Elisabeth Smela

Preface

A portion of this work was presented in 2009 ASME International Mechanical Engineering Congress and Exposition, FL. Nov. 13~19; 2009 International Semiconductor Device Research Symposium, MD. Dec. 9~11; 2010 Hilton Head Workshop: A Solid State Sensors, Actuators and Microsystems Workshop, SC. June 6~10; 2010 Miniaturized Systems for Chemistry and Life Science, Gronngen, The Netherlands, Oct. 3~7; 2011 Biophysical Annual Meeting, Baltimore, MD Mar 5~9; 2011 Miniaturized Systems for Chemistry and Life Science, Seattle, WA, Oct 2~6; and 2012 Biophysical Annual Meeting. San Diego, CA, Feb 25 ~ 29. The chapters that are published as journal papers are declared in footnote.

Dedication

To my beautiful wife Xinxin Chang (常馨心), who supported me in every way in this endeavor.

To my parents Jianguo Shao (邵建国) and Saiyue Xu (徐赛月), who raised me with life-long love and encouragement.

Acknowledgements

There are numerous people who provided support for my Ph.D project financially, scientifically and emotionally.

First, I would like to express my deepest gratitude to my research advisor Dr. D. DeVoe, who provides both financial support and scientific guidelines for my project. His knowledge and experience in integration of different parts of knowledge has led me through my difficult days. I am also deeply indebted to my co-advisor Dr. M. Colombini from Biology department, who not only led me into biophysics world with two intriguing courses, but also guided me to study one of the most interesting biological phenomena. Also, thanks to Dr. S. Bergbreiter, Dr. S.R. Raghavan, Dr. S. Solares and Dr. Smela for providing on-going academic support as my thesis committee members.

Second, I would like to thank my collaborators in the PPM project, including Eric Kendall in Maryland MEMS & Microfluidics Lab (MML) and Bing Sun from Dr. Colombini's lab. They instilled the project with critical thinking and collaborative effect and produced very nice discoveries. Detailed documentation from previous effort from MML alumnus Dr. L. P. Hromada is also greatly acknowledged. I also want to thank my colleagues and friends in our MML family, Kunqiang Jiang, Renee Hood, Annie Lu, Isaac Misri, Omid Rahmanian, Prakruthi Hareesh, Alex Sposito, Michael Wiederoder, Jake Yang, Jikun Liu, Steve Chen, Kevin Tsao, and co-workers in Dr. Colombini's lab, ShangHsuan Lin, Toan Nguyen, Meenu N. Perera and Vidya Ganesan, for their continuous support and research advices throughout the project. A

special "thank you" goes to Toan Nguyen and his guitar, whose music provided comforting accompany to me, Mr. Membrane and Mr. Ceramide-Channel in a number of late nights.

My "thank you" also goes to a lot of personnel in shared UMD facilities, including Larry Lai and Charlie Chen from NIPS Lab and Amy Beaven from Imaging Core Facility.

Table of Contents

List of Tables

List of Figures

applied by increasing the level of the solution on one side of the membrane. Inset: Empirical equations were fit to the data in each curve in the main figure. Using these expressions, the difference in pressure needed to achieve the same membrane area with and without $LaCl_3$, was calculated. As the subtraction involved the difference between two empirical equations, the full function was plotted in the inset. The results shown are typical of two independent experiments. 79

Chapter 1: Introduction

This chapter introduces the background on lipids, lipid membranes, planar phospholipid membranes, membrane ion channels, and ceramide channels that are needed to understand this dissertation. References are given for readers who want to know more about lipids and ion channel biochemistry. The development and current limitations of microfluidic based PPM systems are reviewed, and the motivations of this project are briefly discussed.

1.1 Background

1.1.1 Lipid Membrane Fundamentals

Lipids are broadly defined as molecules that have both hydrophobic ("water-hating") and hydrophilic ("water-loving") regions. The most common lipids in biology are glycerophospholipids [1], or phospholipids in short, which consist of a glycerol core, two fatty acid tails, a phosphate group, and a head group. Typically, two fatty acid molecules are esterified to two hydroxyl groups in the glycerol backbone, forming a hydrophobic region. The third hydroxyl group forms a phosphoric ester with a phosphate group to which a head group is attached, forming a hydrophilic region. Fig. 1 shows a cartoon model of one typical lipid, 1,2-diphytanoyl-sn-glycero-3-phosphocholine (DiPhyPC), which has a choline head group. Sphingolipids, which are based on sphingosine instead of glycerol, are another type of lipid that is very important in this study. A fatty acid is linked to sphingosine through an amide linkage. A molecular model of N-palmitoyl-D-erythro-

sphingosine (C_{16}-ceramide) is shown in Fig. 2. For a comprehensive discussion of lipid biochemistry, please refer to [1].
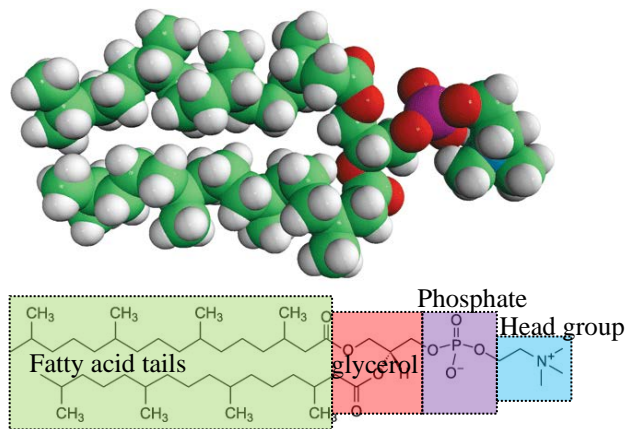
Figure 1 Structure of DiPhyPC, a glycerophospholipid.[1]
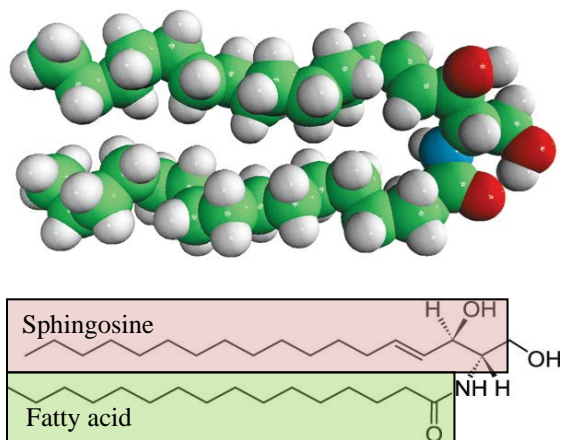
Figure 2 Structure of C_{16}-ceramide, a sphingosine based lipid.[2]

Because non-polar regions in lipids are unable to form hydrogen bonds with water molecules, their exposure to water breaks existing hydrogen bonds of surrounding water molecules and forces them to form a new hydrogen bond network that adapts to the non-polar surface. It increases the system energy by lowering the

---

[1] Source of image: www.avantilipids.com
[2] Source of image: www.avantilipids.com

entropy. Therefore, lipids tend to reorient themselves spontaneously to hide hydrocarbon chains from water molecules to minimize the energy. This entropy driven interaction is called the hydrophobic interaction[2]. Depending on different lipid concentrations and boundary conditions, lipids can form micelles, liposomes and planar lipid bilayers (shown in Fig. 4). Micelles are a spherical form of lipid aggregates in which the hydrophobic tails face inward, while hydrophilic head groups make contact with water. They usually form in free aqueous solutions with concentrations greater than the critical micelle concentration (CMC). Alternatively, two lipid sheets can orient their hydrophobic tails to face each other and form a bilayer. Liposomes and vesicles are composed of a spherical bilayer lipid membrane with an aqueous core. They are widely implemented as carrying vehicle in organisms, and commonly chosen as vehicles for drug delivery by bioengineers. With proper boundary conditions, a flat bilayer membrane can be formed (planar phospholipid membrane, PPM), which will be the center of this study.

Lipid bilayers are impermeable to hydrophilic small ions, ideal for serving as a barrier and containment for cells and intracellular organelles. They maintain the right pH, ion concentration, membrane potential and other important physiological conditions in different compartments. Liposomes are important transport vehicles in cells, as they carry signal molecules in or out of cells in processes called endocytosis or exocytosis. Moreover, cell membranes and organelle membranes host a wide range of proteins that are essential for the fundamental functions of cells, such as cell potential regulation, signal transmission, and neurotransmitter communications [3]. Among these membrane proteins, ion channels are of great interest. They are

typically multi-unit proteins with a hydrophobic region that helps anchor them to the lipid membrane and a hydrophilic opening that allows water to flow through. Ion channels can be categorized based on their gating properties, such as voltage-gating, ligand-gating, mechanically gating and independently stable. Please refer to [4] and [5] for more detailed discussions in structures and functions of ion channels .

Ceramide, a sphingosine based lipid, is one of my research focuses in this dissertation. Because ceramide concentration is elevated before mitochondrion outer membrane (MOM) permeation in apoptotic cell death, the general consensus is that ceramide plays an important role in apoptosis. Dr. M. Colombini's group at UMD proposed that ceramide molecules are able to aggregate and form dynamic ion channels that are large enough to render MOM permeable to large apoptotic proteins. Fig. 3(a) shows a C_{16}-ceramide structure model with electron donor in the blue box and acceptor in the pink box. They can form inter-molecular hydrogen bonds that link ceramide molecules into a column. A circular arrangement of ceramide columns can further link to form a pore in a phospholipid membrane. (Fig. 3(b)) The ceramide channel has a curvature so that exposure of hydrophobic tails to water is minimized. Fig. 3(c) shows a ceramide channel which consists of 24 columns of ceramide molecules. A number of papers have been published in support of this hypothesis, including ones based on macro scale planar membrane tests [6-10], isolated mitochondria tests [8-11], molecular dynamics simulations [12], and comparison between ceramide and its analogues [13, 14]. For a recent review on ceramide channels and their roles in apoptosis, please refer to [15] .
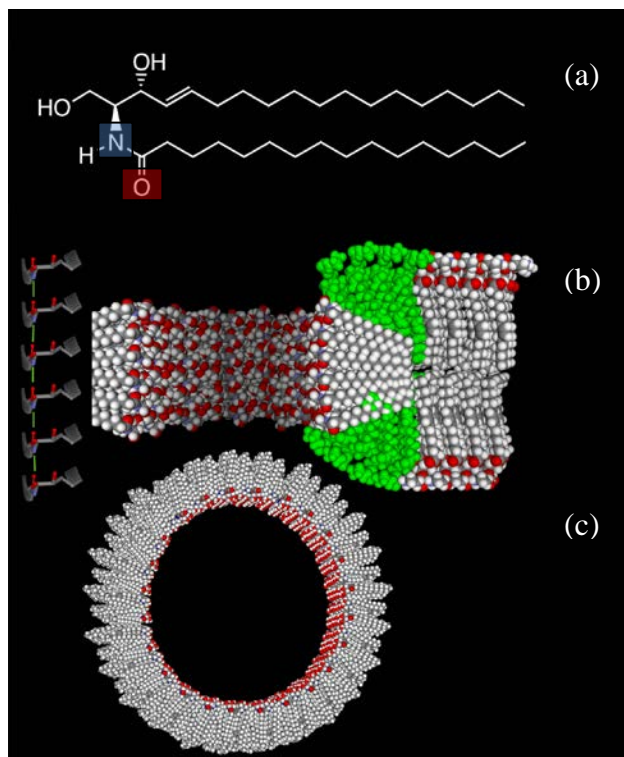
Figure 3 Ceramide channel model.

Because of their fundamental functions in cell signaling, it is important for cell biologists to understand the native structures of ion channels and how they change their conformations in execution of their functions. The main method to study channels is to measure the current flowing through their aqueous cores. Invented in late 1970s, patch clamp is the primary research tool to this end [16, 17]. Briefly, a glass pipette is placed next to a cell and a small negative pressure is applied to suction a small patch of the cell membrane to the orifice of pipette and form a tight seal. Using two electrodes, one placed in the glass pipette and the other in the cell medium, the current flowing through the small patch or the rest of cell membrane can be measured, depending on different configurations. Because of its high detection sensitivity, the patch clamp method is widely used in electrophysiology studies. For a recent review of patch clamp technology by the inventors, please refer to [18].

1.1.2 PPM Technology

Unlike the patch clamp technique that is performed on cells *in vivo,* planar phospholipid membranes (PPM) are reconstituted from lipids *in vitro* [19]. Because PPMs support the study of purified ion channels without interference from other cell components and allow the flexibility of using different lipid system, they serve as a great alternative to patch clamping for the study of ion channels and membrane physics. There have been a few variations in PPM setup (see terminology[3] and examples in Figure 4) since its invention in early 1960s [20-22], but the essential configurations remain same. Typically a PPM is hosted at an aperture on in a hydrophobic partition between two aqueous chambers, which contain buffer solutions mimicking extracellular and intracellular spaces. After introducing ion channels to the PPM, one can measure the current through the ion channel using electrodes in the two chambers. As shown in Fig. 4, three types of PPMs, i.e. free standing membranes, supported membranes, and suspended membranes have been developed. Free standing membranes are usually confined in small glass pipettes [23] or microchannels [24, 25] and are free to move. A supported membrane is formed usually by spreading lipids on a substrate (solid [26-34] or porous [28, 35-38]), which minimizes the impact of mechanical disturbance to fragile membrane and thus improves its stability. An extra tethering structure can be introduced between the

---

[3] Historically the acronym BLM is referred to Black Lipid Membrane to indicate that bilayers often display grey or black color in certain angle of incident under microscope because reflective light from two leaflets is cancelled out at that particular angle (20.   Mueller, P., et al., *Reconstitution of Excitable Cell Membrane Structure in Vitro.* Circulation, 1962. **26**(5): p. 1167-1171.). Later, BLM is widely referred to Bilayer Lipid Membrane to indicate its difference to micelles and monolayer, but it might cause confusion since cell membrane and liposome also has bilayers. To lessen the confusion, BLM in this study is used to refer to any lipid structure with bilayers, and PPM (planar phospholipid membrane) is used in situation where liposome or cell membrane should be excluded.

membrane and the substrate to further stabilize the membrane [39-44]. However, the physics (such as lipid diffusion) in supported PPM is considered different from native cell membrane, and it is difficult to access the chamber adjacent to the substrate. Thus supported PPMs are considered as a biosensor platform but are a less preferable platform for the study of ion channel activity. Nevertheless, due to their mechanical stability, they are widely implemented in AFM or fluorescence imaging techniques [36].

Figure 4 Terminology and examples of different types of lipid systems.[4]

There are two basic methods to form suspended lipid bilayers: the painting method [20-22], and the monolayer folding method [47, 48]. Fig. 5 shows the process of the painting method. Briefly, after the chambers are filled with aqueous buffer, one can use a small brush to gently paint lipid solution (typical concentration 10mg/mL in n-decane or n-hexadecane) across the aperture. As the solvent is retained on the aperture and lipids self-align their hydrophobic tail towards solvent, a "thick" lipid plug can be formed on the aperture. When the solvent wicks towards the partition, the plug becomes thinner. Eventually it reaches a critical point when the Van Der Waals force between two leaflets is large enough to squeeze solvent away [49], and a bilayer can be formed in a zipper-like manner with a thick perimeter bridging between bilayer and aperture edge, called the annulus (Fig. 5). The annulus contains most of the solvent and a quantitative study [50] shows it has an important impact on the stability of the membrane.
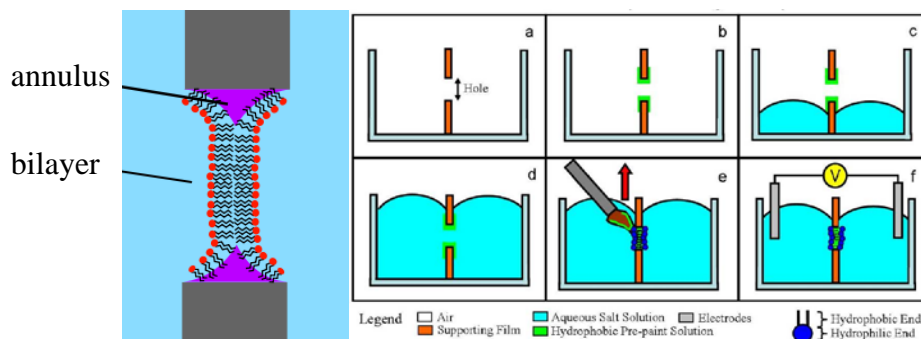
Figure 5 (*Left*) The painting method results in an annulus supported membrane. Annulus is a reservoir of lipids in organic solvent that connects a 5nm bilayer to a micron thick substrate. (*Right*) Procedures for painting a PPM.[5]

---

[5] Source of image: annulus supported membrane: http://en.wikipedia.org/wiki/Model_lipid_bilayer
Painting method: Page 9 in 51.   Hromada, L., *Bilayer Lipid Membrane (BLM) Integration Into Microfludic Platforms With Application Toward BLM-Based Biosensors*, in *Department of Mechanical Engineering* 2007, University of Maryland: College Park.

Fig. 6 shows the process of the monolayer folding method. Briefly, aqueous solution is added to two chambers just below the aperture and a small amount of lipid solution (typical concentration 10mg/mL in n-hexane or n-pentane) is added to both chambers. When the solvent vaporizes completely, the lipids form a monolayer on the water surface, with tails aligned upward because of hydrophobic interactions. Raising the left side buffer creates an upright lipid monolayer across the aperture, and when right side of the buffer is raised, two monolayers attach to each other and form a thin bilayer (Fig. 5). Since there is only a minimum amount of solvent involved in this method, it is also called "solvent free" method. To facilitate the membrane formation and increase the stability of the PPM, a tiny amount of hydrophobic pre-coating materials, typically n-decane/n-hexadecane, is usually applied to the aperture before folding[48].
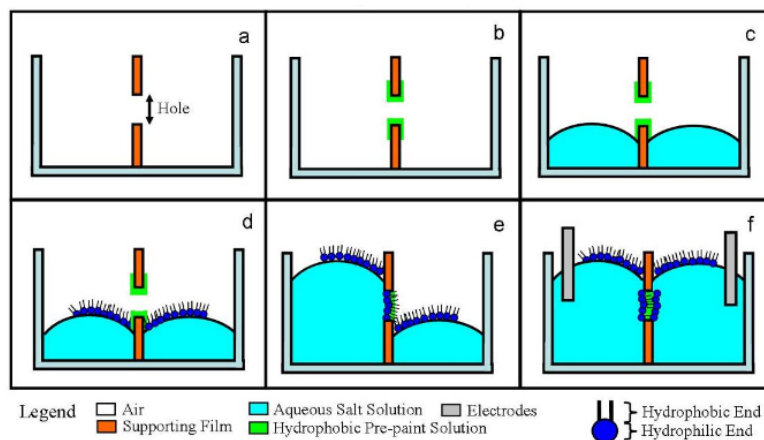
Figure 6 Procedures for forming a PPM by monolayer folding method.[6] [51].

Because their intrinsic fragility, there are a number of methods developed to maximize the stability of membranes, such as lipid polymerization [52-55], solvent freezing [56] and gel protection [57-60]. In lipid polymerization technique, a

[6] Source of image: Page 29 at Reference 49

9

chemical reaction crosslinks unsaturated lipid tails or modified headgroups permanently after lipid bilayer is formed, thus increases its resistance to mechanical disturbance. The solvent freezing method takes advantage of the fact that hexadecane has a freezing point around room temperature. After a hexadecane-containing lipid bilayer is formed, a slight temperature drop can freeze the bilayer and annulus, The stabilized bilayer can then be warmed upbefore use. Gel protection usually involves applying a porous gel structure (common choice is agarose) around the lipid membrane to minimize mechanical instability.

1.1.3 Comparison between PPM Technology and Patch Clamp

Although patch clamping is an exclusive tool to study ion channels in context of other cell components, there are a number of advantages that planar phospholipids membrane can offer to accommodate studies that patch clamp may not support.

1. The patch clamping method is very difficult to perform on ion channels native in intracellular organelle membranes. Locating a glass pipette next to an organelle and applying an appropriate suction to isolate a membrane patch is too sophisticated to perform properly. The only way to perform isolated channel measurements in this case is to purify ion channels and reconstitute them in PPM [61].

2. Ion channel studies on PPMs are completely isolated from interference of other complex factors that may exist *in vivo* cell patch clamping. This may sometime fail to reveal downstream cascade reactions which are also responsible for ion

10

channels' function, but it will provide gains in baseline understanding of ion channels that are newly discovered or are in early stage of their investigation.

3. The composition of the membrane and ion channels can be controlled according to experimental purposes. It is very useful to perform control studies to understand the relationship between ion channel activity and lipid composition, channel point mutants, or external modifications.

4. More ion channels become available in purified form and PPM system is able to take advantage of such advances to perform clean and controlled ion channel studies.

1.2 Microfluidic PPM System

1.2.1 Advantages of Microfluidic PPM System

Miniaturization of PPM system into microfluidics adds unique advantages, as listed below:

1. Disposable chips and mass production. Low cost massive production of microchips will enable researchers to use fresh device every time to avoid sample cross contamination.

2. Array devices and parallel testing. Parallel testing in PPM arrays in a single device is ideal for high throughput screening experiments, where a number of comparisons can be done at one single run with strictly controlled conditions.

3. Reduced reagent volume. The typical chamber size in macro scale PPM step is 1 mL compared to a few μL in microfluidic PPM systems. Exchanging 1 mL buffer at the presence of bilayer often induces a trans-membrane pressure that can break the membrane easily. Reduced reagent volume in microfluidics not only reduces experiment cost but also makes perfusion experiments possible and easier. Chapter 3 in this dissertation shows that with an appropriate design in microfluidics, researchers who would have to spend more than half an hour to exchange buffers in macro size chambers will need only several minutes to do the same job in a microchip.

4. Reduced thermal mass. For those ion channels that have very important and/or interesting thermodynamics in their gating mechanism, study of their temperature responses might be one of the most useful experiments to understand their structures or functions. With lower thermal mass inherent in microchips, changing and sensing temperature can be faster and more accurate.

5. High bandwidth for high frequency event detection. Low system stray capacitance will help increase system bandwidth, making it easier to detect high frequency ligands-ion channel interactions.

6. Compatibility to advanced imaging techniques. Because the PPMs in microfluidic devices are naturally horizontal, they are much easier to fit with confocal microscopes.

1.2.2 Micro-PPM Systems Review

The first PPM that was formed on a microfabricated device and was capable of detecting single channel activity was reported by Schmidts, et al. in 2000 [62]. Manipulated by electrophoresis, negatively charged unilamellar liposomes were fused into a surface-modified silicon aperture and form PPMs. The alamethicin channel activity was detected in the membranes hosted in those devices. Earlier in the same year, a device with gold-coated SU-8 structure was reported to hold thin bilayer layer by Ogier et al. [63]. In the next year, they reported the detection of single channel activity in the same devices [64]. Another silicon-based chip that showed single ion channel activity in a free-standing membrane within a silicon aperture was published by Pantoja, et al. [65]. Glass pipette PPM systems were developed by Fertig and coworkers [66, 67]. Although they all took advantage of microfabrication techniques, they had large aqueous chambers and, thus, were not microfluidic systems.

The first microfluidic PPM system was reported by Suzuki, et al. in 2004 [68]. deep reactive ion etching (DRIE) and tetramethylammonium hydroxide (TMAH) anisotropic etching was employed to pattern microchannels and apertures on silicon. A layer of parylene is deposited over Si wafer for electrical insulation and to increase the hydrophobicity of surface for better membrane stability. Two glass slides with pre-defined electrodes and reservoirs were bonded to both sides of Si wafer to enclose the upper and bottom chambers. Fig. 7(a) shows the conceptual schematic of the chip and Fig. 7(b) shows a cross-section view of PPM sitting on the silicon aperture. A similar device but fabricated with polymethyl methacrylate (PMMA) was reported by the same group in 2006 [69]. The membrane-supporting structure in this case is thick

but tapered PMMA aperture which was carefully drilled by a precision CAD/CAM 3-D machine. Fig. 7(c) shows the schematic and Fig. 7(d) the cross-section view of the PPM. In addition to capacitance studies, they demonstrated the incorporation of alamethicin, gramicidin, and alpha-hemolysin channels and reported their gating events that were consistent to their signature activities detected in macro-scale PPM devices.
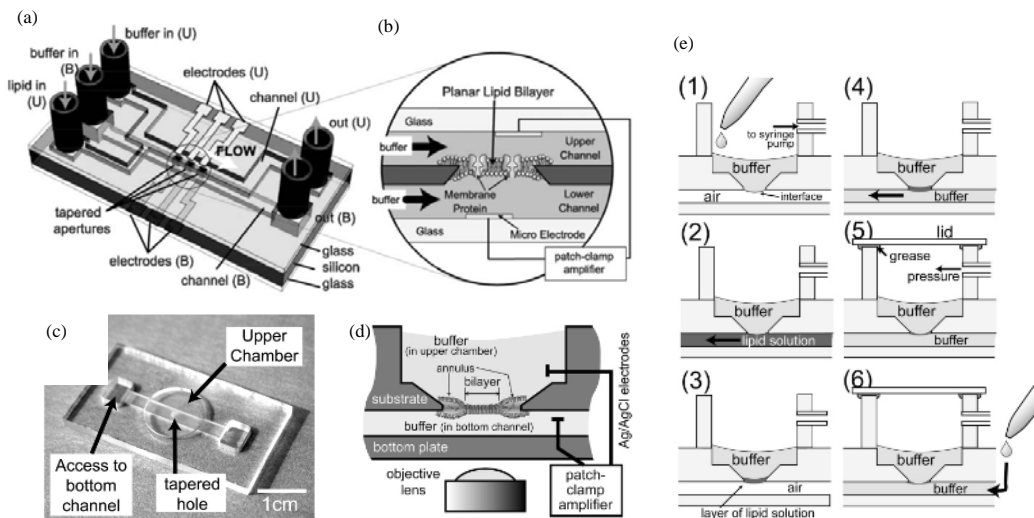
Figure 7 Review of PPM microdevices by Suzuki et al. [7]

The membrane formation methods employed in these devices are essentially the same. Firstly, one chamber is filled up with buffer but the buffer does not snap through the aperture because of surface tension at the water-air interface (Fig.7(e).1). Then ~ 10nL lipid solution is slowly pumped at the other half (Fig.7(e).2), leaving a layer of lipid solution on the surface of buffer at the aperture (Fig.7(e).3). Buffer is

[7] Source of Images: 68.   Suzuki, H., et al., *Planar lipid bilayer reconstitution with a micro-fluidic system.* Lab on a Chip, 2004. **4**(5): p. 502-505, 69.   Suzuki, H., et al., *Highly reproducible method of planar lipid bilayer reconstitution in polymethyl methacrylate microfluidic chip.* Langmuir, 2006. **22**(4): p. 1937-1942.

then injected into the other chamber (Fig.7(e).4), leaving a lipid plug at the interface (Fig.7(e).5). Then the lipid plug is allowed to thin into a bilayer (Fig.7(e).6), when excessive solvent wicks away from the bilayer. In the case of PMMA chip, a positive pressure can be applied through the upper chamber to facilitate the thinning process (Fig.7(e).5).

As an analog to monolayer folding method in microfluidics, another microfluidic bilayer formation was demonstrated by the same group in 2006 [25]. Briefly, two streams of buffer was injected perpendicular to channel filled up with lipid solution. A lipid monolayer was formed on each of the two interfaces (Fig. 8(a)). Pushing those monolayers by pumping syringes forces them contact each other to form bilayer (Fig.8(b)). Importantly, after the bilayer is ruptured, the chip can be easily flushed and used for bilayer formation again (Fig. 8(a)). This concept was later developed by Dr. Bayley's group into another rich topic: droplet interface membranes (DIMs) [70-73]. Instead of having two buffer streams to create monolayers, DIM method uses two aqueous droplets in bulk lipid solutions (typically in hexadecane). When two droplets are brought together, a bilayer can be readily formed and electrical signals can be monitored through electrodes that are inserted into the droplets. DIMs are useful because they can form electrical networks consisting of multiple droplets [70, 71] , asymmetric lipids constitutions [72], and superior membrane stabilities [73].
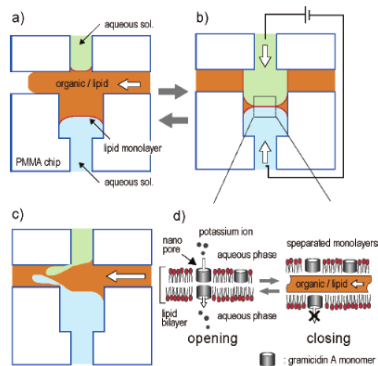
Figure 8 Forming PPM in microchip by contacting two monolayers.[8]

An automatic bilayer formation method in poly(dimethylsiloxane) (PDMS) was reported by Malmstadt, et al. in 2006 [24]. Controlled by pneumatic valves, a droplet of lipid solution is sandwiched by two streams of aqueous buffer in PDMS based microchip (Fig. 9(a)). Solvent partitions into PMDS but lipids do not. After solvent is completely extracted into PDMS, the lipids will form a solvent free bilayer inside the microchannel (Fig. 9(b, c)). This method is essentially labor-free and requires minimal expertise compared to other existing membrane reconstitution methods. Alpha-hemolysin (alpha-HL) channel activities were demonstrated in the membrane formed by this method. However, since the aqueous chambers are coupled in the same microchannel, it might be difficult to manipulate the aqueous buffer conditions to study ion channels in practice.
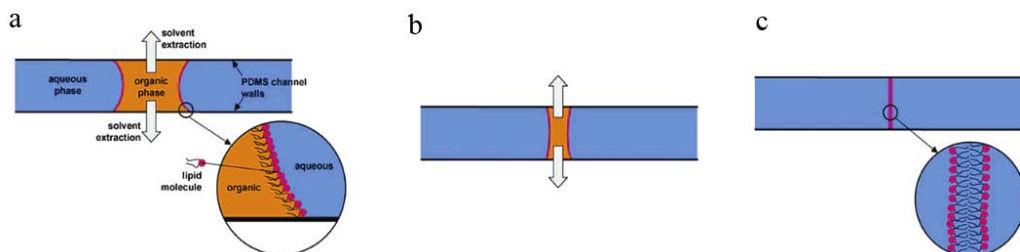
[8] Source of Image: 25.   Funakoshi, K., H. Suzuki, and S. Takeuchi, *Lipid bilayer formation by contacting monolayers in a microfluidic device for membrane protein analysis.* Analytical Chemistry, 2006. **78**(24): p. 8169-8174.

Figure 9 Solvent extraction based PPM formation method in PDMS chip. [9]

Rapid fabrication of PPM devices by hot embossing and laser micromachining was reported by Sandison et al. in 2005 [74]. Two layers of dry films were laminated onto a glass slide and worked as protective layers in glass wet etching. The glass template was then used to imprint PMMA at its glass transition temperature. In the same chip, apertures were patterned with laser micromachining on polytetrafluoroethylene (PTFE), polyethylene terephthalate (PET) and fluorinated ethylene propylene copolymer (FEP).

Sandison et al. reported microfluidic PPM devices based on glass in 2007 [75] to avoid problems associated with polymers, such as low chemical resistance and poor optical properties. An outstanding feature of these glass devices is that they can tolerant aggressive solvent rinsing and cleaning after each experiment so that every device can be recycled. They used a simple spark assisted chemical engraving (SACE) process to create glass apertures that are subsequently salinized to render highly hydrophobic surface for better PPM formation.
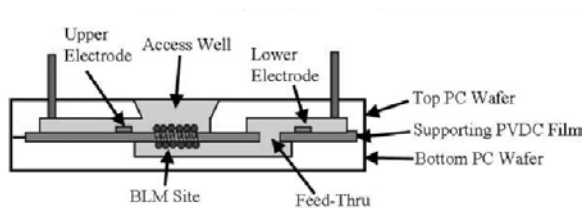
Figure 10 PC-PVDC-PC based bilayer lipid membrane device. [10]

---

[9] Source of Image: 24.   Malmstadt, N., et al., *Automated formation of lipid-bilayer membranes in a microfluidic device.* Nano Letters, 2006. **6**(9): p. 1961-1965.
[10] Source of image: 76.   Hromada, L.P., et al., *Single molecule measurements within individual membrane-bound ion channels using a polymer-based bilayer lipid membrane chip.* Lab on a Chip, 2008. **8**(4): p. 602-608.

A micro-PPM device that was able to host α-HL channels for size discrimination of polyethylene glycols (PEGs) was reported in 2008 [76]. Polycarbonate (PC) and polyvinylidene chloride (PVDC) was used as chip material and membrane supporting material, respectively. With a new PPM formation method called diffusion painting, based on a mixture of 90% hexanol, 10% hexadecane as the lipid solvent, a bilayer formed spontaneously after the water-miscible portion of solvent diffuses into the aqueous phase (Fig. 10). Alpha-HL channel solution was pumped through upper channel to the open well until one single channel is incorporated into bilayer. The ion channel solution was then withdrawn to ensure only one channel was inserted. With PEG prefilled in the bottom channel, the high frequency interaction between PEG and alpha-HL can be resolved, thanks to high bandwidths achieved by microfluidics. With its high level of integration, this device was claimed as a step towards high performance micro-biosensors based on bilayer lipid membrane.

Figure 11 Illustration of success rate in PPM array reported in [77].

There is an ongoing effort to create lipid membranes array in microfluidic platform [77-79], to fully realize the mass production power of microtechnologies.

18

The highest yield achieved so far is 44/96 by Sukuzi et al., as shown in Fig. 11 [77]. In this 96-well array device, parylene was used as supporting material and metal traces were directly patterned on the parylene sheet. By sweeping lipid solution in microchannel, lipid membrane can formed in the aperture (Fig. 11). While the PPM array technology is promising to provide high throughput screening (HTS) capability for ion channel studies, there still exist several challenges before its practical application:

1. Tunable buffer solutions. HTS requires that reagent conditions be able to be adjusted in each of the PPM unit so that responses of ion channels to different conditions can be studied. Individual buffer chambers for each ion channel would create a very complicated channel network, while shared buffer chambers may cause cross contamination or electrical coupling.

2. Decoupling of the electrical signals and parallel measurements of ion channel activities. Limited by availability of electrophysiological setups, it is experimentally expensive to have one logger for each of the ion channel. With fast development of CMOS based amplifiers and digitizers, this problem might be solved in the near future.

1.3 Project Overview

To this date, there are a number of successful fabrication techniques and membrane formation methods that give rise to different versions of micro-PPM platform. Nevertheless, the advantages of miniaturization have not been explored entirely and there are a lot to be done. In particular, this study goes beyond membrane

formation demonstration in microfluidics, and focuses on mainly its utility of studying ion channels and membrane physics dynamically. The device in my vision will not only have all the capabilities that traditional PPM systems have, but also will offer neat solutions to problems that traditional system suffers from. This dissertation places great focuses on 1) taking advantage of small buffer volume to achieve dynamics study capabilities and 2) developing an electro-optical chip that allows biologist to study ion channel or membrane physics with simultaneous electric measurements and optic visualization.

1. A PPM device that fully supports high flow rate, high resolution dynamic perfusion (Chapter 3). This device will remove the limitation of macro PPM devices on how reagents should be added and removed. With careful device design and experimental procedures, the concentration of reagents in one side of the chamber can be changed in less than 1 minute. This will be fast enough to resolve kinetics between ion channels kinetics and external conditions with time constant larger than 1 minute. Examples are given on ceramide channels on La^{3+}, EDTA, and Bcl-x_L proteins. In Chapter 4, a comprehensive dynamic study of the response of ceramide channel to La^{3+} is presented and a novel elastic model is proposed to interpret the experimental results.

2. A novel *in situ* "kiss and retreat" PPM formation is developed to replace somewhat clumsy painting. It forms a PPM after the chip is placed on a confocal microscope and lipid microdomains are imaged as a demonstration of its dynamic electro-optical capabilities. (Chapter 5)

3. As an extension of Chapter 5, a double PPM microchip is developed for studies of (bio)chemical and mechanical interactions between membranes (Chapter 6). Preliminary results of creating two membranes simultaneously and bulging membranes up to 200 µm are presented.

4. A prototype PPM device which can be used to probe ion channels activities in different temperatures ranging from room temperature to 50°C (Chapter 7). With smaller thermal mass in microdevices and variety of microfabrication techniques available, it is easier to control and sense the temperature of ion channels. This is potentially useful for the study of the thermodynamics of ion channels or the temporal temperature response of temperature sensory ion channels such as TRPV families.

Chapter 2: PPM Chip Design and Fabrication

This chapter discusses the design philosophy and fabrication techniques involved in creating a PPM microchip, including polycarbonate and PMMA chip patterning, PVDC thin film patterning, polymer chip thermal bonding, and electrode fabrication and integration. They apply to all micro-PPM chips in this dissertation, with a few modifications when noted.

2.1 PPM Chip Design

2.1.1 Design Overview

PPM microchip design remains essentially unchanged since its birth: two buffer chambers are separated by a hydrophobic partition where a bilayer is hosted at an aperture with a diameter from 50 to 250 µm. However, considerable practice is needed for a new researcher to become an expert who can perform PPM formation routinely. Even slight variations in fabrication, lipid introduction, fluids handling, or ion channel incorporations may result in unsuccessful bilayer experiments. Thus it is very important to make the final system user friendly, convenient to use, and robust by deciding what materials should be chosen, what the best fabrication method is, how to create the PPM repeatedly, how to optimize the stability of membrane, and how to lower the cost. In this study, polycarbonate or PMMA is chosen over glass or silicon for chip material because they can easily be patterned by CNC with low cost. PVDC is chosen over Teflon for the bilayer supporting material because previous efforts have shown that high quality PVDC apertures are easier to create with controllable size. Also, although lower than Teflon, the hydrophobicity of PVDC is

proven to be enough to support PPMs well. Fig. 12 shows a conceptual diagram of a perfusion PPM chip connected with syringe pumps and Fig. 13 shows a closer look of the current flowing through ion channel between upper chamber and lower chamber.
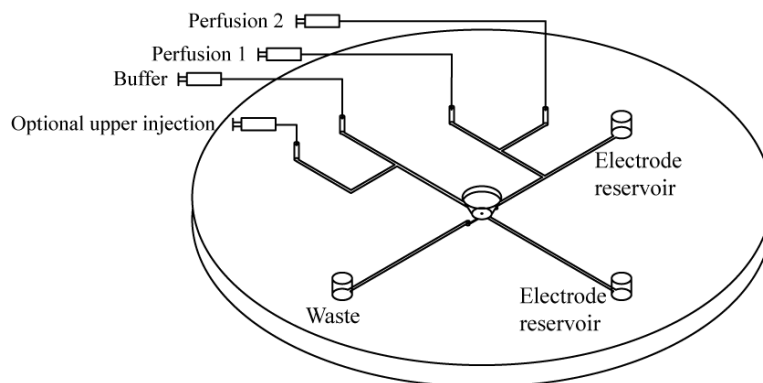
Figure 12 Schematics of PPM perfusion Chip
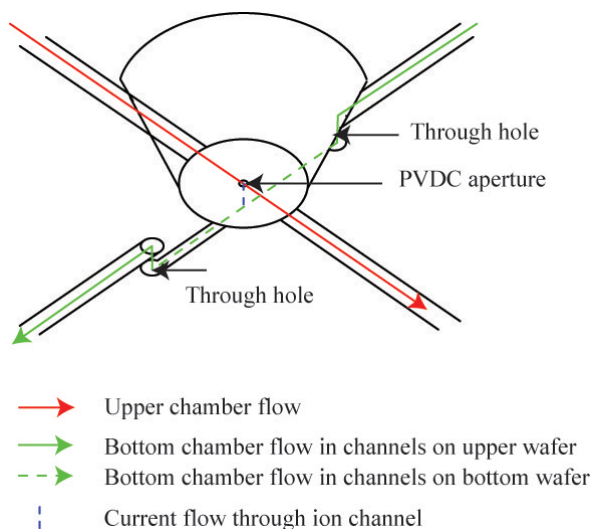
Figure 13 Schematics of current flow through ion channel

The microchip consists of three layers: upper polycarbonate (PC) wafer (2.38 mm thick, 8.9 cm diameter; McMaster-Carr, OH), a polyvinylidene chloride (PVDC) thin film (12.5 µm thick; Sheffield Plastics, MA), and bottom PC wafer. An aperture

of 60 ~ 120 µm diameter is burned at the center of PVDC thin film as a formation site for PPM. Most of the microchannels are patterned on the upper wafer except a 6 mm section just below the PPM site (show as green dash line in Fig. 13). This bottom channel is connected to other channel networks on the upper wafer through two holes positioned right above the ends of the bottom channel. One open well is drilled in the center of upper wafer, providing access to the PVDC aperture when lipid is painted manually. The open well is connected to another portion of upper channel network, illustrated in red solid line in Fig. 13. These two separated channel networks are defined as the bottom chamber and the upper chamber.

Buffer can be introduced through the reservoir connected to the open well and all the channel network can be filled up when buffer goes through PVDC aperture and through-holes. Two electrodes can be fixed by wax at the end of the upper chamber and bottom chamber with gas tight seal. Another open reservoir is placed at the other end of the bottom chamber to collect waste introduced by bottom chamber perfusion. Side perfusion channels can be added to the main channels according to experimental needs. Typically, two or three perfusion channels are connected to bottom chamber, enabling alternated introduction of different analytes that are potent to ion channel. For analytes that need to be introduced slowly and progressively, an optional upper injection channel can be used. The solution will mix with buffer in the open well by convection and total concentration will increase in a much slower manner.

Fig. 14 shows a picture of finished PPM perfusion chip. Stainless steel needle segments (51 mm long, 22s gauge, Hamilton, Reno, UT) are inserted to reservoirs

and connection unions (Upchurch, WA) are used to connected to capillary tubing (not shown).
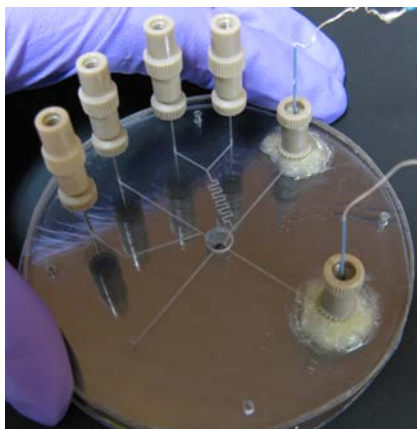
Figure 14 A finished PPM perfusion chip.

2.1.2 Optimize Electrical Performance

To optimize the design of the PPM chip, it is important to understand its equivalent electronic model, shown in Figure 15. Ion channel can be seen as an adjustable resistor in parallel with bilayer membrane capacitance C_m and PVDC partition film capacitance C_p. Connected through resistors in upper chamber R_u and lower chamber R_b, the current flowing through the ion channel R_i is picked up by Ag/AgCl electrodes and converted to voltage in a low noise headstage by a factor of $10^6 \sim 10^8$. The 60 Hz cycle noise in the signal can be removed by a noise eliminator. The signal is then digitized by an Axon Digidata 1440A and recorded by computer (All current data in this dissertation were acquired this way.) The recorded data is then processed in pClamp 10.0 software package and Matlab.

In an ideal system, any events occurring in ion channel, such as ligand - ion channel interactions or ion channel conformation changes, should be detected and

differentiated by the electronics. In reality, however, the ability to resolve fast events is limited by the system bandwidth. Based on the electrical model illustrated in Figure 15, the bandwidth of system can be obtained by Thevenin's theorem:

$$B = \frac{1}{(C_p + C_m)(R_u + R_b)} \, [51]$$

It can be maximized by minimizing stray capacitance of supporting film, capacitance of the bilayer and resistance of the microchannel.
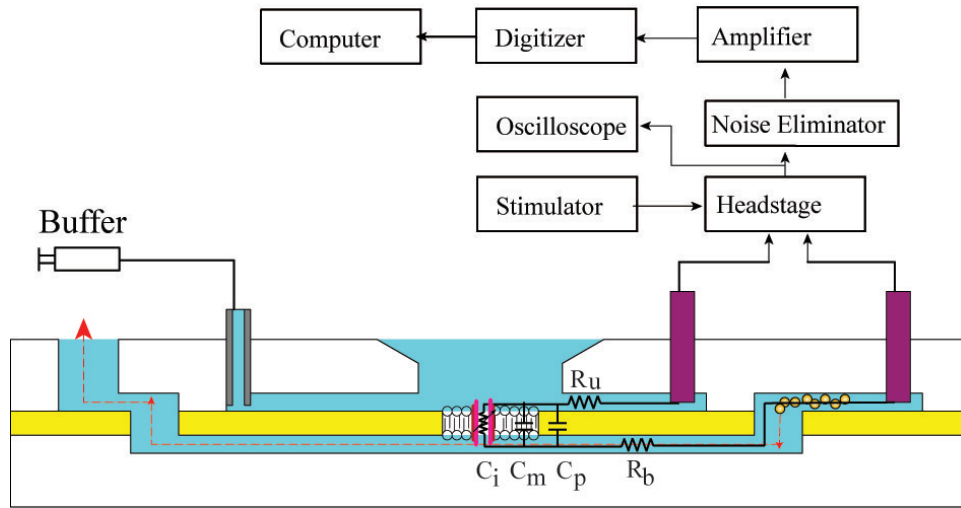
Figure 15 Electric schematics of PPM chip.

1. The stray capacitance of supporting film can be estimated by equation $C = \frac{\varepsilon \varepsilon_0 A}{d}$, where ε_0 is permittivity of vacuum and ε is permittivity of the partition; A is the partition surface area exposed to both chambers; d is the thickness of the partition. PVDC is selected since it was successfully used as supporting layers for bilayer membranes. Other hydrophobic materials such as PTFE or polyvinylidene fluoride (PVDF) can also server PPMs well but there is no practical method to bond

them to polycarbonate due to their high glass transition temperatures. Meanwhile, the aspect ratio of the membrane aperture is proven critical to the stability of the membrane, thus the thickness of the PVDC may not be altered at will. The exposure area is also constrained by the fabrication method. In this study, 12.5 µm thick PVDC is used and the stray capacitance of PVDC is measured as 0.2 pF.

2. The capacitance of a bilayer can be determined in the same equation $C = \dfrac{\varepsilon \varepsilon_0 A}{d}$. The thickness and permittivity of the bilayer formed by same method are constant. Thus it is beneficial to keep area of bilayer A as small as possible to minimize capacitance. Smaller bilayers also have better stability. However, limited by the magnification of stereo microscope, apertures smaller than 50 µm in diameter cannot readily be resolved during experiments, and it is difficult to paint the lipid solution properly. In this study, the bilayer capacitance C_m ranges from 6.4 pF (50 µm in diameter) to 55 pF (140 µm in diameter). It is worthwhile to mention that this is slightly different from a theoretical estimation of bilayer capacitance based on the aperture area ($1\mu F/cm^2$), because the bilayer doesn't cover up the whole aperture in painted membranes due to existence of an annulus.

3. The resistance of upper and bottom channel can be determined by the equation $R = \dfrac{L}{GA}$, where G is the conductivity of buffer, A is the cross section area of the channel and L is the length of the channel. Unfortunately, the type and conductivity of buffer needs to be chosen carefully in accordance with the native environment of the ion channel. The ionic strength and/or presence of particular ions

may affect ion channel behavior, and we cannot change it arbitrarily. For example, 1 M KCl or lower, 1mM MgCl$_2$ and 5mM PIPES buffer is a standard buffer for ceramide channel experiments. The dimensions of the channel are limited by the fabrication method. For example, if an SU-8 template is used to hot emboss a polycarbonate chip, both of the channel width and depth cannot exceed 50 µm to avoid demolding failure in the embossing process. If a silicon template pattern by DRIE is used, then channels cannot be deeper than 100 µm. In this study, we use CNC direct machining to pattern PC and the dimension limitations can be relaxed. The upper channel here is 460 µm wide and 120 µm deep. With 1 M KCl, the total resistance of the system is 50 kΩ.

Table 1 A Comparison of PPM System Bandwidth *

System	Bandwidth**
Macro PPM system	3.5MHz
Micro-PPM system described in [51]	0.8MHz
PPM system in this study***	2.7MHz

* Chambers filled with 1 M KCl buffer.
** Bandwidth is theoretically calculated. In experiment, it is lowered by downstream electronics.
*** Based on 50 µm diameter PPM.

2.1.3 Minimize Back Pressure Introduced by Perfusion

A moving flow in the bottom channel creates a back pressure which will bulge the PPM upward. A PPM subjected to this pressure bursts when the pressure reaches a critical point. In fact, in macro scale PPM devices, it is not uncommon that the PPM ruptures due to very tiny mechanical disturbance. Thus it is important to understand the inherent physics that limits membrane pressure resistance quantitatively before a perfusion chip is developed. The back pressure at PPM site can be determined by:

$$p = Q \cdot R_h,$$

28

where Q is the volumetric flow rate and R_h is the hydraulic resistance between PPM site and the waste reservoir. R_h can be further determined by:

$$R_h = \sum_{i=1}^{n} \frac{8\eta l_i}{r_{hi}^2 A_i},$$

where η is viscosity of water, l_i is length of ith segments of the channel, A_i is the cross section area of the of ith segments of the channel, and r_{hi} is the hydraulic radius of ith segments of the channel, which can be determined by:

$$r_{hi} = \frac{2A_i}{P_i},$$

where P_i is the perimeter of the cross section.

Combining these three equations together, we know that deeper and wider channels have significantly lower hydraulic resistance and thus lower back pressure. In this study, the perfusion downstream channel consists of two segments, one of length 3 mm in the bottom wafer, and other of length 27mm in the upper wafer. Since free PVDC may sag into the channel during thermal bonding wider than 100 µm, a modification to thermal bonding recipe is made. PVDC is bonded to the bottom wafer in the first thermal bonding step, and then further bonded to the upper channel with PVDC already fixed to the bottom wafer. Thus, only the bottom channel is restricted by the maximum channel width. Here the bottom channel width is 90 µm, and depth 120 µm. Upper channels are again 460 µm wide and 120 µm deep. By theory, this dimension will give a back pressure of approximately 40 Pascals at 3.5 µL/min.

2.2 Patterning of Thermal Plastics

Well known for their low manufacturing cost, good optical, physical and chemical properties, plastics have been widely used for microfluidic devices since late 1990s. In contrast to laborious and expensive silicon/glass fabrication, rapid casting of elastomer PDMS provided a prototyping alternative which would cure into full functional devices less than two days [80]. For biochemical applications that involve strong chemicals and high internal pressures, however, PDMS is not an ideal material because of its poor solvent resistance and low bonding strength. Thermal plastic has emerged as a strong alternative to this end. Plastics commonly used by microfluidic researchers include PMMA, PC and cyclic olefin polymer (COP) or cyclic olefin copolymer (COC). There are a number of fabrication methods available for thermal plastics, such as casting, injection molding [81], laser ablation [82], hot embossing [83] and direct machining [84]. For a review on plastic based microfluidic devices, please refer to [85].

Among those methods, hot embossing and direct machining are at the center of this study because of their exceptional design flexibility and low fabrication cost. Unlike SU-8 based hot embossing described in [51, 76], hot embossing in this study is primarily done with silicon template patterned by deep reactive ion etching (DRIE). The higher mechanical strength of silicon helps maintain features created by DRIE from run to run compared to SU-8 features. However, because of demolding difficulty between polycarbonate and silicon wafer, only 100 μm deep channels can be achieved. As discussed in previous session, it would limit our ability to lower the

back pressure caused by perfusion. All PPM chips discussed in this dissertation were fabricated with CNC machining.

2.2.1 Hot Embossing by Silicon Template Etched by DRIE

The DRIE process is a highly anisotropic dry etching method to create microstructures with aspect ratio as high as 20:1. DRIE typically consists of alternated activation and passivation steps. Briefly, in the activation step, etchant gas (SF_6 for silicon) is introduced into the etching chamber and a high power RF source breaks the gas molecules into ions. The ions are accelerated vertically towards wafer surface and materials that are not protected by a mask are etched and sputter away by the high energy of plasma. In the passivation step, a chemically inert gas (C_4F_8 for silicon) is deposited to the wafer side wall and trench bottom surface to protect against etchant. By cycling activation and passivation, the substrate can be etched down almost vertically.

Bare silicon is rinsed extensively by acetone, methanol and isopropanol and then put into hot oven at 150 ℃ overnight to remove any possible moisture which would cause adverse effect in DRIE process by reducing adhesion between photoresist and silicon. Degassed silicon is put on a spin coater (Specialty Coating Sytems G3P, Cookson Electronics Co, IN) and several drops of adhesion enhancer Hexamethyldisiloxane (HMDS) are added onto the wafer. Spin coater ramps from 0 rpm to 3000 rpm in 5 seconds and dwells at 3000 rpms for 120 seconds before ramps down to 0 rpm in 5 seconds. High resolution positive photoresist AZ 9245 is then poured on the wafer and the spin coater is activated at 3000 rpm for 60 seconds. A soft bake is performed

on a hot plate at 70 ºC for 2 minutes, and then UV exposure is carried on with film mask (Fineling Imaging INC, CO) fixed on the wafer. The PRX-1000 UV source (Tamarack Sci, CA) is used for UV exposure. With output intensity ranging from 20 – 30 mW/cm^2, the typical exposure time is 120s. Then a hard bake is performed at 110 ºC for 10 minutes before the wafer is placed in AZ 400 bath for development. It is very important to optimize the recipes of UV exposure and photoresist development to achieve the right size of final feature. Usually variation of UV power from day to day can be compensated by a careful dosage calculation. Meanwhile, it is recommended to check the feature of photoresist during development frequently to make sure there is no over-development or under-development.

After development, the wafer is transfered to DRIE machine (STS DRIE system, Surface Technology System, Newport, UK). The DRIE recipe is set as 10 seconds for activation (etching) and 6 seconds for passivation. The silicon wafer is taken out of STS etcher after 10 minutes to estimate the etching rate which is used to calculate the etching time for second round etch time with a total depth of 100 µm. Fig. 16 shows a work flow to use DRIE patterned silicon template for polycarbonate impriting.
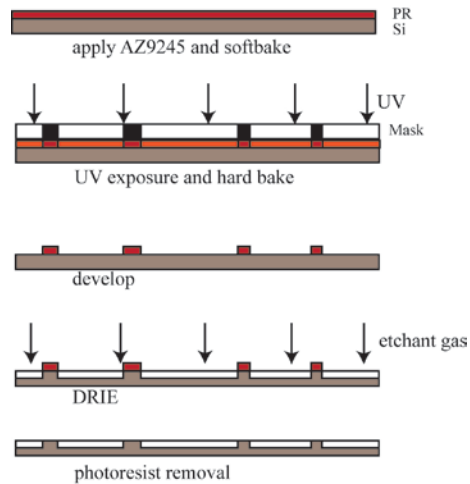
Figure 16 Workflow of silicon template fabricated by DRIE.

The finished silicon template can be permanently fixed into a 6 inch by 6 inch stainless steel plate by a thermal curable adhesive layer (FR0111, DuPont, DL) in a hot press (AutoFour/15, Carver, IA). The stack, from top to bottom including a 762 µm Teflon sheet, silicon template, a layer of FR0111 and stainless steel plate, is pressed under 2000 lbs at 188 ℃ for 3 hours.

The polycarbonate imprinting recipe is slightly modified from that in [51]. Briefly, a 6 inch by 6 inch stainless steel fixture and a glass plate fixture are fixed at the bottom and top platform respectively. Polycarbonate (8.9cm in diameter, 2.38mm thick, McMaster-Carr, CA) should be put into 100 ℃ vacuum oven for degassing at least 8 hours before imprinting. PC and the silicon template are put on the fixture and the hot press temperature is set towards 177 ℃. Then the hot press is closed until only a few centimeters left between upper glass plate and polycarbonate sheet. After temperature rises to 150 ℃, the hot press is closed with load 700 lbs. When the temperature rises to 160 ℃, the load is increased to 2700 lbs. When the temperature

33

rises to 166 ℃, the water cooling is initialed. When the temperature hits 147 ℃, the hot press is opened up and the patterned PC wafer will be stuck to the glass plate. The PC wafer is peeled off from the glass at temperature 135 ℃. The temperature in this recipe should be optimized in testing trials since thermocouple readings in hot press might not represent the temperature at the polycarbonate precisely enough. Usually two thermocouples are implanted into the steel fixture and glass plate fixture to provide better readings than the built-in thermocouple in hot press. After imprinting, the marked positions in PC are drilled manually as electrode reservoirs, needle reservoirs, waste reservoirs and open well. Several alignment holes are drilled at the matching position in upper wafer and bottom wafer. Later on in the bonding process, small spring pins are inserted to the alignment holes so that bottom channel can be precisely aligned to upper channel network. Fig. 17 shows work flow to create a PC wafer ready for bonding. Fig. 18 shows a set of SEM images of imprinted polycarbonate.
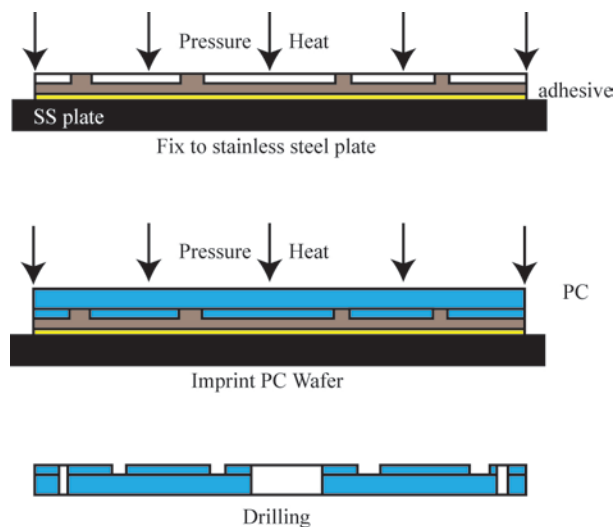
Figure 17 Work flow for creating a PC replica using a silicon template fabricated by DRIE
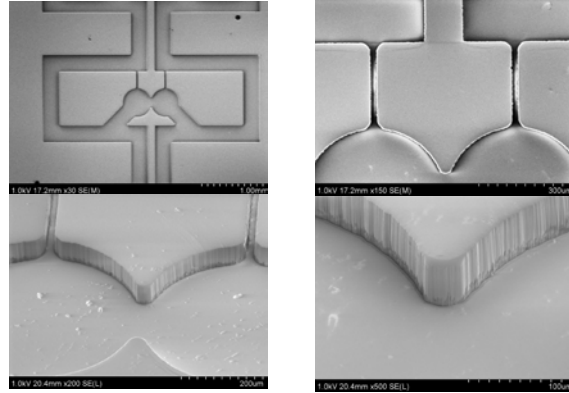
Figure 18 A set of SEM images of imprinted PC using described procedure. These chips were designed to produce droplet interface membranes (DIMs). Details of DIMs were not covered in this dissertation.

2.2.2 CNC machining

CNC direct machining is a great alternative to cleanroom based patterning techniques. For glass or other hard materials, CNC direct machining might not be as cost effect as lithography because of overwhelming cost for diamond based milling tip. For thermal plastics, however, the cost is significant lower. Other advantages includes its ability to pattern features of different depths, to drill reservoirs and mill channels in single machine run, rapid design turnaround, and higher overall robustness. All my PPM chips are fabricated using CNC machining.
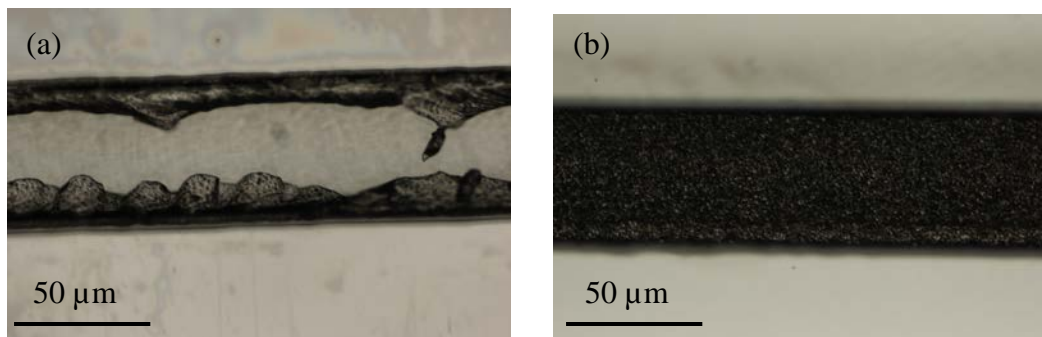
Figure 19 Comparison of milled microchannel in PC before and after sonication.

460 ~ 470 µm wide channels in upper wafer are milled by 18 mil end mill (Performance Micro Tool, Janesville, WI), and 85 ~ 90 µm wide channel in bottom wafer is milled by 5 mil end mill. Width variations is in the allowed range of CNC machine precision specified by manufacturer (Roland MDX-650, Roland DG Corp., Tokyo, Japan), and usually channels are 5 ~ 10 µm wider than the tip of the end mill. The depth of the channels is 120 µm, although it can be increased further to lower hydraulic resistance and electrical resistance. Part of the reason not to go deeper than 120 µm is that channel deeper than 120 µm is very difficult to clean. As a brittle material, PMMA has a nickname acrylic glass and is well known for its good machinability. PC, however, is much more ductile and milled channels in PC are covered by machine debris. Fig. 19 (a) shows a picture of milled PC channel. Aggressive ultrasonication is performed to remove all the debris, shown in (b). For channels deeper than 120 µm, debris is difficult to remove.

All the needle reservoirs (0.65mm diameter), waste reservoirs (2.9mm diameter), open well (2.9mm diameter) and alignment holes (#52 drill bits) are drilled together with milling.

After CNC machining and sonication, the devices are put into 100 ℃ vacuum oven until further use.

2.3 Patterning of PVDC Films

Before patterning PVDC, the bottom wafer with a channel patterned by CNC is removed from vacuum oven. After the wafer cooled down to room temperature, a 12.5 µm PVDC layer (Sheffield Plastics, MA) with diameter 8.5 cm is applied to

bottom wafer. Extreme care should be taken to avoid dust in this step because any particles in the bottom channel may later affect the bonding strength of final PPM chip.

To better support the PPM, the hole in PVDC should range from 50 µm to 140 µm with smooth edge. A hot needle apparatus was constructed by Hromada to achieve this goal [51]. Briefly, a stainless steel needle is wrapped with Cr-Ni wire and a thermocouple is planted adjacent to needle tip. A DC voltage supply is connected to the wire and the temperature of needle will go up as the voltage source is increased. Temperature can be read out from a thermometer. A needle with smaller tip size (20 ~ 40 µm in diameter) at temperature 250 ~ 300 ℃ is used to burn the PPM aperture, and bigger needle (40 ~ 60 µm in diameter at temperature 350 ~ 400 ℃ is used to burn the through holes (460 µm).
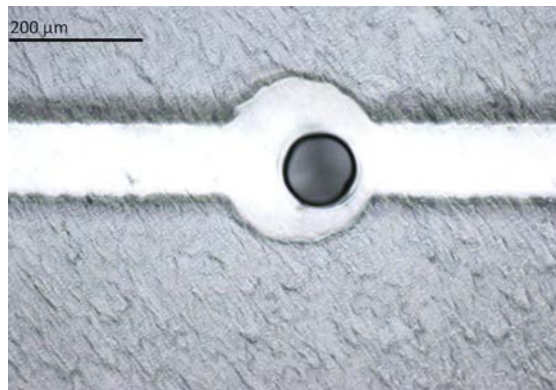
Figure 20 10X view of PPM aperture

The whole apparatus is placed on a probe station and a 3-D positioner can hold the wafer just above the needle. By observing through microscope while adjusting the positioner and voltage supplier, we can controllably lower the wafer and

burn the PPM hole and through holes to the right sizes. Fig. 20 shows a 10X view of a typical PPM aperture.

2.4 Thermal Bonding of Polymer Chips

The first bonding thermally bonds bottom wafer and PVDC together after PVDC is properly patterned. A stainless steel and a glass plate fixture are put into the hot press just as in imprinting. A Teflon sheet (0.762 mm thick) is put on the wafer to prevent adhesion between PVDC and glass plate. To avoid the impression of surface PVDC around PPM site by rough Teflon surface, which affects the PPM stability later on, an opening is cut out on the Teflon just above the PPM site. The bonding recipe is shown in Table 2. Briefly, the hot press is programmed towards 141 ℃ and the stack is put under 700 lbs after the temperature has risen from room temperature to 115 ℃. As soon as the temperature hits 141 ℃, water cooling is on and the device can be taken out after the temperature falls to 90 ℃. The purpose of this bonding is to fix PVDC onto bottom wafer so that it doesn't sag into wide channels in upper wafer. Thus the load and temperature is lower than 2nd bonding.

Table 2 Recipe for 1st thermal bonding

Bonding Material	Bottom PC + PVDC
Bonding Temperature	141 ℃
Dwell Time	0
Bonding Pressure	700 lbs
Press Open Temperature	90

The upper wafer is taken out of the vacuum oven and cooled down to room temperature. By inserting spring pins into alignments holes through upper and bottom wafer, the interconnection between upper channel and bottom channel via through holes can be assured. Microscopes can be used to make sure they are properly aligned

before putting them into hot press for final thermal bonding. It is critical to avoid any particles during the assembly process. The recipe for 2nd thermal bonding is shown in Table 3. All the processes are the same except for there is no needed for opened Teflon sheet.

Table 3 Recipe for 2nd thermal bonding

Bonding Material	Upper PC + PVDC + Bottom PC
Bonding Temperature	144 ºC
Dwell Time	5 minutes
Bonding Pressure	2700 lbs
Press Open Temperature	90

Fig. 21 shows a summarized work flow to create a PPM chip from CNC machining to final assembly.
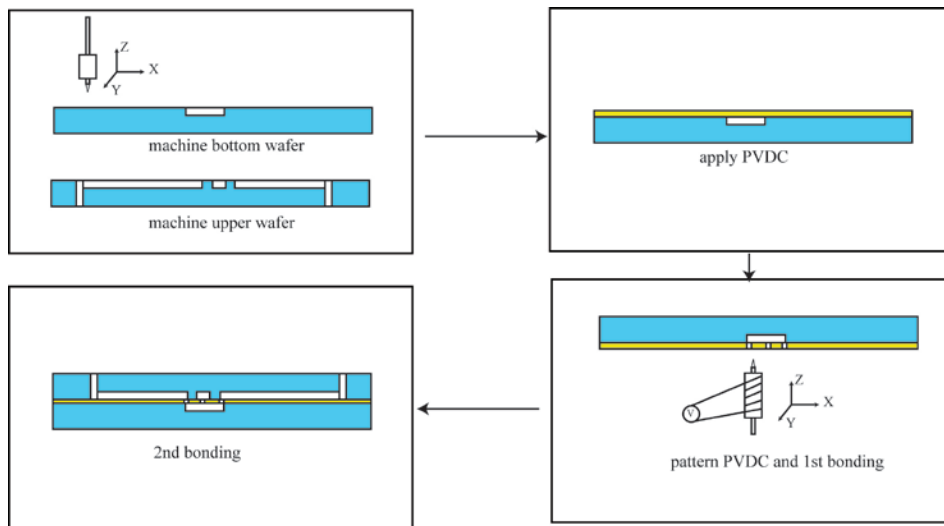
Figure 21 Workflow of bonding two milled PC wafer into a full functional PPM Chip. The chips imprinted from silicon templates are bonded in same way.

2.5 Incorporation of Fluidic and Electrical Interfaces

Stainless steel tubing segments (51 mm, 22s gauge, Hamilton, Reno, UT) are inserted into needle reservoirs assisted by stereomicroscope. To avoid the needle clogging the opening of the microchannel, it is recommended to insert needles to only

4/5 depth of the needle reservoir. The resulting chip-to-world interface has low dead volume and is widely used in plastic chip fabrications in our lab [86]. Standard fused silica capillaries (2000023-10M, OD 360 µm, ID 100 µm, Polymicro, Phoenix, AZ) are connected to stainless steel needles through unions (shown Fig. 14).

Electrodes used in electrophysiology system are usually Ag/AgCl. When connected with a DC voltage source and with KCl as electrolyte, reactions in anode are (where current goes into anode): $AgCl + e^- = Ag + Cl^-$. Reactions in cathode (where current departs) are: $Ag + Cl^- = AgCl + e^-$. Due to its reversible nature, its electrode potential is very stable as long as there is AgCl coating. It is critical to have electrodes with identical electrode potentials in electrophysiology experiments to avoid interference of undesired electrode disparity voltage.
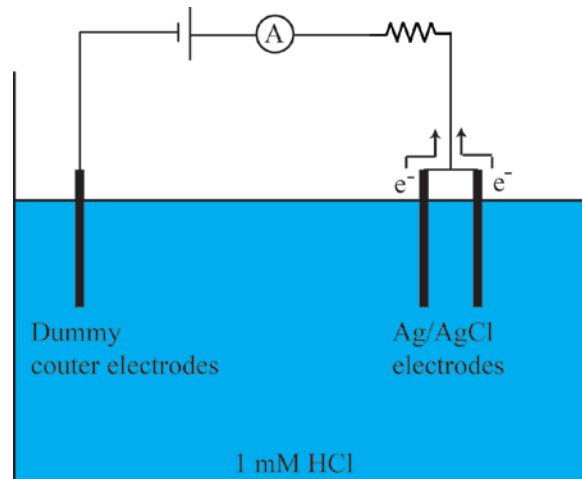
Figure 22 Schematic of fabrication of Ag/AgCl electrodes with minimum asymmetry

To fabricate an electrode pair with minimum disparity, following procedures are taken (instructed by Dr. Colombini). A 1M NaCl solution is put into a petri dish covered with an aluminum foil and two identical silver wires (640 µm, PN 783500, A-M Systems, WA) were put into the petri dish to remove any oxidized Ag by

electrochemical reactions. After the silver wires return to shiny bright color, they are dipped into 1 mM HCl solution as cathode and another dummy electrode work as anode (shown in Fig. -22). It is necessary to reverse the polarity of the DC voltage source several times at the beginning. It roughens the silver surface and helps prevent delamination of AgCl from Ag wire in usage. After the silver wire is properly roughened, a 20 minutes coating with current limited within 1 mA range will result in a pair of nicely coated Ag/AgCl electrodes. The asymmetry of the electrode potentials should not exceed 0.2 mV.

When in storage, the coated electrodes are shorted in saturated KCl solution to keep asymmetry low. When in use, electrodes are inserted to Nanoports (PN N-124S, Upchurch, WA) and sealed by standard sleeves. Then the electrode-nanoport assemblies are attached to the electrode reservoirs of PPM chips by reversible wax (C11444 Center Softseal Tackiwax; Cenco Scientific, IL). The buffer level in the reservoir should be controlled so that no buffer leaks when electrodes are inserted because water leakage will impair the attachment of wax. The dry wax seal prevents buffer leakage from the microfluidic channels while allowing the electrodes to be removed from the chip for reuse. Unlike thin film electrodes, it also allows replacement of electrodes when electrode polarization is observed, the chip will not have to be disposed because of electrode degradation. In high flow rate perfusion experiments, perfusion flow may leak at the bottom electrode reservoir when they are supposed to pass by the membrane. In this case, electrodes need to be removed and the electrode reservoir should be cleaned and dried before new wax is used to attach the electrodes.

There is always a tradeoff between "open" free dipping electrodes [69, 87-89] and "closed" electrodes [68, 76, 77]. Free dipping electrodes suffer from vibration noise, low mechanical robustness and in perfusion case, lack of resistance to pressure generated by perfusion. Closed electrodes don't have any of these concerns but are not suitable for a long time electrophysiology experiment since thin AgCl layers can easily run out and they are difficult to recondition. The method reported here practically fits the need in perfusion experiment by maximizing the flexibility to replace electrodes and reducing electrode vibration at the same time.

Chapter 3: Micro-PPM System Enables Perfusion[11]

While the ability to perform perfusion within microfluidic PPM platforms is often noted as another important advantage of these systems, there has thus far been little progress in demonstrating ion channel measurements in the presence of time-varying chemical inputs. Indeed, despite significant overall advances in microfluidic PPM platforms, a practical system for dynamic ion channel studies remains elusive. Existing microfluidic systems rely on diffusive transport, either by directly depositing reagents into an open chamber in fluidic contact with the membrane, or through an interconnecting microchannel. For example, Suzuki et al. pipetted gramicidin into a reservoir connected to a channel positioned below the bilayer membrane, with diffusion leading to incorporation of gramicidin into the bilayers [69]. In an alternate approach, Hromada et al. studied the interaction between poly(ethylene glycol) (PEG) with alpha-hemolysin ion channels by pre-filling a channel with PEG solution before forming the membrane through an open well above the channel [76].

In the case of diffusive transport, the long time scales required to achieve the desired interactions between chemical inputs and membrane-bound channels precludes the implementation of high-frequency dynamic studies. More generally, diffusion does not: allow for precise time-varying control of reagent concentration at the ion channel sites, enable specific time courses of chemical inputs with both increasing and decreasing concentrations, or provide a means for modulating the

---

[11] First 5 sections of this chapter and part of chapter 2 has been published as "Micro Planar Phospholipid Membrane System Enabling Kinetics Studies of Ion Channels". *Annals of Biomedical Engineering*, 2011, **39**, 2242.

concentrations of multiple reagents. To our knowledge, reagent addition and removal using a pressure-driven perfusion channel in a microfluidic PPM system has not yet been reported. Thus the ability to rapidly perfuse chemicals to membrane-bound channels by pressure-driven convective transport would open the door to a wide range of ion channel studies which are not presently feasible using established technologies.

This chapter will focus on the demonstration of a rapid perfusion scheme compatible in any thermoplastic microfluidic chip to investigate the response of ceramide ion channels under the application of time-varying chemical concentrations. Firstly, a small peptide dimer ion channel gramicidin is used to prove the membrane formed in this microchip works well for ion channels. Then a bit more fundamental and hypothesis about ceramide channel is discussed. Finally perfusion tests on inhibitor La^{3+}, chelator EDTA and potent protein inhibitor $Bcl-x_L$ is discussed.

The microfluidic system employs novel design elements that serve to minimize pressure gradients across the bilayer membranes during perfusion, enabling rapid pumping of reagents to the ion channel sites without disrupting the fragile membranes. The microfluidic chip is found to support volumetric flow rates above 3 µL/min for continuous perfusion, and significantly higher flow rates up to 20 µL/min for rapid pulse injection of reagent plugs. The resulting system provides a convenient platform to manipulate chemical conditions in the presence of fragile bilayer membranes, broadening our toolbox for dynamic studies of ion channels.

3.1.1 Gramicidin Ion Channels

Gramicidin is widely used to confirm the existence and quality of PPM because its characteristic gating behavior cannot be confused with a non-specific conductance. It forms channels when two monomers (one in each monolayer) link together into a dimer. If the film is significantly thicker than a bilayer, channels are not formed. Thus it provides uncontestable proof of the formation of a PPM [90].

Gramicidin is a monovalent cation ion channel whose gating is almost not affected by voltage. The characteristic of gramicidin activities in bilayer is pS range conduntance fluctuations in time scale of seconds, as shown in Figure 23 [69]. This reflects the dynamic association and dissociation of monomer population in bilayers [91]. A conceptual diagram of gramicidin gating is shown in Figure 24.
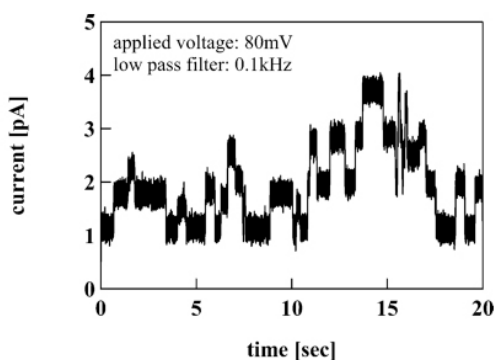
Figure 23 A typical current trace indicating dynamic nature of gramicidin ion channel. Picture reprint from [69].
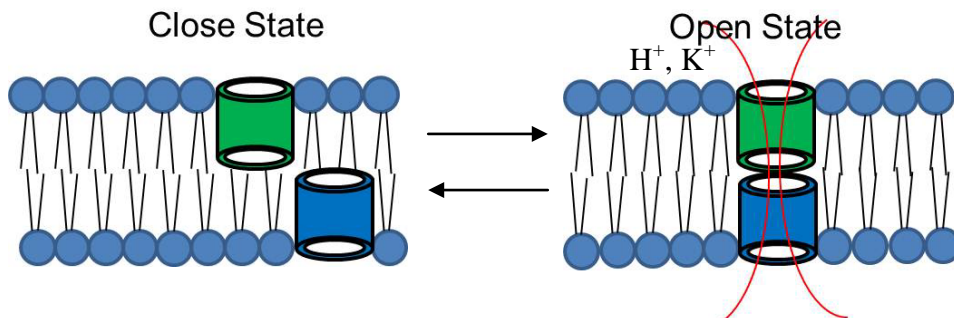
Figure 24 Conceptual schematics of gating of gramicidin ion channels

3.1.2 PPM Formation in Microchip
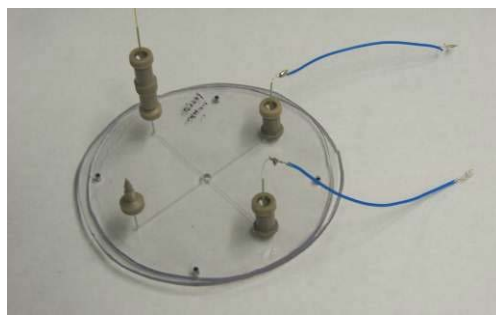
Figure 25 Picture of a PPM chip without perfusion channel

The experiment is done in a chip without perfusion channels (shown in Figure 25). The planar bilayer is formed with a "diffusion painting" method developed by Dr. Hromada [76]:

1. After the chip is freshly assembled or cleaned by isopropanol and deionized water (if reuse the chip after previous test), the chip is fully dried under nitrogen stream.

2. $0.3 \sim 0.6$ µL of DiPhyPC in hexane (2 mg/mL) is pipetted onto the PPM site through the open well. A stream of nitrogen is used to evaporate the solvent. This step is found necessary to facilitate the formation of PPM in step 4.

3. After pre-coating the aperture, a buffer solution of 2 M NaCl and 10 mM MES, pH adjusted to 7.5 is injected through the needle reservoir to filled up both upper and bottom channels.

4. Lab gas flare is used to burn a glass pipette into a glass brush with round tip size 250 ~ 350 µm. Some DiPhyPC solution in hexanol/hexadecane (v/v 10:1, 10mg/mL) is gathered by rolling the glass brush in solution vial. Then the lipid solution is transferred to the PPM site by wiping the glass brush across aperture. It is likely that we need to repeat the procedure until a small plug of lipid solution is left on the PPM aperture, which can be identified by an almost zero conductance in oscilloscope.

5. Wait for the hexanol to diffuse into aqueous solution and the bilayer to thin into bilayer. It can be judged by reading the square wave in oscilloscope if a triangle wave stimulus is applied.

This recipe of PPM formation is used throughout this study and some variations might be made according to different experiment purposes. For example, the lipid composition for ceramide channel experiment will be altered to 1,2-diphytanoyl-sn-glycero-3-phosphocholine (DiPhyPC, 5 mg/mL), asolection (soybean phospholipids, 5 mg/mL), and cholesterol (0.5mg/mL). To facilitate the formation of ceramide channels, C_{16}-ceramide is added to the painting lipid solution with 1:50 in molar fraction to total phospholipids. In this case ceramide channel will form spontaneously several minutes after the membrane thins to its bilayer state.

3.1.3 Confirm PPM Formed in Microchip by Gramicidin

Gramicidin is delivered to membrane by adding into open well. As shown in Figure, after membrane is formed, at time point A, 3 µL of 0.01 µg/mL gramicidin solution in 3DMSO (dimethyl sulfoxide) / 2DMF (dimethylformamide) was added, and characteristic assembly and disassembly of individual channels were observed. After several minutes, 1 µL of 1 µg/mL gramicidin in 3DMSO/2DMF was added at time point B. As expected, high density of channel formation events were observed, resulting in exponential conductance growth due to the formation of large numbers of gramicidin dimer channels. The conductance of a single gramicidin channel was 15~20 pS, consistent with previous report, indicating a well-functioning planer bilayer for ion channel studies.
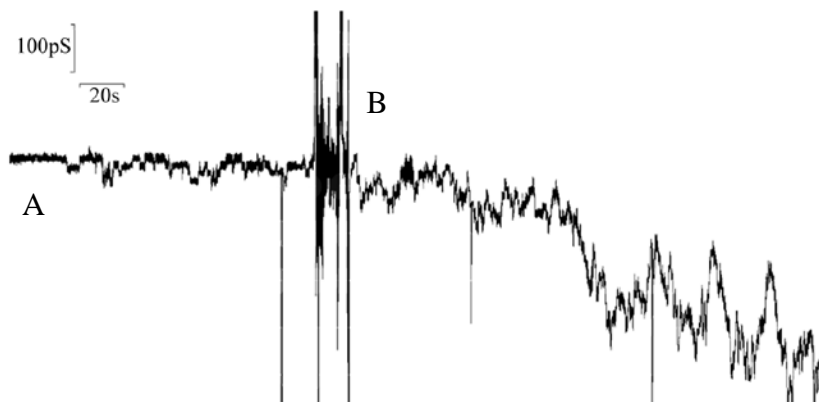
Figure 26 A current trace with gramicidin ion channel activities confirms the PPM formed in microchip is suitable for ion channel study.

3.2 Dynamic Ion Channel: Ceramide Channel

3.2.1 Dynamic Nature of Ceramide Channel

Ceramide channel model is proposed to explain the decision-making role of ceramide in apoptotic cell death process [6-11, 13]. Unlike any other ion channels that at least have one peptide, ceramide channel is completely comprised of ceramide lipid. This structural difference results in a number of interesting aspects of ceramide channel:

1. Compared to complex hierarchy structures of proteins, lipid molecules have simpler molecular structures thus are considered to have less potential structure variations to adopt different conformations. The fundamental energy driving force of ceramide channel gating might be different from protein ion channels.

2. The size of hydrophilic ion pathway in ceramide channel has to be very large so that big proteins (apoptosis induce factors, cytochrome c, etc) can be introduced to cytoplasm from mitochondria.

The proposed model successfully answers the above questions. The hydrogen bonds between oxygen atoms and nitrogen atoms in amide groups makes it possible to assemble a large population of ceramide molecules into a cluster. Thus the conformation change from a ceramide raft [12] into ceramide channel involves

---

[12] Ceramide molecules in phospholipid membrane tend to accumulate into small region, called rafts, with ceramide composition significantly higher than overall ceramide concentration. Imaging of such raft in both fluorescence and atomic force microscopy (AFM) can be referred to reference 92.
    Chiantia, S., et al., *Role of ceramide in membrane protein organization investigated by combined AFM and FCS.* Biochimica Et Biophysica Acta-Biomembranes, 2008. **1778**(5): p. 1356-1364.

dissociation of hydrogen bonds of ceramide to water molecule, reforming hydrogen bondis between ceramide molecules, rotation of rafts from horizontal to vertical direction, squeezing the fluidic membrane to make up room for the ion channel passage and an entropy change associate with change of organization degree. The size of such ion channel may be decided by a large number of factors besides those listed above. For example, it is hardly imaginable that two columns of ceramide can form an ion channels since the curvature of such channel will be not bearable for the hydrogen bonding. It is possible that the micro-scale "strain" associated with the curvature of the inter-column hydrogen bond also affect the channel size. Likewise, the strain inherently existing in the bilayer might affect the ion channel in same manner. In short, ceramide channel, if exists, should be very dynamic in its nature.

The biological activities of ceramide and ceramide channel can be studied *in vivo*, with relationship with other species revealed by control experiments. For example, spectrometer is used to measure the oxidation rate of reduced cytochrome c released from mitochondria in cell assay to determine the relationship between ceramide concentration/type/mutation and degree of permeability of mitochondria [8]. Studies *in vitro* should be able to answer more fundamental questions: what factors govern the dynamics of ceramide channel and how? What is the secret in the ceramide structure that enables channel formation? How can we answer this question quantitatively?

Numerous experiments have been done to answer these questions. It is shown that in order to increase permeability of membrane the ceramide channel prefer to become larger by recruiting more ceramide molecules from bilayer than forming new

50

ion channels (shown in Fig. 27) [6]. Energetically speaking, the energy barrier of nucleating a new channel might be much larger than the energy of recruiting. Thus it is possible that ceramide channel can become large enough to allow apoptotic proteins to pass through, just by recruiting enough ceramide molecules. Figure 28 shows a typical channel activities in a solvent free planar membrane [6]. Molecular dynamics studies is also done to seek proper molecular arrangements for ceramide channel (shown in Figure 29) [12]. It is found that an aqueous pore surrounded by C_{16}-ceramide columns in POPC bilayer (Figure 29.A) can self-aligned into hourglass-liked shape (Figure 29.B) ion channel. It might be partially because the hydrophobic interaction favor the ceramide hiding the hydrophobic tails from water molecules.
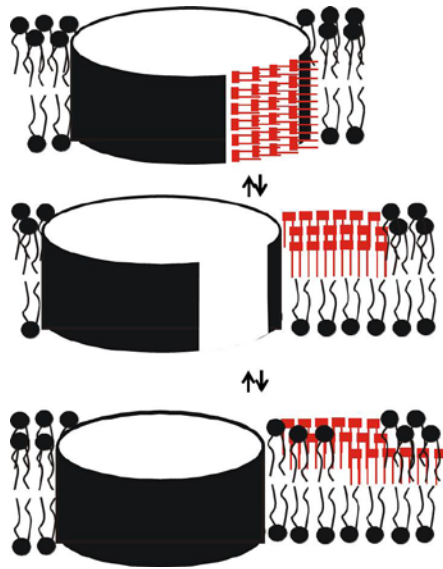
Figure 27 Conceptual schematics of enlargement and shrinkage of ceramide channels by population recruitments or releasing. [13]
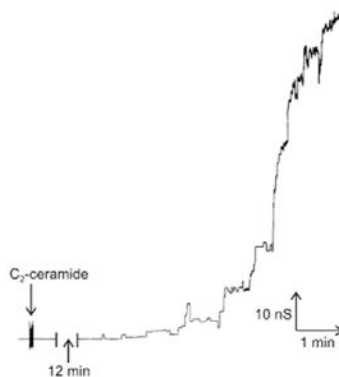
Figure 28 A typical ceramide channel current trace. [14]
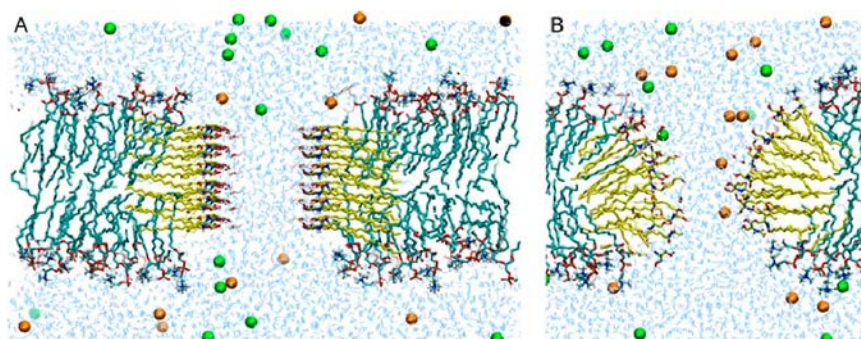
Figure 29 10ns molecular dynamics simulation indicates that columns of ceramide molecules bend to form a nanopore. Similatuion time 10 ns. [15].

3.2.2 Response of Ceramide Channel to Outside Stimulus

It is found that La^{3+} ion can eliminate ceramide channel conductance completely in solvent free planar membrane experiment [6]. Indeed, it becomes a signature behavior of ceramide channel and it is common practice to confirm the identity of ceramide channel by checking if conductance can be inhibited by La^{3+}. EDTA is known to chelate multivalent cations like La^{3+} and usually is used to revive ceramide channel after La^{3+} addition. However, it is not completely clear how La^{3+}

[14] Source of image: 6.   Siskind, L.J., et al., *Enlargement and contracture of C-2-ceramide channels.* Biophysical Journal, 2003. **85**(3): p. 1560-1575.
[15] Source of image: 12.   Anishkin, A., S. Sukharev, and M. Colombini, *Searching for the molecular arrangement of transmembrane ceramide channels.* Ibid.2006. **90**(7): p. 2414-2426.

ions dissemble ceramide channel and what happens after the channel collapse (see Chapter 4 for a preliminary study on this question). It is plausible that ceramide molecules diffuse away from the channel after disassembly, such that probability of spontaneous channel reformation would decrease with longer time intervals before EDTA perfusion. This question will be investigated further by dynamic experiments using this system in Chapter 4.

Interesting active ligands to ceramide channel include Bcl-2 family proteins, which are also important game players in apoptotic cell death. In fact, the role of BAX, BAD, Bcl-x_L etc and ceramides in apoptosis are in the center of debate about what is major factor in mitochondria apoptosis pathway. Anti-apoptotic Bcl-2 familty proteins are found to inhibit ceramide channels [9] while pro-apoptotic proteins are found to enhance them [10]. It is intriguing to explore the molecular mechanism of such interaction, and one approach is the use of point mutations at critical sites. Both the potency and the kinetics of reversal can be determined using our platform.

3.3 Response of Ceramide Channel to La^{3+}, EDTA

3.3.1 Addition of La^{3+} to Open Well

Before a bottom chamber perfusion experiment is down, the response of ceramide channel in membrane formed in our microdevices are studies by adding La^{3+} to open well.

Shown in Figure 30, ceramide channel is formed in membrane in a stepwise manner. Buffer contains 0.25M KCl, 0.25mM MgCl2, 20mM PIPES, pH 6.98. After

three shots of 2 µL 10mM La^{3+} to the open well, the conductance decreases correspondingly but didn't completely go to zero. It suggests that the existence of hexadecane in membrane might affect the inhibition ability of La^{3+}. Since it is well known that La^{3+} binds to bilayers [93-99], it is likely that La^{3+} indirectly induce ceramide channel collapse by introducing external stress to the membrane.
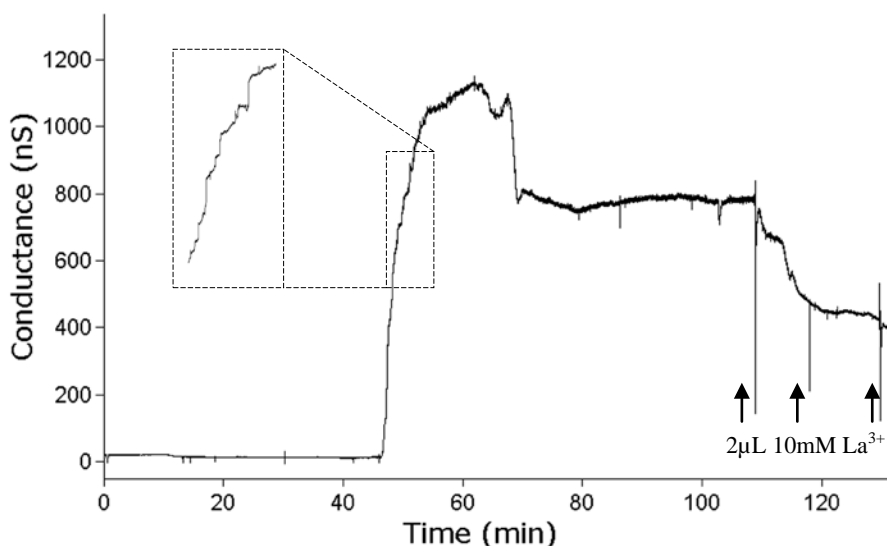
Figure 30 Response of ceramide channel in micro-PPM system to La^{3+} added into open well.

3.3.2 Perfusion EDTA to Enable Ceramide Channel

In experiment shown in Figure, buffer contains 1M KCl, 1mM MgCl$_2$, 20mM PIPES, pH 6.98. 50 µM LaCl$_3$ is perfused to bottom chamber channel as soon as thick lipid plug is formed on PVDC aperture. There is no ceramide channel formation in more than 15 minutes waiting time. Then 50 µM EDTA is injected through bottom perfusion channel at a flow rate 0.2 µL/min. Channel formation is observed upon delivery of a total perfusion volume of 2.8 µL, as expected given the 2.3 µL perfusion channel volume between the inlet and membrane aperture. The stepwise fluctuations

of the channel reveal the dynamic nature of the membrane/channel system as a result of the channel's continuous recruitment or loss of free ceramide molecules from the membrane. In this test, the total perfusion time is 14 minutes, nearly matching the time needed for EDTA to be perfused to the membrane site.
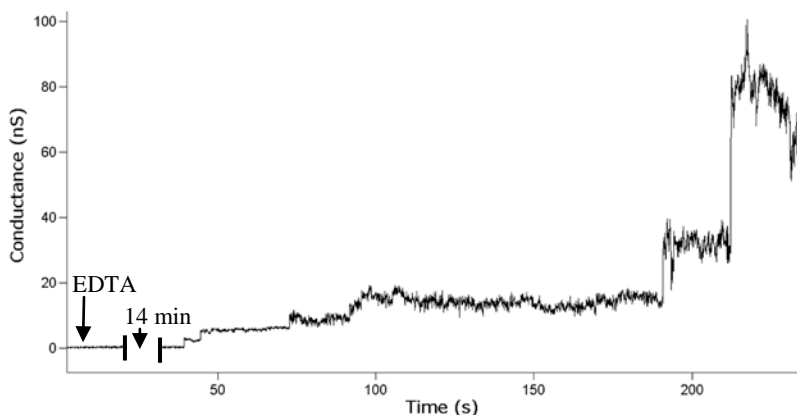
Figure 31 Ceramide channel forms when EDTA is perfused in bottom channel to remove and chelate inhibitor La^{3+}.

3.3.3 Repeated Perfusion of La^{3+} and EDTA

To provide stronger evidence that the reviving effect of EDTA chelating La^{3+} to revive ceramide channel shown in 3.3.2 is not a coincidence, a double inhibition-reviving is demonstrated.

In an experiment shown in Figure 32, all the buffer conditions are same as in 3.3.2. PPM are formed in microdevices and the current trace is shown starting from the formation of ceramide channel. La^{3+} and EDTA perfusion are alternately perfused to the membrane, using a flow rate of 20 µL/min to enable rapid transitions between the chemical boundary conditions. In the initial membrane, a ceramide channel formed with a stable conductance of ~320 nS. Perfusion of 50 µM La^{3+} in base buffer at 20 µL/min partially disassembled the ceramide channel, reducing the conductance

55

to ~20 nS. As EDTA (50 µM in base buffer) displaced La^{3+} within the perfusion channel, residual La^{3+} in the PPM was chelated and the channel conductance returned to ~300 nS. Due to the high perfusion flow rate used in these tests, both La^{3+} and EDTA were delivered to the ion channels within 10 s of initiating perfusion, and changes to the channel conductance were observed within 1 min. The accumulative effect of multiple reagents with controlled time interval can be easily probed in this method. All together, the perfusion capability demonstrated here would enable researchers to conceive new experiments that are not realistic in macro device, deepening the mechanistic understanding of ion channels.
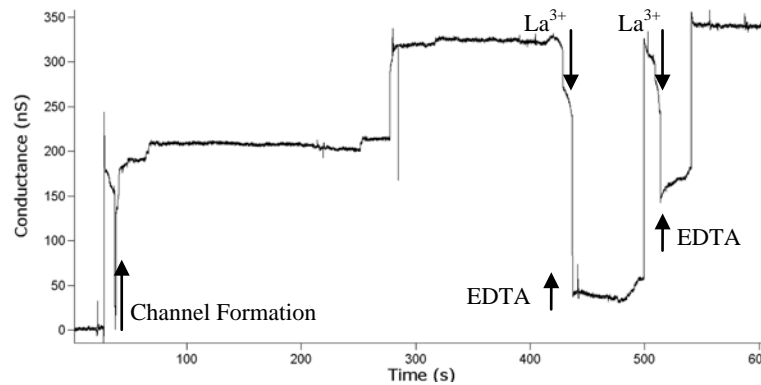
Figure 32 Alternative perfusion of La^{3+} and EDTA. It is a solid demonstration of perfusion capability of micro-PPM device.

3.4 Response of Ceramide Channel to Bcl-x_L Mutant Protein

This part experiment is done by Dr. Bing Sun in Dr. Colombini's lab in Dept. of Biology, University of Maryland using micro-PPM devices presented in this work. I include this part of work in my dissertation to demonstrate the usage of devices to study the dynamic response of ion channel to more complex samples such as proteins.

The description below may only contain part of information to achieve the performance in presented results.

3.4.1 Bcl-x$_L$ Protein Brief Introduction

Bcl-x$_L$, a potent apoptosis inhibitor, is found both in the cytosol and attached to mitochondrial membranes in healthy cells [100, 101]. Overexpression of Bcl-x$_L$ in the B-lymphocyte cell line WEHI231 protected against ceramide-induced apoptosis without altering the cellular level of ceramide [102]. By directly introducing Bcl-x$_L$ to lipid membrane, we previously reported that full length BcL-x$_L$ can disassemble C$_{16}$ ceramide channels formed in planar phospholipids membranes, strongly suggesting a direct interaction between Bcl-x$_L$ and the ceramide channel [9]. It is intriguing to explore the molecular mechanism of such interaction, and one approach is the use of point mutations at critical sites. Both the potency and the kinetics of reversal can be determined using our platform.

3.4.2 Perfusion Bcl-x$_L$ to Ceramide Channel

Here we present an example in which the reversible interactive between the Y101K mutant of Bcl-x$_L$ and ceramide channel is demonstrated. Bcl-x$_L$ Y101K mutants were prepared following procedures in [103] and [104].Y101K is mutant of wild type Bcl-x$_L$ with a mutation of amino acid 101 from tyrosine to lysine, which blocks the ability of Bcl-x$_L$ to heterodimerize with Bax. However, it retains the ability to prevent membrane permeabilization but with lower activity [105]. In this study, C$_{16}$-ceramide channels formed on a phospholipid membrane in the

57

microfluidic chip were disassembled by Y101K, with conductance of the single channel knocked down almost to baseline in multiple steps. When Y101K-containing solution was displaced by continuous perfusion with base salt buffer, the ceramide channel began to reassemble in as a series of stepwise conductance increments (Figure 7). The ability to observe the reversal in the minute time scale indicates a direct but not strong interaction between Y101K and ceramide channel.
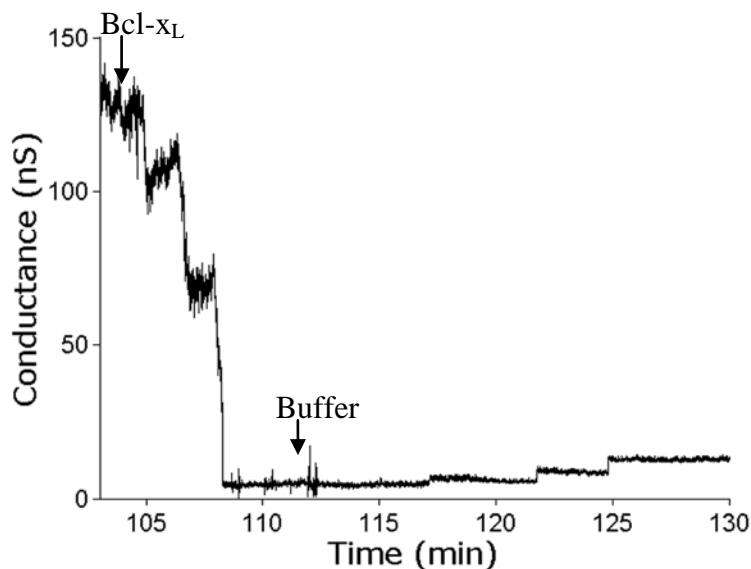
Figure 33 The response of ceramide channel to perfused Bcl-x$_L$ which then replaced by buffer.

3.5 Perfusion Capability

3.5.1 Membrane Responses to Perfusion

Essentially, the principles of PPM perfusion microfluidic system presented in this chapter are same as some other microfluidic devices. It is the careful design that enables the device to do better job in perfusion. Besides the geometry optimization discussed in section 2.1.3 which works to minimize the backpressure when flow is

perfused in bottom chamber, it is also important to note there is another factor helping

stabilize the PPM.

Figure 34 shows the capacitance of planar phospholipid membrane change

over different flow rate. The flow rate is tuned from 0 to 3.2 µL/min. It is found that

when flow rate is lower than 3µL/min, the membrane stays same with some small

changes probably due to fluctuation of bilayer boundary. When flow rate reaches 3.2

µL/min, the capacitance increases dramatically almost 4 folds while the outward

migration of boundary is observed under stereo microscope (pictures not shown).

Remarkably, the capacitance will return to original state when perfusion flow is

stopped. It suggests that the presence of annulus actually helps stabilizing the

membrane at low flow rates.

As revealed in the membrane capacitance measurements shown in Figure 35,

disturbance of the membrane was negligible for flow rates up to 2.5 µL/min, while

direct optical observation of the membrane revealed that the bilayer diameter

remained unchanged over this range of perfusion flows. However, for flow rates

above this level, the boundary of the bilayer was observed to expand toward the edge

of the aperture together with a corresponding increase in membrane capacitance. This

can be interpreted as a combination of slight membrane bulging and consequential

annulus thinning, when lipids and solvent in the annulus was continuously pulled out

of annulus and taken up by the bilayer. Indeed, halting the perfusion resulted in a

rapid return to the initial capacitance level as lipid within the membrane was allowed

to return to the annulus reservoir. However, as pumping at flow rates at or above 3.5

µL/min continued over long time periods, annulus could no longer support the bilayer

59

bulging which finally became irreversible and led to membrane rupture. The pressure

calculated from the burst capacitance 280 pF, is found to be 1420 Pa, consistent with

the pressure directly calculated from channel geometry and the flow rate. For shorter

perfusion cycles, however, the membrane was found to remain stable at significantly

higher flow rates. The highest flow rate employed in this work was 20 µL/min.
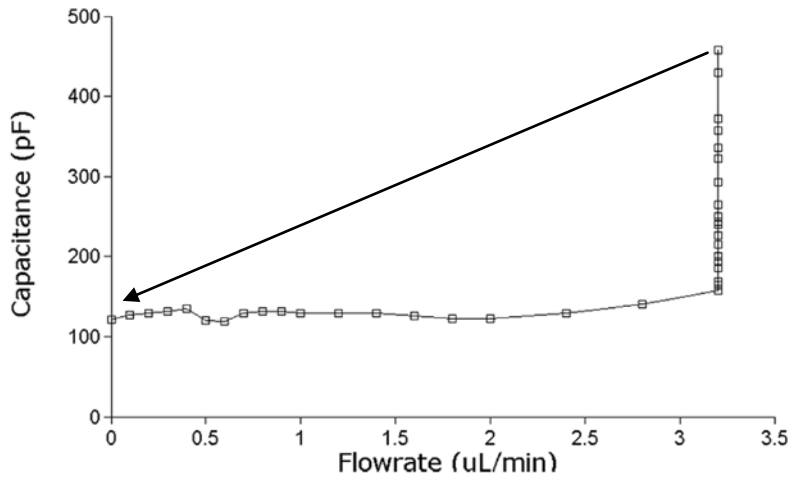
Figure 34 Capacitance change of bilayer when flow rate is adjusted. The error indicates the membrane returns to its initial state if the flow is stopped before rupturing the membrane.
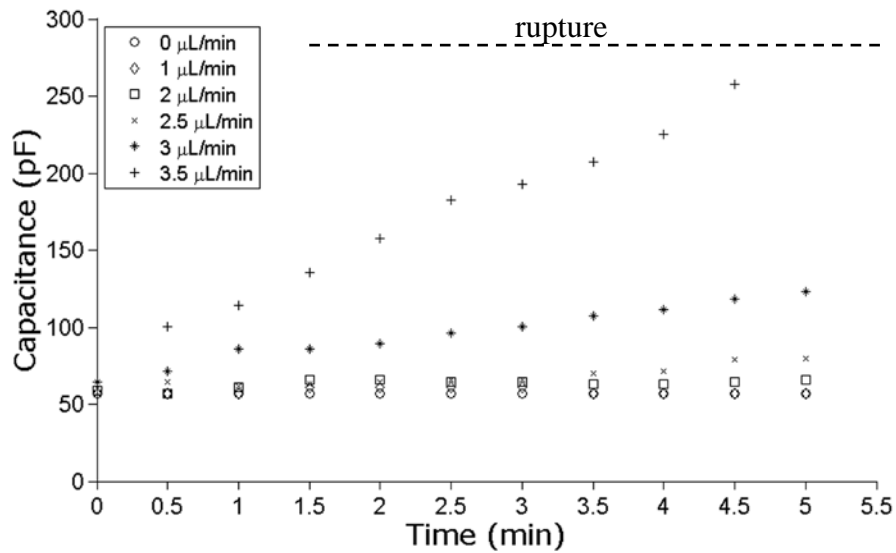
Figure 35 Capacitance change over time at different perfusion conditions.

3.5.2 Kinetics Resolution

Since the transport in this perfusion process involves both convection and diffusion, the sharp interface initially between present bathing solution and perfusion solution is blurred downstream. Thus the ion channel may experience a ramping concentration profile and it is important to know whether the observed dynamic response of ion channels to perfused reagent is true kinetics or limited by ramping concentration. If the kinetics time constant is much smaller than ramping time scale, e.g. the reaction of ion channels to solutes is much faster than change of concentration, then the change of ion channel current trace is just a reflection of concentration ramping, losing the kinetic insights we are looking for. If the ramping happens much more rapid than kinetics, then the concentration change can be considered as a step function, and the current trace activities can reflect the kinetics between ion channel and solute at target concentration. To ensure the ion channel – ligand interaction is properly resolve in our device, the latter case is preferred.
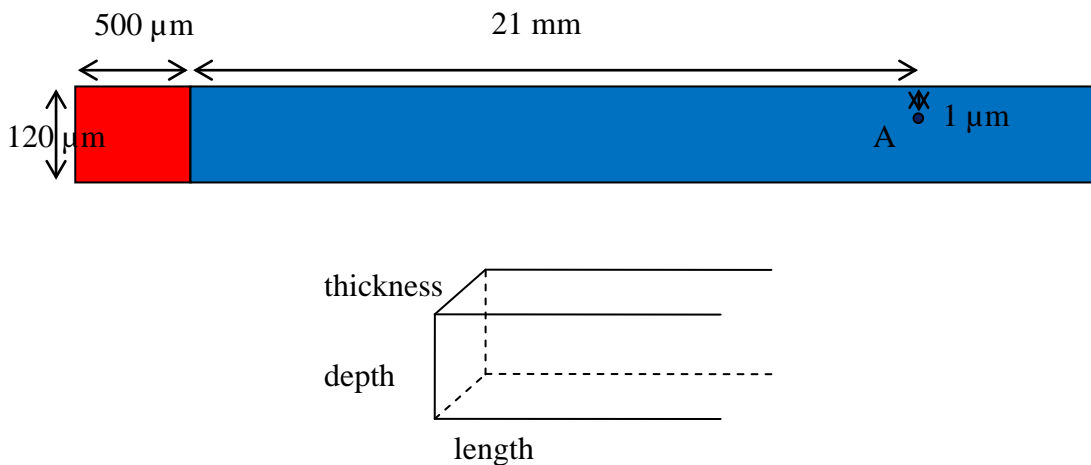
Figure 36 The simplified 2-D model only depicts the microchannel in depth and length. The thickness is taken account when volumetric flow rate is converted to linear velocity.

To find out the kinetics resolution limit of our device, i.e. the fastest kinetics it can resolve, following simple model is discussed (Figure 36): a segment of microchannel (120 µm deep, longer than 21 mm) is filled up with buffer with concentration C=0 for species 1 (blue in Figure 36, and it has direct contact with another segment (120 µm deep, 500 µm long) filled up with buffer with concentration C=1 for species 1. These two channels are 460 µm in thickness. Complicate mixer geometry is replaced with straight channels to simply the analysis. At time t=0, the velocity of the whole domain is zero. Let left end boundary have volumetric flow rate as a step function at time t=0 to Q and following questions are asked:

1. When (t_1) will the PPM local concentration rise to 5% of the target C?

2. When (t_2) will the PPM local concentration rise to 95% of the target C?

3. What is the rampting time Δt= t_2- t_1?

Reynolds number for this problem can be calculated as:

$$\text{Re} = \frac{vL}{v} \approx \frac{0.75e - 3m/s * 2e - 4m}{1e - 6m^2/s} = 0.15$$, indicating it is laminar flow.

With no-slip wall boundary condition (the velocity of fluids just next to fixed wall is assumed to zero), the velocity profile across the channel depth is parabola:

$$u(y) = u_o(1 - \frac{(y - \frac{d}{2})^2}{(\frac{d}{2})^2})$$, where $u_0 = \frac{3}{2}u = \frac{3Q'}{2d}$ is maximum x-direction velocity, u is

mean velocity and Q' is the 2-D flow rate considering the thickness of the channel, d is the depth of the channel.

Because perfusion is performed by pressure-driven flow, it is necessary to consider the degree to which lateral diffusion of perfused molecules to the PPM site located at the channel surface occurs. To understand if lateral diffusion is sufficiently rapid to produce a nearly uniform distribution of molecules across the channel width in the presence of a parabolic flow field resulting from convective Poiseuille flow, the Taylor condition [106] is calculated $: \frac{d^2}{4\pi^2 D} \square \frac{l}{u}$, or $\frac{D}{u} \square \frac{d^2}{4\pi^2 l}$, D is the diffusion coefficient, l is the channel length between the perfusion inlet and PPM site, and u is the average fluid velocity. For the chip described here, $d = 120$ µm, $l = 21$ mm, D/u $\gg 1.74$ x 10^{-8} m. Using diffusion coefficients of 6.2×10^{-10} m^2/s for La^{3+} and 8.5×10^{-11} m^2/s for the Bcl-x$_L$ mutant, the maximum average flow velocities that will yield nearly uniform reagent distributions across the channel width are found to be 35.7 mm/s and 4.89 mm/s for La^{3+} and Bcl-x$_L$ mutant, respectively. For the channel geometry used in the PPM chip, these velocities correspond to volumetric flow rates around 118 µL/min for La^{3+} and 16 µL/min for Bcl-x$_L$ mutant. By Taylor dispersion theory, the distribution of solutes for flow rates well below these limits can be reduced to a one-dimensional longitudinal diffusion problem, with a solute front moving at half the maximum velocity ($u_o = 3u/2$) of the convective flow, and a diffusive profile relative to this moving boundary defined by an effective diffusion coefficient of

$$D_{eff} = D + \frac{d^2 u^2}{192 D}$$

In this case, the relative concentration of solute at the PPM a distant L from the injection point is given by

$$\frac{C}{C_o} = \frac{1}{2} erfc(\frac{L - u_0 t/2}{2\sqrt{D_{eff}t}})$$

Solving t_1 and t_2 for C/C_0 = 0.05 and 0.95, the switching time of concentration at PPM site from 5% to 95% of time can be determined by $\Delta t = t_2 - t_1$. With typical perfusion flow rate 2.5 µL/min used in this study, the switching time is 36.5 seconds and 13.2 seconds for Bcl-x_L and La^{3+} respectively. Therefore, kinetics with time constant slower than this time scale can be readily resolved in our device, with PPM local solute concentration treated as sharp step function. The kinetics resolution power can be further improved to by using larger flow rate. When 20 µL/min flow rate is used, the switching time Δt can be reduced to less than 5 seconds for La^{3+} ion and 15 seconds.

Extremely rapid buffer exchange by pulsed flow injection demonstrated here will further push the kinetics resolution down to order of 10 s. By integrating multiple perfusion inlets, the accumulative effect of addition or removal of multiple reagents with controlled time interval can be easily probed in this method, thus experiments that are not realistic in macro device can be performed in this device. For example, ion channel behavior can be studied by changing exposure time of ion channels to ligands, time interval between ligand exposure and sequence of ligand exposure. It is also useful to perform multiple kinetic tests on same ion channels by restoring initial conditions with base buffer perfused between different ligands, to avoid possible artifacts that affect ion channel reproducibility. It is believed to be very important to obtain meaningful quantitative information for ceramide channel whose constitution may vary even when conditions are strictly controlled.

3.6 Summary

As kinetic studies of ion channels receive increased attention from both biologists and pharmaceutical industry, there is urgent need for a new benchtop platform suitable for the dynamic study of channels. In this chapter, a new microfluidic system with controllable perfusion capability is described. The system allows for easy formation of the PPM by the painting method. The improved fabrication methods significantly reduce hydraulic resistance of the perfusion channel and thus back pressure imposed by flow, allowing a continuous perfusion up to 3 µL/min or a pulsed perfusion up to 20 µL/min. Using this platform, we studied the interaction between the ceramide channel and its inhibitor La^{3+} and reversed the inhibition using the chelator EDTA. Both the kinetics and the subconductance levels can be resolved showing the feasibility of performing a detailed analysis, which might lead to a further understanding of the ceramide channel formation mechanism. Similarly, the kinetic features of the ceramide channel and its selective ligands can be investigated as demonstrated by experiments showing a reversible ceramide channel inhibition by the Y101K mutant of Bcl-x_L. Although we only tested this platform with a ceramide channel, it should work with other types of ion channels. This technology represents a step towards a robust, user-friendly and cost effective micro-PPM system enabling effective kinetic studies of ion channel interactions.

Chapter 4: Dynamics of Ceramide Channel Detected Using Micro-PPM System[16]

Chapter 3 explains the working principle of the perfusion scheme in a PPM microchip and demonstrates that we can observe ceramide channel conductance changes in response to dynamic perfusion of different analyst to PPM site. This chapter shows that this system can be used to study ceramide channel dynamics quantitatively.

Ceramide, a proapoptotic sphingolipid, has been shown to form channels, in mitochondrial outer membranes, large enough to translocate proteins. In phospholipid membranes, electrophysiological studies and electron microscopic visualization both report that these channels form in a range of sizes with a modal value of 10 nm in diameter. A hydrogen bonded barrel-like structure consisting of hundreds of ceramide molecules has been proposed for the structure of the channel and this is supported by electrophysiological studies and molecular dynamic simulations. To our knowledge, the mechanical strength and deformability of such a large diameter but extremely thin cylindrical structure has never been reported. Here we present evidence for a reversible mechanical distortion of the cylinder following the addition of La^{3+}. A microfluidic system was used to repeatedly lower and then restore the conductance by alternatively perfusing La^{3+} and EDTA. Although aspects of the kinetics of conductance drop and recovery are consistent with a disassembly/diffusion/reassembly model, others are inconsistent with the expected

---

[16] This work has been composed to a manuscript "Dynamics of Ceramide Channels Detected Using a Microfluidic System" and accepted by PLoS One.

time scale of lateral diffusion of disassembled channel fragments in the membrane. The presence of a residual conductance following La3+ treatment and the relationship between the residual conductance and the initial conductance were both indicative of a distortion/recovery process in analogy with a pressure-induced distortion of a flexible cylinder.

4.1 Introduction

The self-assembly of molecules and macromolecules into higher-order structures is commonplace within cells and critical to life as we know it. Common examples are the mitochondrial respiratory complexes, microtubules and microfilaments, ribosomes and membranes. Whereas it is normal and accepted that proteins and RNA form well-organized high-order structures, lipids are relegated to the formation of lipid or solid phases. It is generally assumed that lipids cannot form highly ordered structures save for crystalline or paracrystalline structures. An exception to this has emerged. Ceramide, a sphingolipid, has been shown to form highly-organized channels in phospholipid membranes [6-11, 13, 15, 107, 108]. Although the dependence of ceramide channel stability on membrane lipid composition is still under investigation, the propensity for the formation of these channels does vary from one natural membrane to another. The erythrocyte plasma membrane is refractory to ceramide channel formation whereas the mitochondrial outer membrane is very sensitive to the formation of these channels [11]. Model-building [15], molecular dynamic simulations [12], and transmission electron microscope (TEM) visualization [108] indicate that these channels are formed by columns of ceramide monomers that span the membrane and assemble to form a

67

barrel-like structure (Fig. 3). In these models, the amide linkage in ceramide forms the hydrogen bonds that connect ceramide monomers into columns, in much the same way that the hydrogen bonds of the amide linkages stabilize the secondary structure of proteins. Adjacent columns are proposed to be connected by the hydrogen bonding of the twin hydroxyls on each ceramide molecule with corresponding residues on adjacent columns. The hydroxyl-hydrogen-bonded network would form the inner lining of the channel, favoring interactions with water and giving the structure mechanical strength. As shown in Fig 3b, the channel is proposed to interface with the phospholipid bilayer by curvature of both the channel and phospholipid bilayer structure. Thus this higher-order structure requires the particular environment of the phospholipid membrane and the interface with the water phase.

The dynamics of a ceramide channel, a structure composed of hundreds of individual molecules, is largely unexplored because of the difficulty of making structural measurements. The ceramide channels are in dynamic equilibrium with either ceramide monomers or non-conducting ceramide complexes in the membrane. Experimental observations indicate that only about 1% of the ceramide in the membrane is participating in the channel structure. This makes the use of spectroscopic methods to explore the ceramide structure, very difficult. This dynamic equilibrium can be shifted toward channel disassembly by an anti-apoptotic protein called Bcl-x_L [9] or by La^{3+} [6]. The latter may be acting by applying lateral pressure to the channel by binding to negatively-charged phospholipids in the membrane. This is how La^{3+} acts to inhibit the function of stretch-sensitive channels [109]. Addition of La^{3+} to ceramide channels formed in planar phospholipid membranes results in

disassembly of the channels. This disassembly has features that clearly point to a highly-structured cylindrical barrel-stave channel. The large conductance drops are quantized. They have a strong preference for being multiples of a fundamental unit, 4.0 nS, in 1.0 M KCl [107]. Theoretical calculations show that 4.0 nS is consistent with the loss of a pair of ceramide columns in the working model of the channel. Thus multiples of 4.0 nS indicate disassembly by the preferential loss of an even number of ceramide columns [107]. This is consistent with columns arranged in an anti-parallel fashion, each pair stabilized to some extent by dipole-dipole interactions. The dipoles would come from the alignment of the amide linkages in the columns, similar to the origin of the dipole in the alpha helix. The pattern of large conductance decrements could only be modeled by assuming a rigid cylindrical structure. If the structure was assumed to be flaccid or non-cylindrical the calculations did not produce histograms of conductance changes comparable to the experimental data. La^{3+}-induced disassembly occurred at sub-micromolar levels of free La^{3+} and resulted in total loss of conductance.

These previous studies of the structure and dynamics of ceramide channels were performed on planar phospholipid membranes made from monolayers without the use of a liquid hydrocarbon solvent. Current studies use phospholipid membranes made in such a way as to produce a planar membrane attached to the plastic partition by a hexadecane-containing annulus. This annulus is both a source and sink of phospholipids. In this system, La^{3+} additions result in a very different outcome. The ceramide channel remains but its conducting properties change drastically. This is a different type of stress-induced dynamics.

Whereas transient, unstable "lipidic pores" have been described in various contexts [110, 111], ceramide forms large stable channels in phospholipid membranes. This property is, to date, unique for cellular lipids. Ceramide channels form pores that vary greatly in size with a modal value of 10 nm in diameter. The channels are believed to be in dynamic equilibrium with ceramide monomers and ceramide aggregates in the membrane. The channel size observed is presumably the result of this equilibrium and different local conditions result in different sizes. The mechanical stability of a cylindrical structure with such a small aspect ratio (height/diameter) composed of small units that are non-covalently bound and indeed under dynamic equilibrium with non-channel structures, is an unexplored area. Beyond assembly and disassembly, the dynamics of such structures is totally unknown. Here we provide an initial glimpse into what we conclude to be the distortion of the cylindrical channel and the accompanying recoil/relaxation as the original structure is restored.

4.2 Results

All the experimental performed on microchip are same as Chapter 3.

The membrane stretching experiments were performed with a Lucite chamber consisting of two hemichambers separated by a PVDC partition containing a circular hole 0.43 mm in diameter. Each hemichamber contained 2.5 mL of the aqueous buffer specified above. A membrane was pained across the hole using a the same lipid solution as above except that it did not contain either hexanol or ceramide. The hexanol is washed away in the microfluidic system whereas this chamber was not perfused. Ceramide was not used because the intent was to assess the influence of

70

La^{3+} on the properties of the phospholipid/cholesterol membrane. Transmembrane pressure was applied by addition of aqueous solution to one side of the membrane resulting in a hydrostatic pressure gradient. Changes in membrane area were calculated from capacitance measurements obtained by using a triangular voltage wave (±12 mV, 29.4 Hz) and taking the unit membrane capacitance as 0.8 µF/cm^2 [112]. After each change in pressure the membrane was allowed to relax to its new condition prior to collecting capacitance measurements. Measurements with and without 50µM La^{3+} were made on the same membrane. La^{3+} was either added as LaCl$_3$ (12.5 µL of 10mM LaCl$_3$) or as a La^{3+} buffer. When the La^{3+} buffer was used, the solution was supplemented with 6.00 mM ethylenediamine-N,N'-diacetic acid (EDDA) prior to membrane formation. At the point of La^{3+} addition, 25µL of 213 mM LaCl$_3$ and 20µL of 400 mM KOH were added (the KOH consumed the protons released by La^{3+} binding to EDDA maintaining pH 6.9). The design of the La^{3+} buffer and binding constants were published previously [6]. The La^{3+} buffer compensated for loss of La^{3+} from binding to surfaces and was expected to be a better mimic of the perfusion system. However, essentially the same results were obtained by either method.

4.2.1 La^{3+} Addition Results In a Reduction of Membrane Conductance

The perfusion of the solution on the lower side of the planar membrane with the same solution but supplemented with 50 µM LaCl$_3$ resulted in a drop in conductance as previously described [6] but with a critical difference. The conductance drop only resulted in a partial loss of conductance in most experiments (e.g. Figure 37). Previous results with membranes made from monolayers invariably resulted in a total

71

loss of conductance. The partial conductance drop observed with the microfluidic system could be due to partial disassembly of the channel or channels resulting from a La^{3+}-induced shift in the dynamic equilibrium between ceramide in channels and ceramide monomers or non-conducting structures in the membrane. The increase in lateral pressure induced by this lanthanide [109] could be responsible for altering the dynamic equilibrium by favoring structures with a reduced occupied membrane area. The 2-dimensional pressure in the membrane times the area occupied by a ceramide structure is part of the energy of the structure. Reducing the area by disassembling into structures without an aqueous pore would reduce the energy and thus favor the loss of conductance. The virtual insolubility of ceramide in the aqueous phase excludes the possibility that ceramide leaves the membrane thus ceramide molecules leaving the channel must remain in the membrane in other forms. If this interpretation were correct one might expect that increasing levels of La^{3+} would shift the dynamic equilibrium further toward channel disassembly. However, the use of La^{3+} levels that were 10 times greater did not result in detectably different extents of conductance drop, indicating that some sort of maximal effect had been achieved. The removal of the La^{3+} by perfusion with EDTA generally restored the original conductance level, somewhat surprising for an assembly/disassembly mechanism. As is evident from Figure 37, this change in conductance can be repeated many times by sequential perfusion with EDTA and La^{3+}. The results appear consistent with a two-state structural model.
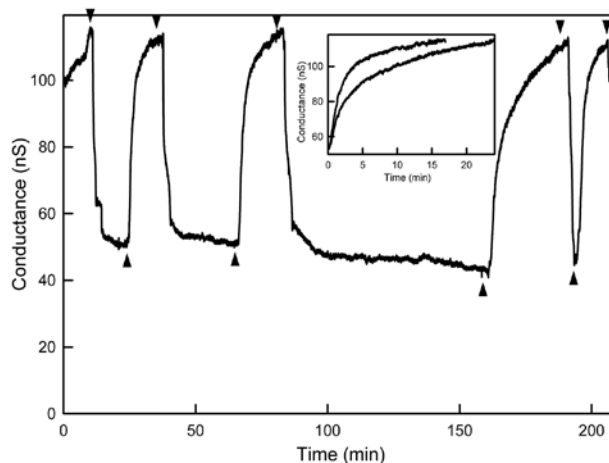
Figure 37 Cyclic changes in ceramide channel conductance following alternative perfusions with La³⁺ and EDTA-containing medium. Downward arrowheads indicate the start of perfusion with La³⁺ medium whereas upward arrowheads indicate the start of perfusion with EDTA-containing medium. The inset shows the overlap of conductance increases following EDTA treatment for short (upper curve) and long (lower curve) pretreatments with La³⁺.

4.2.2 Evidence for a Ceramide Channel Disassembly and Reassembly Model

In contrast to the traditional planar membrane system where turbulent mixing is used to change solute concentrations in large aqueous compartments, with the laminar flow dominated flow in the microchip, changes in the local concentration at the membrane as a function of time can be precisely predicted by using a mathematic model [113]. Using a flow rate of 10 µL/min, the concentration of perfused substance next to the membrane reaches 95% of the final value in 3.6 s. Thus, compared to the rates of change in conductance observed in Figure 3, the concentration change of La³⁺ and EDTA can be taken as step functions. Thus the time dependent measurements of channel conductance effectively reflect the dynamics of the channel.
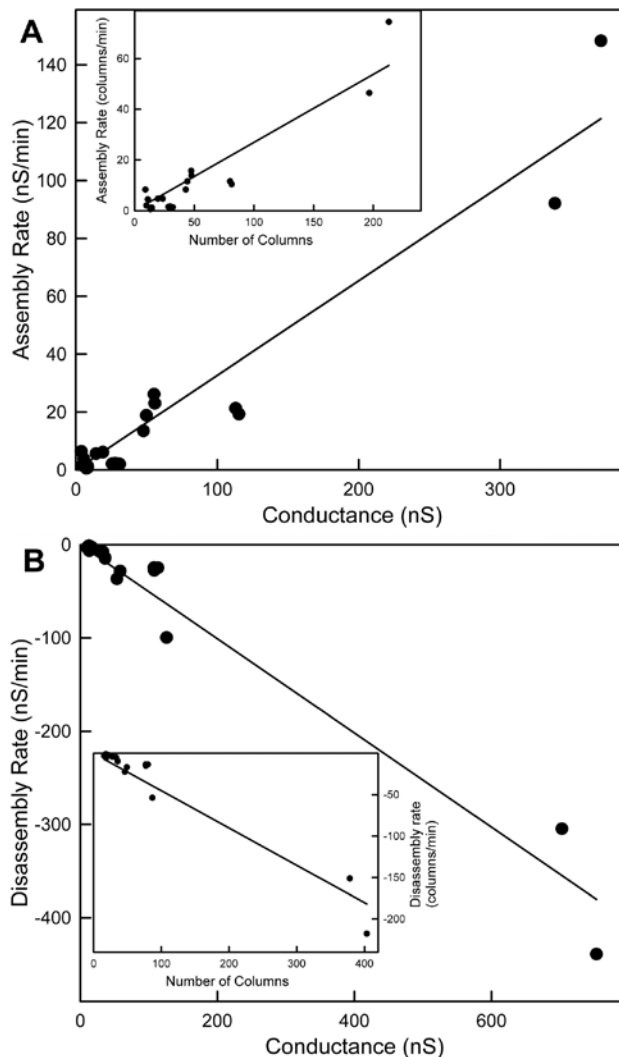
Figure 38 Correlations between the rates of conductance increases and decreases with channel size. The initial rate of conductance decrease (nS/min) is proportional to the starting conductance (nS) (A) and the calculated initial rate of column loss (columns/min) is proportional to the starting circumference of columns (inset in (A)). The initial rate of conductance increase (nS/min) is proportional to the conductance (nS) just before EDTA perfusion (B), and the calculated initial rate of column reassembly (columns/min) is proportional to the circumference of columns before EDTA perfusion (inset in (B)).

The initial rates of conductance change were determined by using a linear fit to the initial change in conductance. Both the rates of conductance decrease following exposure to La^{3+} and increase with EDTA perfusion correlated linearly with the conductance before delivery of either La^{3+} or EDTA (Figure 38). This is consistent with a greater conductance translating into a greater reaction surface.

Whether considering one or many channels, a greater conductance would be consistent with more sites at which ceramide columns could leave the channel or insert into the channel. Indeed, considering the formation of a single channel, from the initial conductance the circumference of a cylindrical channel was calculated and the rate of conductance change correlated linearly with the calculated circumference. Thus the results would be consistent with the conclusion that La^{3+} favors channel disassembly and EDTA favors channel growth (by removing La^{3+}).

By varying the time interval between La^{3+} and EDTA perfusions one observes changes in the kinetics of conductance increase. If conductance increase represents channel growth, the changes in kinetics indicate a reduced rate of channel growth with time even though the final conductance achieved remained unchanged (Figure 37, inset). Previous findings showed that ceramide channel disassembly involved conductance drops consistent with the loss of multiple ceramide columns with preference for the loss of an even number of columns. Thus channel disassembly could result in the formation of structures that reassemble in a channel more easily than the typical ceramide assemblies that may normally exist in the membrane. With time such assemblies could break down or diffuse away resulting in slower rates of channel reassembly. This interpretation fits with the observation of a delay between EDTA perfusion and conductance increase (Figure 39) and this delay increasing with increasing time between La^{3+} treatment and EDTA treatment. The results from the four experiments were pooled and sorted into three bins (Figure 39, inset). By doing so a statistically significant difference was obtained between intervals shorter that 10 min and those longer than 30 min.
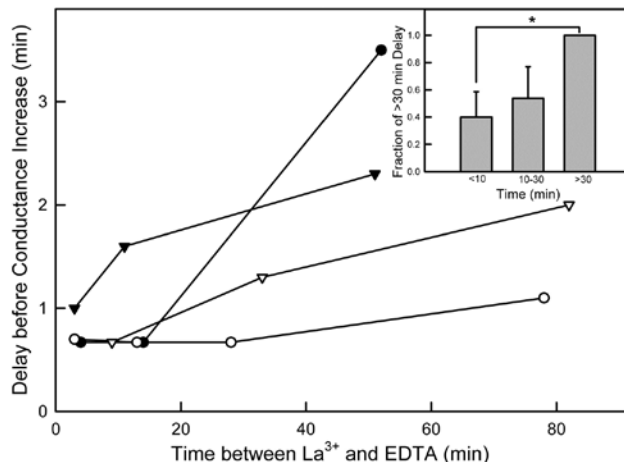
Figure 39 The delay between the delivery of EDTA and the initiation of conductance increase correlates with the time of exposure to La^{3+} prior to EDTA treatment. Each curve is from an independent experiment. Inset: For each experiment, the delay times between the start of EDTA perfusion and the start of conductance increase were grouped as follows: <10min, 10-30min, and >30min based on the length of time of LaCl$_3$ treatment and then normalized to the result of the ">30min" group. The averages ± SD of the relative delay times of the different experiments in each group is shown. The "*" indicates that the "<10min" group was significantly different from the ">30min" group at the 95% confidence level.

While qualitatively consistent with the channel assembly/disassembly hypothesis, the length of time over which the kinetics changed is far too long for a diffusion model. Any fragments that came off the channel would diffuse away rapidly and be unavailable for reassembly during the time at which the conductance increased. Considering the mole fraction of ceramide present in the membrane, there is vastly more ceramide available for channel growth from ceramide in the membrane than any ceramide from a previous putative disassembly event and therefore the changes in kinetics are not easily explained by a disassembly/reassembly model. Furthermore if the channel fragments were to have a special structure allowing preferential reassembly one might expect to measure a reduced conductance recovery after EDTA perfusion that became more pronounced with gap time between LaCl$_3$ treatment and EDTA delivery. In Figure 40, each curve represents multiple alternate

76

perfusions with $LaCl_3$ followed by EDTA. Although there seems to be a negative trend, there is no statistical correlation with gap time when results are grouped (Figure 40, inset).
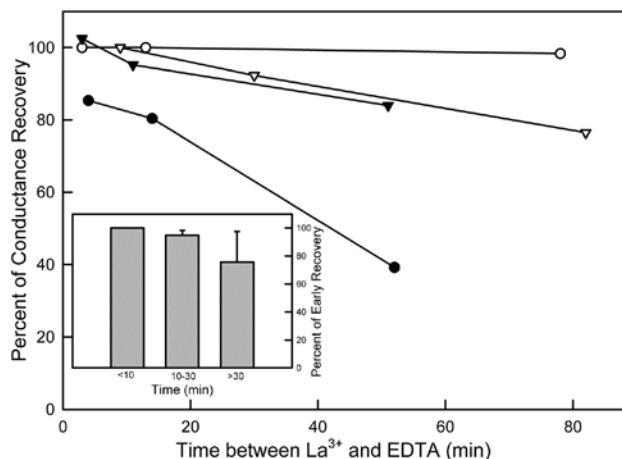
Figure 40 Lack of statistically significant correlation between the percentage of conductance recovery following EDTA treatment and the prior time of exposure to $LaCl_3$. Each curve is an independent experiment. The averages of the relative percentage of conductance recovery of different experiments in each group are shown in the inset. The results were grouped and normalized to the values of the "<10min" group. No statistically significant difference was observed.

The observation that is most inconsistent with the assembly/disassembly mechanism is the residual conductance after the La^{3+}-induced conductance drop. This and the other inconsistencies are best explained by a different dynamic mechanism.

4.2.3 Evidence for a Ceramide Channel Distortion Model

An alternative to the assembly/disassembly model is the possibility that a large cylindrical channel could be distorted by the addition of La^{3+}, resulting in a reduced cross-sectional area and thus a reduced conductance. La^{3+} removal would allow the channel to relax to its previous state. Lanthanides are known to inhibit the opening of stretch-sensitive channels by changing the transmembrane profile of the

77

lateral pressure [109, 114, 115] resulting in an increase in the lateral pressure in the hydrocarbon region by 45 mN/m. In a "free" membrane, one is able to expand or contract without outside constraints, and the integral of the membrane tension as a function of distance through the membrane should remain zero. However, the experiments described were performed on a membrane connected to a plastic partition by a torus of phospholipid/cholesterol and hydrocarbon. The partitioning of the lipids between the membrane and the hydrocarbon can be influenced by La^{3+}. We performed experiments to test this using the same lipid mixture and hexadecane solvent in the torus. The results are shown in Fig. 41. Note that, in the presence of 50µM La^{3+}, a higher transmembrane pressure was needed to increase the surface area of the membrane by introducing curvature. The effect was greater when La^{3+} was added to both sides of the membrane as compared to just one side. This result is consistent with a greater lateral pressure in the membrane keeping phospholipids from flowing in from the torus. As the transmembrane pressure was increased, the lateral pressure in the membrane was reduced until a critical value was reached that allowed phospholipids to flow from the torus into the membrane. The force introduced into the membrane by the transmembrane pressure is countered by two processes: the interlipid cohesion and the resistance to bending of the membrane. In the experimental procedure used, one cannot increase the membrane area without decreasing the radius of curvature. Thus at the same area change, the radius of curvature is the same regardless of treatment with La^{3+}. Thus, in the inset, the added transmembrane pressure needed to achieve the same area increase in the presence of La^{3+} is plotted as a function of the fractional area increase. For the one-sided La^{3+}

addition, for low changes in area, the added pressure needed is fairly constant, independent of area, indicating the portion of the applied forces needed to balance the greater lateral pressure in the membrane induced by La^{3+}. At larger changes in area, the required added transmembrane pressure increased, indicating that the force needed to bend the membrane is greater in the presence of La^{3+}. A similar result is seen in the case where La^{3+} was added to both sides. There the constant region is quite limited. Nevertheless, it is interesting that this added transmembrane pressure is roughly double for the two-sided La^{3+} addition as compared to the one-sided addition.
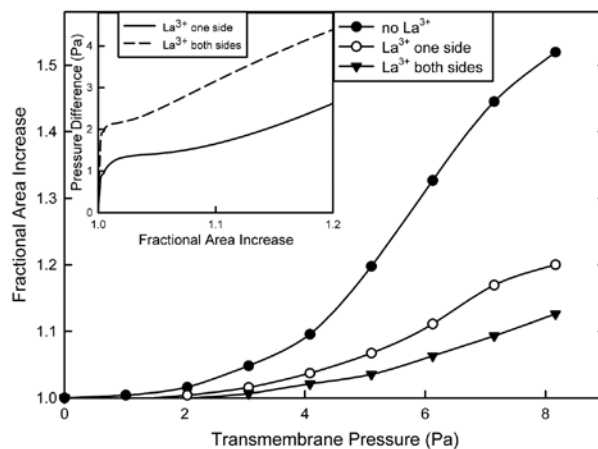
Figure 41 Lanthanum chloride addition increases the transmembrane pressure needed to increase the area of a planar phospholipid membrane. The data of the pressure/area curve was first collected in the absence of LaCl₃. Then 50 μM LaCl₃ was added to one side of the same membrane and the data was collected again. Finally 50 μM LaCl₃ was added also to the other side of the same membrane and the final data set was collected. For the experiments illustrated, the La³⁺ buffer was used. Pressure was applied by increasing the level of the solution on one side of the membrane. Inset: Empirical equations were fit to the data in each curve in the main figure. Using these expressions, the difference in pressure needed to achieve the same membrane area with and without LaCl₃, was calculated. As the subtraction involved the difference between two empirical equations, the full function was plotted in the inset. The results shown are typical of two independent experiments.

The increased lateral pressure induced by La^{3+} must favor a structure with a smaller cross-sectional area. The lateral pressure times the area change is the

negative energy change that would drive the change in structure. However this change would also result in a change in curvature of the channel wall and this is likely a positive change in energy. For any change to occur the former must be greater than the latter. Experiments show that the structural change occurs slowly and thus it is reasonable to assume that the lateral pressure of the liquid hydrocarbon tails acts uniformly on the channel wall and the tension in the wall counteracts the lateral pressure. Thus the tension in the wall should be uniform at all locations. However, the curvature of the wall cannot be the same at all sections of the wall. Assuming that any stress on the wall would be distributed throughout the structure drastically limits the possible structures. The simplest solution is for the cross-sectional shape of the channel to change from a circle to a biconcave structure. This produces two radii of curvature: one positive and the other negative (shown in Fig. 42). Circles 1 and 2 define the radii of curvature of the negatively and positively curved regions respectively. The ratio of the radii (r_1 and r_2) of the circles reflect the resistance to bending of the wall of the channel in the convex and concave direction (from inside the biconcave structure). α and β are the angles. d_1 and d_2 are the distances from the center of the drawing to the center of circles 1 and 2. The circumference of the biconcave structure = $4r_1\beta + 4r_2(\pi-\alpha)$. The area of the biconcave structure = $2d_1d_2 + 2r_2^2(\pi-\alpha) - 2r_1^2\beta$. As the distortion of the circle into the biconcave structure was performed, the circumference was kept constant. Let $r_1/r_2 = x$, then the area of the

biconcave structure $= r_2^2\left[(x+1)^2 \sin(2\alpha) + \dfrac{\pi}{2} + \beta - x^2\beta\right]$, and the area of the

original circle $= r_2^2\left[\dfrac{4x^2\beta^2}{\pi} + \dfrac{4\beta^2}{\pi} + \pi + \dfrac{8x\beta^2}{\pi} + 4x\beta + 4\beta\right]$. Note that the ratio of

the areas is independent of the radii of the circles as long as the ratio of the radii was kept constant.
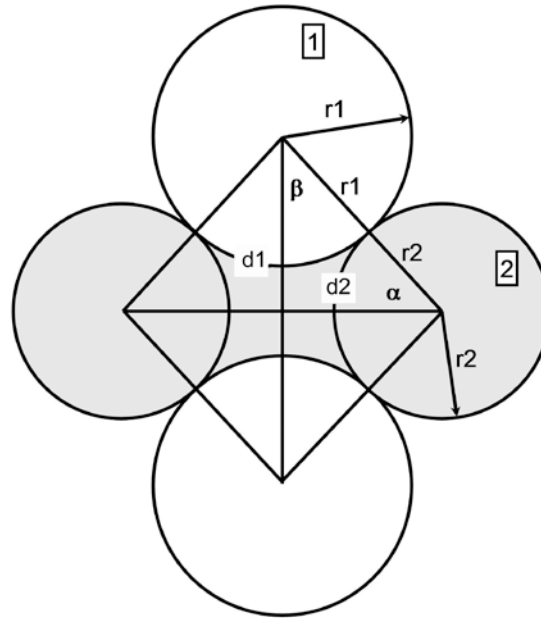
Figure 42 One of the biconcave structures is shown in grey along with the geometrical tools needed to quantitate the relevant parameters.

The cross-section of such a structure is shown in Fig. 43 at various degrees of distortion. Since the force needed to produce a positive curvature could be different from that required to generate a negative curvature, three plots are shown: one with the radius of negative curvature is half that of the radius of positive curvature (inner curve); the second with both radii having an equal magnitude; the third with the negative curvature being twice that of the positive curvature. In each case, the tension at all parts of the wall of the channel is the same with the ratio of the radii determined by the ratio of the forces needed to generate the two different curvatures. The other constraint is that the circumference is kept constant as the shape changes. With these constraints calculated structures were obtained at increments until the two arcs of negative curvature touched. The area of the biconcave structure as a fraction

81

of the area the original circle is plotted (Fig. 43) against the ratio of the distortion

length (see figure) to the radius of the original circle. As long as the ratio of the two

radii of curvature is kept constant, the fractional area change is independent of the

size of the original circle. This is consistent with the linear dependence of the data

shown in Fig. 44. Furthermore, in Fig. 44, the slope for the conductance ratios of the

experimental data, 0.42, is very close to the value of the final area ratio when the two

walls with negative curvature touch: 0.43. Similar values were obtained for the other

curves. The closeness of the theoretical and experimental values provides confidence

that the theory describes the molecular process.
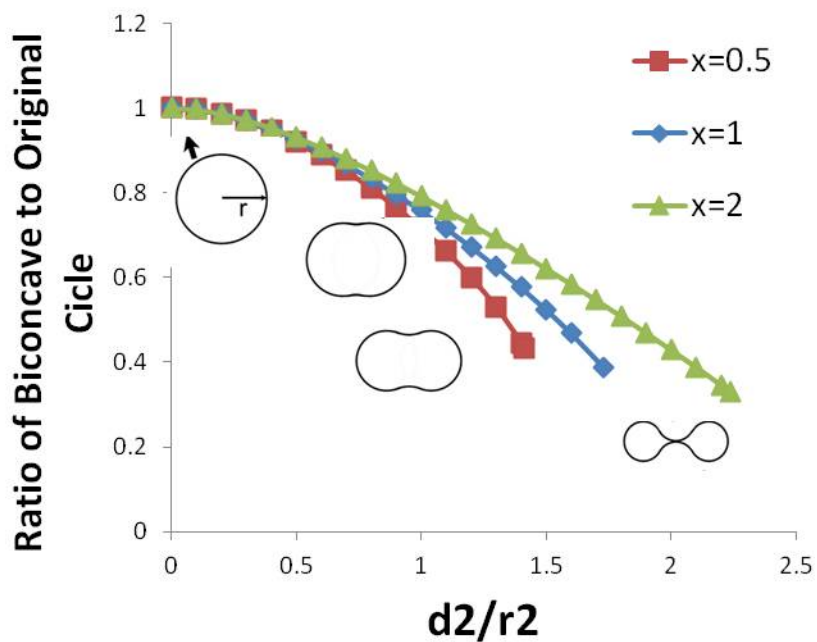
Figure 43 Theoretical calculations of cross-sectional area changes resulting from the formation of a cave structure with positive and negative radii of curvature. The perimeter of the structure was maintained constant as the axial ratio was increased while maintaining the absolute value of the ratio of the two curvatures (negative/positive) at 0.5, 1 and 2 as shown. Calculations were performed at the plotted points. The cross-sections shown are the results of calculations and are to scale relative to each other.
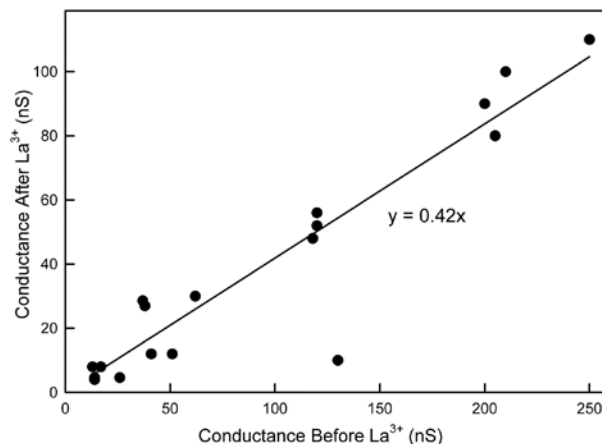
Figure 44 There is a linear relationship between the conductance (nS) of a ceramide channel after LaCl₃ treatment and the conductance (nS) before LaCl₃ perfusion.

The energetics of the distortion has two counteracting components, the lateral pressure times the area change and the bending of the channel wall times the length of arc associated with the bend. The bending of a structural element, even at the molecular level tends to have a parabolic energy curve (e.g. [116]). Thus the greater the bend the stronger the restoring force, until collapse of some structural element. The results reported with the ceramide channel indicate an elastic restoring force and thus no structural collapse. Thus one would expect that a low-energy minimum might exist, formed by these opposing energy changes. However a comparison of experimental results and theory indicate that the lowest energy is the point at which the two concave surfaces touch, not any point before this event. Supporting this is the observation that regardless of the size of the channel, the ratio of the conductance before and after La^{3+} are the same (Fig. 42). Since the channel is not a continuous material but is composed of staves, the contact between each stave must be the weak point, the hinge that allows the distortion to proceed. With channels of different sizes, the change in the angle between the staves would vary and so would the tension

and the restoring force. Thus the fact that the conductance ratio remains constant regardless of channel size, in the size range studied, indicates that the energy change associated with the change in curvature is smaller than the associate energy change due to the decrease in cross-sectional area. Distortion seems to stop when the two negatively curved surfaces make contact, indicating that further distortion results in a structure with a higher energy level.

The changes in kinetics with time considered in light of the assembly/disassembly model can also be understood in the framework of the distortion model. The complexity of the interactions of adjacent ceramide columns would easily accommodate adaptations following the distortion of the structure. These adaptations would reduce the rate of relaxation following the removal of La^{3+}. Hysteresis would be expected when an external force is applied to a system made up of hundreds of interacting components.

4.3 Conclusion

Except for channel growth and disassembly, the dynamics of ceramide channels have never before been described. Thanks to the capabilities of the planar membrane microfluidic system developed to study channel dynamics, evidence is presented that ceramide channels can undergo reversible structural changes in response to La^{3+} exposure. The observations are consistent with a partial collapse of a cylindrical channel into a cylindrical structure with a biconcave cross-section. The distortion stores mechanical energy resulting in restoration of the original structure upon chelation of the La^{3+}. These finding are consistent with a channel structure that

is highly cross-linked by hydrogen bonds and these provide the degree of rigidity and

flexibility necessary for both the dynamic motion and the restoring force.

Chapter 5: Electro-Optical Micro-PPM System Enabling Dynamic Imaging of Order Lipid Domains[17]

5.1 Brief Introduction of Lipid Rafts and Lipid Phases Separation

There is growing recognition that, rather than behaving merely as inert and homogeneous boundaries for cell organelles or platform for membrane proteins, cell membranes possess rich heterogeneities including asymmetric leaflets [117, 118] lipid caveolaes [119-122], and lateral dynamic nanoscale organizations [123-126] that play central roles in cellular function. In particular, various membrane components, including sphingsolipids and cholesterol, segregate into microdomains, termed lipid rafts, by intermolecular interactions including van der Waals interactions between fully saturated acyl chains and hydrogen bonding between adjacent glycosyl moieties of glycosphingolipids.[123] Membrane proteins can be either incorporated in or excluded from lipid rafts based on their physical properties. Rafts in the exoplasmic leaflet of the plasma membrane may serve as a platform for controlling interactions with the cell's fluidic surroundings, playing important roles in protein sorting[127-129], ion channel regulation[130], membrane traffic[131], and cell signaling[132-135]. Mediation of membrane proteins by lipid rafts is vital in defining their functional roles[136]. Examples include the internalization of HIV-1 Tat protein by lipid raft interactions[137, 138], trafficking of L1 cell adhesion protein involved in fetal alcohol syndrome[139, 140], and raft-induced aggregation of the peptide amyloid beta in the progression of Alzheimer's disease[141, 142]. Therefore,

---

[17] Part of this chapter has been published in Lab on a Chip

understanding the biophysical properties and biological roles of lipid rafts may provide critical insights toward cell function and disease progression.

Because lipid rafts in biological cells are small domains on the order of 10-200 nm, they are below the diffraction limit for light microscopy, preventing direct visualization using standard optical methods. As a result, alternative approaches are needed to more fully elucidate the characteristics of lipid rafts. Detergent extraction of lipid raft components from cells has proven to be a valuable technique for evaluating raft-associated molecules following the exposure of cells to various inputs, but this approach does not provide direct observation of the lipid microdomains and may be subject to artifacts that limit its ability to accurately assess lipid raft composition[143]. To avoid these limitations, in vitro model bilayer membranes produced using predetermined lipid mixtures are invaluable for elucidating the mechanisms of lateral heterogeneity in cell membranes in a protein-free setting. In particular, giant unilamellar vesicles (GUVs) on the order of 10 ~ 100 µm in diameter generated by electroformation [144, 145] are commonly used for exploring the behaviors and interactions of ordered lipid domains[146]. The use of GUVs enables lateral phase separation into liquid disordered (L_d) and liquid ordered (L_o) domains with micrometer length scales that can be directly observed by confocal microscopy. Like lipid rafts, the Lo domains are rich in cholesterol and lipids with high melting temperature lipids such as sphingolipids and 1,2-saturated phospholipids, while the Ld domains mimic the disordered phase of cell membranes which are primarily composed of phospholipids with at least one unsaturated acyle chain. Phase behavior

can be directly observed by 3D reconstruction with z-slicing using confocal microscopy [146-155]

Despite the benefits of GUVs, there are several important drawbacks that limit their utility for lipid domain studies. Because vesicles are closed elements, with no direct fluidic access to the inner compartment of the vesicle, the chemical or biochemical composition can only be readily changed at the outer membrane leaflet. Similarly, isolation of the inner vesicle compartment also prevents effective electrical characterization of the membrane, which would otherwise offer an orthogonal measurement dimension to reveal details of average membrane structure accompanying domain changes that cannot be monitored solely by optical methods. Furthermore, changing the conditions at the outer compartment is a slow diffusive process, making it impossible to evaluate dynamic processes with time constants faster than several minutes. Even when investigating the relationships between static boundary conditions and lipid raft behaviors and interactions, GUVs require laborious experimental efforts to adjust the concentrations of selected solvents and solutes, limiting the density of data that may be extracted from these studies. In addition, GUV surface tension is defined by the vesicle radius, which is difficult to reliably control during vesicle synthesis and cannot be adjusted dynamically. More generally, GUVs are by definition closed equilibrium systems, very different from cell membranes in which lipids are dynamically transported between the plasma membrane and intracellular compartments.[156] Finally, since optical imaging of the spherical vesicles requires three-dimensional scanning microscopy, the frame rate limitations can complicate studies of dynamic phase behaviors such domain

formation, coalescence, and dissolution. As an alternative to vesicles as model membranes, planar supported lipid bilayers enable full-field imaging of lipid microdomains including access by atomic force microscopy.[146, 157, 158] However, because supported lipid bilayers provide direct fluidic access on only one side of the membrane, they suffer from many of the same issues as GUVs. In addition, the behaviors of lipid microdomains within supported bilayers do not accurately reflect the dynamics within biological cells since the supporting substrate impacts diffusion kinetics of both lipids and proteins by an order of magnitude or more.[159] Solid supports also interfere sterically with conformational changes in proteins, and artificially impact the flip-flop dynamics of lipids and membrane-bound components across the membrane leaflets.

Although known for stability issues, annularly-supported BLMs represent an promising membrane model for lipid domain imaging that is compatible with promising microfluidic technologies. [68, 76, 87-89, 113, 160] BLMs are formed across an aperture fabricated in a thin hydrophobic film which separates two buffer chambers. Unlike both GUVs and supported membranes, BLMs provide direct fluidic and electrical access to both membrane leaflets. In addition, horizontal BLM systems compatible with direct microscope observation have been employed to optically and electrically study physics of lipids[161, 162] and ion channels[163-165] simultaneously. Previous efforts toward the characterization of lipid phase separation using macro-scale BLM chambers included real time observation of merger of two domains, dissolution of lipid domains under elevated temperature,[166] and simultaneous electrical and optical measurements.[161] In particular, liquid ordered

domains were formed in an asymmetric planar bilayer,[167] presenting unique usefulness to mimic rafts only in exoplasmic leaflet in cell membrane.

A universal challenge of model membranes as an alternative to native cell membrane studies lies in the variable lipid composition inherent to both vesicles and BLMs. Although the composition of GUVs can be estimated, for example by matching the phase diagram for binary phospholipid mixtures[168] or comparing the bending elasticity of membranes reconstituted from erythrocyte lipid extracts[169] such characterization methods are indirect. Indeed, it remains a key challenge to form a multi-component GUV and directly determine its lipid content.[145] While the lipid composition in BLMs is also uncertain, it can be directly quantified by a mercury droplet extraction method,[170, 171] an approach which has been used to confirm that lipid content in the BLM can differ from the bulk annulus and may change over the lifetime of BLM. However, due to the challenging experimental effort required to perform these various analysis, both indirect and direct methods for determining lipid content of model membranes are seldom employed. Despite this limitation of all established model membrane systems including both GUVs[146, 172] and BLMs[161, 167], these models are routinely employed to study phase behavior of multi-component lipid mixtures without explicit knowledge of the lipid composition by labelling domains with phase-segregating dyes. With a range of fluorescence dyes known to segregate into either L_o or L_d phases,[173] local lipid structure can be qualitatively determined, enabling the evaluation of key membrane characteristics including domain morphology,[174] diffusion behaviour,[175] phase diagrams,[176] and inter-leaflet domain induction[167].

Here we report the extension of a miniaturized and integrated BLM platform[113] enabling precise control over membrane curvature and fluidic boundary conditions toward studies of lipid phase separation. The thermoplastic microfluidic chips support the *in situ* stable formation of annularly-supported planar BLMs that can be monitored by full-field confocal epifluorescent microscopy, allowing direct imaging of lipid microdomains together with the simultaneous characterization of transmembrane impedance for correlated electrical and optical membrane observations. The microfluidic system supports the rapid control of static and dynamic (bio)chemical conditions in either side of membrane via direct perfusion, and also supports controllable modulation of membrane curvature, enabling the impact of surface tension on lipid-lipid and lipid-protein interactions to be readily explored. Collectively, these capabilities serve to extend the available model membrane toolkit toward new studies of both transient and equilibrium-state lipid domain dynamics and interactions.

5.2 A New Micro-PPM System to Study Lipid Domains

5.2.1 Fabrication

The electro-optical microfluidic BLM chips were fabricated from a hybrid glass/thermoplastic multilayer system. Microchannels (460 µm wide, 150 µm deep) were patterned in a 2.38 mm thick PMMA chip by direct computer numerical control (CNC) micromachining to create a microfluidic network supporting *in situ* lipid membrane formation and reagent perfusion. The PMMA chip was then thermally bonded to a 12 µm thick PVDC film containing a 50~100 µm diameter aperture fabricated using a thermal ablation method.[113] To render the chip compatible with

high-magnification confocal optical imaging, a 100 µm thick patterned adhesive polymer layer was patterned on a glass cover slip with average thickness of 110 µm, forming a lower microchannel beneath the membrane site, and bonded to the back side of the PVDC layer. The total distance between the lipid membrane to the bottom of the cover slip averages 210 µm, which enables high magnification confocal imaging of the membrane. Ag/AgCl electrodes were sealed into reservoirs connecting to both the upper and lower perfusion microchannels using a previously-reported process,[113] enabling simultaneous monitoring of transmembrane current. A cross-sectional schematic and photograph of a chip fabricated by this process are shown in Fig. 45. Estimates of transmembrane pressure within this system were established by setting known buffer flow rates through one of the perfusion channels, with the resulting pressure difference across the membrane defined by the product of the volumetric flow rate and estimated hydrodynamic resistance of the microchannel connecting the membrane site with the downstream waste reservoir. Large and balanced reservoirs at each channel outlet minimized the contributions of water column height and capillarity on the overall pressure gradient.
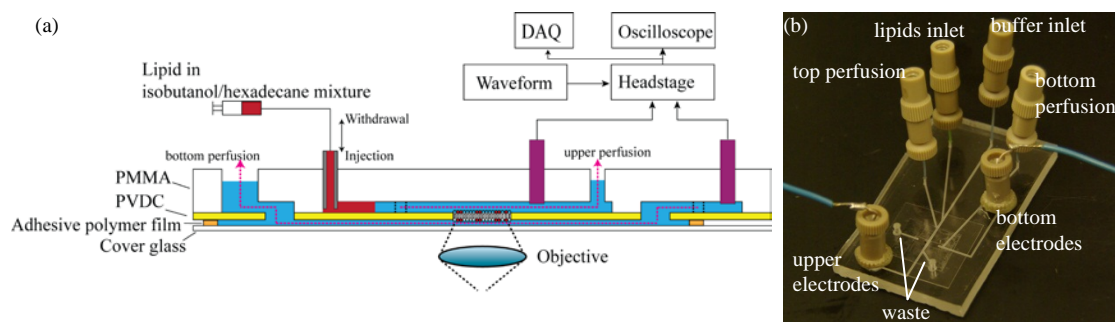
Figure 45 (a) Schematic of a microfluidic BLM chip supporting simultaneous electrical measurements and confocal optical imaging together with active perfusion to either side of the bilayer. (b) A fabricated BLM chip. The chip is 6.0 cm long and 2.5 cm wide.

5.2.2 Optical and Electrical Interfacing

Optical measurements were performed by placing the BLM chip on the imaging stage of a Leica SP5 X confocal microscope. Standard objectives (20X/0.7 NA Plan Apo multi-immersion, 63X/1.3 NA Plan Apo glycerin) were used to provide imaging with up to 60 nm pixel resolution. A laser line at 595 nm was used for excitation with a photomultiplier tube (9624s; Hamamatsu Photonics, Japan) used for fluorescence detection. Frame rates up to 25 frames per second via resonance scanning at 512 by 512 resolution were readily achieved. Video imaging was performed at frame rates ranging from 0.76–1.32 Hz to improve contrast. Leica AF Lite software was used to measure circular domain diameter while irregularly shaped domains were analyzed using ImageJ software. Transmembrane current was converted to a voltage signal by a custom amplifier and monitored using a data acquisition system including a 60 Hz noise eliminator (Hum Bug; AutoMate Scientific, CA), filter (LPF-202A, f_c=10 kHz; Warner Instruments, CT) and digitizer (sampling at 250KHz, Digidata 1440A; Axon, CA). A syringe pump (11 Elite; Harvard Apparatus, MA) with both infusion and withdrawal capability was used to deliver lipid and buffer solutions to the microchip via stainless steel needle interfaces.[86] All data were acquired at a temperature of 27 °C.

5.2.3 In-situ Membrane Formation

A novel technique termed "kiss and retreat" was developed for reliable and semi-automated *in situ* membrane formation (Fig. 46). Briefly, lipid mixture is dissolved in solvent consisting of 1:4 v/v isobutanol and hexadecane. After the microchip is filled with buffer, the lipid mixture is delivered by syringe pump towards

the BLM aperture at flow rates between 0.1–0.5 µl/min until the lipid front reaches the PVDC aperture (Fig 46a,b).
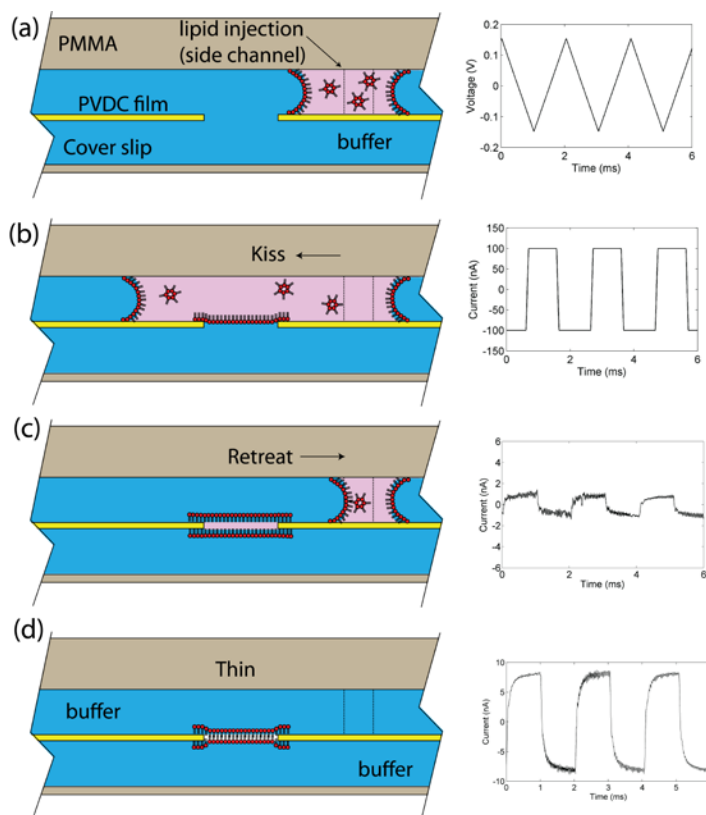
Figure 46 Schematic of the kiss and retreat bilayer formation process and corresponding trans-membrane current traces measured with the integrated chip electrodes. See texts for details.

Immediately after passing the aperture, as determined by optical observation or electrical monitoring of current through the aperture, the lipid solution is withdrawn back towards syringe, leaving a plug of lipid solution that remains attached to the rim of the aperture (Fig. 46c). Isobutanol within the remaining lipid plug diffuses into the surrounding aqueous solution, thinning the lipids into a bilayer supported by a solvent-containing annulus (Fig. 46d). If a bilayer fails to form, the inject/withdraw process is simply repeated until a stable bilayer is formed, as confirmed by electrical characterization of the membrane's specific capacitance using the integrated Ag/AgCl

electrodes. Electrical measurements were performed using a triangle wave with 150 mV amplitude and 500 Hz frequency. The stray capacitance of the chip was measured as 3.33 pF. The 60 µm diameter BLM was formed across an 80 µm diameter aperture. The final measured current corresponds to a membrane capacitance of 26.7 pF (0.94 µF/cm^2) confirming the formation of a bilayer. The sealing resistance of BLM ranged from 1.5 – 2.5 GΩ.

Compared to our previously-reported "diffusion painting" method[76] this technique reliably produces on-chip bilayer membranes with a minimum of human operation. Moreover, like our previous demonstration of *in situ* BLM formation by two-sided lipid/solvent perfusion,[177] the kiss and retreat technique is compatible with a closed chip format enabling controllable buffer exchange to both sides of the membrane, but with a significantly higher success rate above 90% for creating a robust BLM. Using this method, both dynamic and steady-state solution conditions at both sides of the membrane can be freely changed by rapid perfusion. Moreover, because the fluidic passages are only open at waste reservoirs distal from the membrane site, it is possible to control the transmembrane pressure by adjusting the relative perfusion flow rates across the upper and lower membrane compartments, allowing membrane curvature to be modified while maintaining the desired (bio)chemical boundary conditions.

5.2.4 Domain Imaging

TR-DHPE has been widely employed to image the co-existence of lipid phases in solid-supported and GUV model membranes. In particular, membranes formed with DPPC/DPhPC/chol,[178] POPC/PSM/chol, and DOPC/PSM/chol[173,

179] exhibit highly efficient partition of dye to the liquid disordered phase. Similar dynamical evolution of coexisting L_o and L_d domains in both DPPC/DPhPC/chol and POPC/PSM/chol have been observed with TR-DHPE in this system. Fig. 47 shows images at four sequential time points in a membrane formed by DPPC/DPhPC/chol. Selected domains (shaded in the figure) are tracked to reveal the dynamic movement and coalescence of discrete L_o domains using this ternary lipid system. While DPPC/DPhPC/chol mixtures can be readily used for on-chip membrane formation and phase separation experiments, other membrane compositions are of interest to provide greater biological relevance. Specifically, the remainder of the work described in this paper is focused on POPC/PSM/chol. POPC is a 1-saturated, 2-unsaturated PC, representing a large portion of naturally occurring PC.[180] Sphingomeylin is the most abundant sphingolipid in plasma membranes, but has a rather complex thermotropic behavior. PSM was chosen for this study as it exhibits simpler thermotropic behavior but possesses a melting temperature very close to natural SM extract.[176]
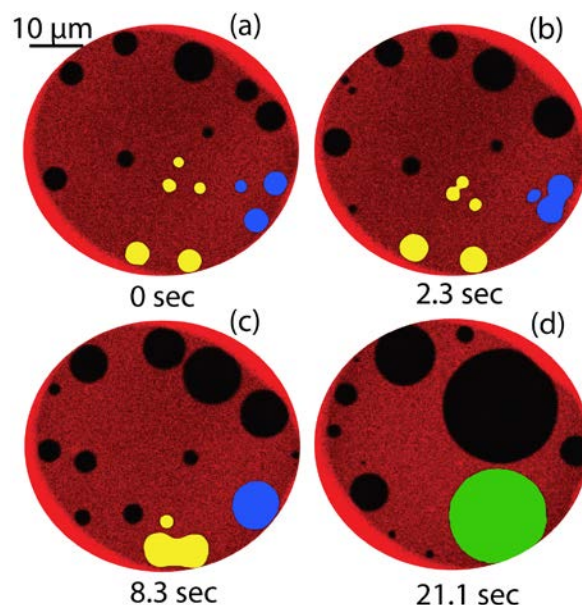
Figure 47 The merger of ordered domains (dark regions) formed by DPPC/chol within a disordered phase composed primarily of DPhPC, with TR-labeled DHPE preferentially segregated to the disordered phase. Two sets of domains are presented in pseudo-color (yellow and blue) to highlight the evolution of multiple merger events leading to the formation of a single ~15 μm Lo domain (green).

One characteristic of the L_o domains that is readily probed in the system is their behavior under free diffusion. Fig.48 shows the diffusion trajectory of a single L_o domain under the application of 0.96 Pa transmembrane pressure generated by buffer perfusion at 300 nL/min. Under these conditions, multiple domains with diameters of several microns were found within the center of the bilayer (Fig 48a). The domains were highly stable and remained detached from the supporting annulus, enabling the Brownian motion of the ordered structures to be observed over long time scales. An average diffusion coefficient of 0.125 μm^2/s for ~1.5 μm diameter domains was determined in this experiment. In comparison, diffusion coefficients ranging from 0.09 ~ 0.20 μm^2/s have been reported for L_o domains in GUVs using a different lipid composition (DOPC/DPPC/CHOL) with a lower cholesterol concentration in the initial lipid mixture.[175]
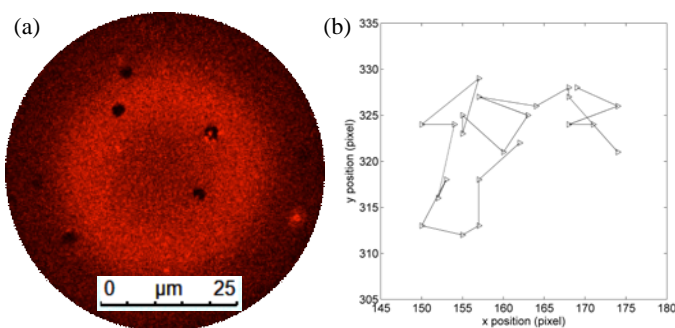
Figure 48 (a) Stable small ~1.5 μm diameter ordered domains in a membrane formed with molar ratio 2:1:2 POPC/DPPC/chol mixture . (b) Trajectory of a single Lo domain with 3.22 s between each time step.

5.3.1 Dynamic Domain Generation During Membrane Stabilization

In the case of GUV model membranes, lipid domain imaging is performed only after the vesicles are formed and fully stabilized. As a result, existing studies of lipid domains have generally focused on evaluating steady-state relationships such as lipid phase space rather than kinetic phenomena. In contrast, because our on-chip BLMs are formed *in situ* after positioning the chip on the microscope stage, the microfluidic system allows the full dynamic processes of ordered domain emergence, formation, and interaction during the early stages of membrane stabilization to be observed. An example revealing the typical behavior of these non-equilibrium processes in a POPC/PSM/chol membrane is shown in Figure 49 and video 1[18].
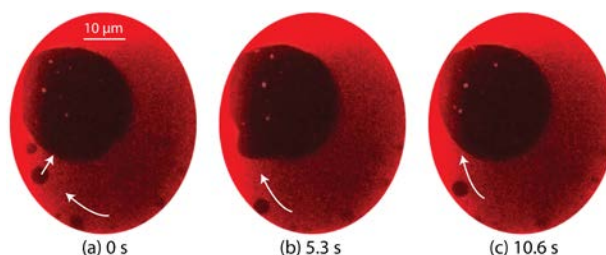
Figure 49 Growth of a large Lo domain in the absence of transmembrane pressure for a POPC/PSM/chol membrane. Ordered domains (dark regions) are generated from the right side of bilayer and driven to the pre-existing large domain, revealing that the composition of bilayer during the first 2-3 min following membrane formation is not in equilibrium with the surrounding annulus.

Immediately after membrane formation across a 60 µm diameter aperture, L_o domains were spontaneously generated at the right side of the bilayer and observed to migrate along the interface of the bilayer and surrounding solvated lipid annulus to the left side, where a large L_o domain had formed immediately at the initial stage of

---

[18] Video one is available in http://mml.umd.edu/si/SI-1.mov

98

bilayer formation. The large domain continued to expand as it absorbed incoming small domains until the composition of the bilayer reached equilibrium. In a typical experiment, L_o domain generation stops within 2–3 min after bilayer formation, with no further changes in membrane organization over an equivalent time period confirming equilibrium. Although different membranes exhibit different initial domain patterns at the moment of formation, the lipid exchange process involving dynamic domain generation and coalescence into a single large stable domain is consistently observed. While small domains can float freely within the bilayer, larger domains tend to attach to the surrounding annulus. This behavior can be interpreted as a measure to minimize the energy state by lowering the contacting circumference length between liquid ordered and disordered domains.

Annulus-supported BLMs have been employed to study membrane biophysics for decades, with static steady-state partitioning of lipids between the bilayer and surrounding annulus routinely assumed. However, the composition the bilayer can differ from the initial lipid solution due to the dynamic partitioning process during the initial stages of membrane formation,[170, 171] as well as dynamic changes that occur following membrane formation.[171] Here we present direct observations of lipid exchange between the BLM and surrounding annulus in the early stages of membrane formation, manifested by lipid phase separation and domain stabilization, which we believe are the first reported visualizations of these dynamic processes. The microfluidic platform may further serve as a fluorescence-based alternative to the mercury droplet extraction method[170, 171] for qualitatively studying membrane composition during these dynamic processes, and may be of particular utility toward

99

examining membranes reconstituted from complex lipid mixture and natural lipid extracts

5.3.2 Effect of Transmembrane Pressure on Domain Stability

Surface tension directly affects the ordering of lipid membranes, and its impact on lipid domains is commonly studied in GUVs by micropipette aspiration or osmotic swelling[181, 182] to control vesicle surface tension. Previous reports have revealed that small domains tend to grow and combine into larger domains as surface tension is increased. This observation can be interpreted as a thermodynamic effect, with increasing lateral tension caused by expansion of the vesicle surface resulting in increased line tension between adjacent lipid phases, encouraging a reduction in ordered domain size to minimize enthalpy. Unlike vesicle membranes, where surface tension of the closed system responds immediately to an osmotic pressure gradient, pressure-induced bulging of a BLM is a kinetic process.[162, 183] As membrane curvature increases, lipids migrate dynamically from the annulus to the bilayer to maintain lower surface tension, thereby expanding the Plateau-Gibbs border that defines the edge of the annulus. This rate-dependent lipid transport process has previously been leveraged to enable high pulsatile perfusion rates while avoiding membrane rupture.[113] In the present study, an estimated transmembrane pressure gradient of 1.63 Pa was defined by applying a constant 500 nL/min buffer flow rate to the microchannel positioned above a POPC/PSM/chol bilayer with an average diameter of 60 µm. Immediately upon perfusion, new L_o domains began to nucleate and grow adjacent to the annulus, followed by migration around the periphery of the membrane toward a large domain which had formed during initial membrane

stabilization. Fig. 50 shows a typical observation of this process, including the transport of lipids from the annulus to the bilayer over time. In this example, perfusion was initiated several minutes after complete stabilization of the membrane, so that all observed domain formation and migration was due solely to energy minimization under the influence of the applied pressure gradient. The generation of new L_o domains under pressure exhibits distinct characteristics compared to the membrane stabilization stage. Comparing the two cases, L_o domains are generated from 4–5x more nucleation sites with the application of transmembrane pressure. The maximum size of generated domains under pressure appears to be limited only by collisions with adjacent domains, while during zero-pressure stabilization the domains do not grow beyond a plateau of around 4 µm in diameter. In addition, the growth rate of individual domains under transmembrane pressure is significantly higher than the growth rate of domains during stabilization (Fig. 51).

(a) 0 s   (b) 27.6 s

(c) 72.3 s   (d) 120.0 s
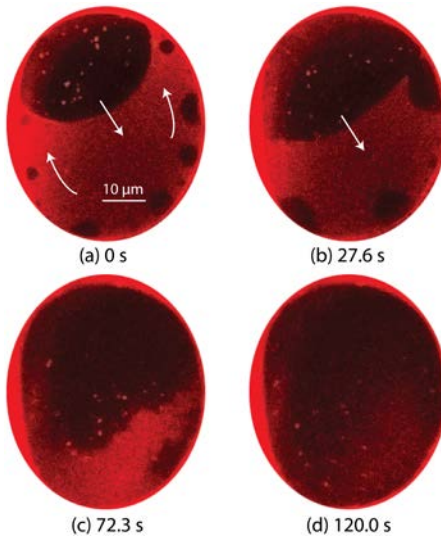
Figure 50 A POPC/PSM/chol membrane exhibiting clear phase separation experienced a topological change when 1.63 Pa pressure was applied across the membrane. (a) Domains generated at the bottom of the image migrate and merge with a large domain created during initial membrane formation. (b-c) As perfusion continues, the boundary between ordered and disordered domains becomes increasingly indistinct, until (d) the L_o and L_d regions become fully miscible.

101
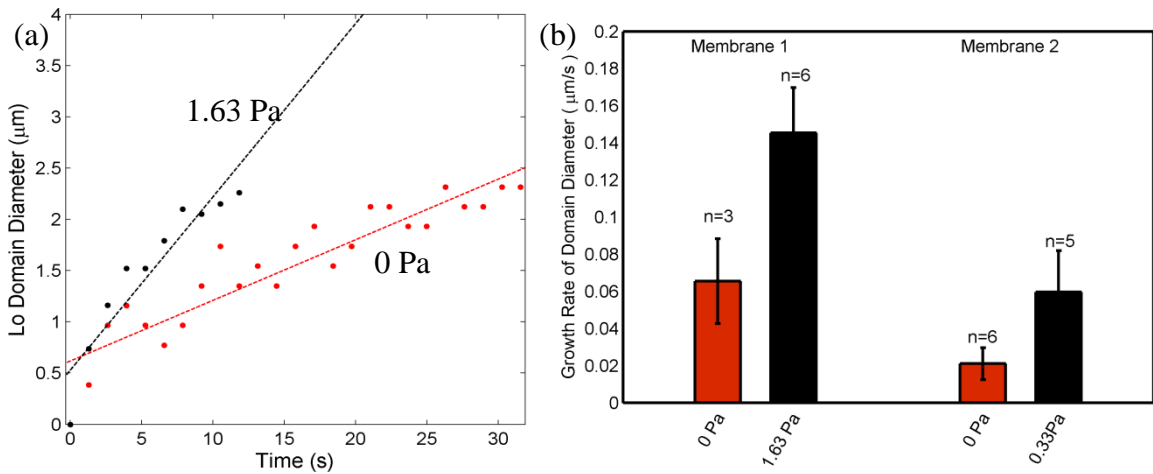
Figure 51 (a) The growth of selected domains during initial membrane stabilization in the absence of external pressure (0 Pa) and applied transmembrane pressure (1.63 Pa). (b) Average domain growth rates extracted from multiple domains under different pressure states for two different membranes. The diameters of individual ordered domains were measured from nucleation at the bilayer boundary through departure from the boundary or merger with other domains. Membrane 1 has an area of ~2400 μm2, while membrane 2 has area of ~4400 μm2.

Following the initial growth and coalescence of L_o domains, continued application of the 1.63 Pa transmembrane pressure led to the boundaries between ordered and disordered phases becoming indistinct, until the discrete ordered domains ultimately dispersed, resulting in uniform fluorescence intensity across the bilayer (Fig. 50c,d). The change from well-defined circular boundaries to irregular shapes, and finally phase miscibility, reflects a reduction in the contribution of line tension to the overall energy of the system. The reduction in line tension at the phase boundaries is presumably due to increasing surface tension in the bilayer that occurs when lipid migration from the annulus can no longer compensate for increasing membrane curvature. The higher surface tension provides larger space for the free motion of individual molecules within the bilayer, such that POPC, PSM and cholesterol can assume preferable interactions with water and lipid molecules without segregating to

different phases. This observation is similar to the behavior of a Langmuir monolayer exposed to a change in surface pressure, where the increased space available to each lipid allows the monolayer to undergo a transition from L_o to L_d states.[184] Since L_o domains maintain their circular shape in presence of high line tension to lower energy, reduced contribution of line tension to the overall enthalpy of the system would lead to reduced roundness of the domain shape. The process of L_o domain distortion, dispersion, and dissolution has been consistently observed over repeated experiments, together with the recovery of partially-dispersed L_o domains following removal of the applied pressure gradient, with recovery times on the order of several tens of seconds. A video showing the full process of pressure-induced domain generation, migration, and dispersion over the course of a typical experiment is provided in Video-2.[19]

5.3.3 Gel Phase Domain Growth

In a similar study as in 5.3.2, we did an experiment with same lipid mixture as Figure 47 (equal molar DPPC/DPhPC/CHOL) but in a lower temperature (22 ºC). We observed a similar growth of gel phase upon trans-membrane pressure while it is easy to see from the gel phase growth that the growth point is at the boundary between bilayer and annulus (show in Figure 52).

---

[19] Video-2 is available at http://mml.umd.edu/si/SI-2.mov
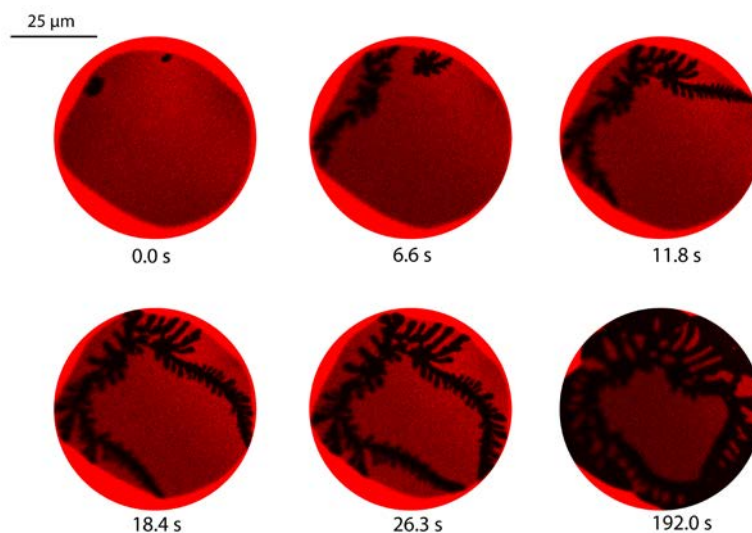
Figure 52 Real-time imaging of gel phase growth under transmembrane pressure. The expanding gel phase reveals that DPPC is pulled out of supporting annulus as a result of applied transmembrane pressure. Membrane was formed with same solution as Fig. 47. Images were taken at 22 ºC.

5.4 Summary

As a useful alternative to GUVs and supported bilayers, planar BLMs better represent the native environment of biological membranes, with fluidic access to both membrane compartments, dynamic lipid exchange between the membrane and supporting annulus, and a free-standing configuration that does not impede the motion of lipid components within the membrane. The present work describes a microfluidic BLM system that supports *in situ* stable bilayer membrane formation with nearly perfect success rates, simultaneous electro-optical measurements of the bilayer, and rapid independent control over (bio)chemical boundary conditions at both sides of the membrane. To demonstrate the utility of the microfluidic system, phase-segregating dyes were introduced to the lipid solutions and used to successfully observe lipid phase separation in two different ternary lipid compositions, with high

resolution confocal imaging of the resulting L_o domains. The chips have enabled, for the first time, direct optical observations of the initial lipid exchange between the bilayer and supporting annulus immediately after membrane formation, and full-field video of on-chip membranes have revealed details of the movements of L_o domains that provide a new view of energy minimization processes during membrane stabilization. Control of transmembrane pressure has been used to show that L_o domain generation and dissolution dynamics depend directly on membrane surface tension, and may allow future experiments to elucidate surface tension dependent phase diagrams for different lipid compositions or explore the response of mechanosensitive ion channels. By applying a moderate transmembrane pressure, the formation of small stable domains has also been demonstrated, allowing the diffusion coefficients of L_o domains undergoing free Brownian motion to be measured. Overall, the microfluidic-enabled platform represents a powerful and convenient model membrane system that can significantly extend the scope of biophysical and biochemical studies of lipid membranes, lipid rafts, and ultimately their interactions with membrane-bound proteins and exogenous agents delivered to the membrane by dynamic perfusion.

Chapter 6: Double Bilayer Lipid Membrane Chips

6.1 Motivation

Lipid membrane fusion plays a range of important roles in cellular processes. Despite extensive study, the mechanisms controlling the association and fusion of membranes remains unclear [185]. While giant unilamellar vesicles (GUVs) are a natural choice of model membrane for fusion studies, they are enclosed elements, with no direct fluidic access to the inner compartment of the vesicle such that the chemical or biochemical composition can only be readily changed at the outer compartment. Similarly, isolation of the inner vesicle compartment also prevents effective electrical characterization of the membrane, which would otherwise offer an orthogonal measurement dimension to elucidate details of average membrane structure. This is particularly important for studies of membrane fusion, where electrical characterization may provide new insight into the formation and propagation of defects at the interfacing membranes that ultimately lead to fusion. Planar BLMs offer an excellent alternative model system to address these limitations. The membrane formation discussed in Chapter 5, namely "kiss and retreat" method is essentially compatible and easy to create two parallel membranes a single time. here we describe thermoplastic chips enabling double BLM (dBLM) formation

6.2 Fabrication and Design Principle

Figure 53 shows the schematic of the dBLM chip design. The dBLM microchip is fabricated from an upper PMMA layer bonded to a BLM-hosting PVDC film, a second thin PMMA sheet containing a middle microchannel, a second PVDC partition, a polymer adhesive film, and finally a cover glass for optical imaging. The

membranes can be brought into contact by a transmembrane pressure introduced by top and bottom perfusion, while perfusion in the middle channel supports the delivery of fusion proteins (e.g. SNARE) or adhesion receptors to the membrane.
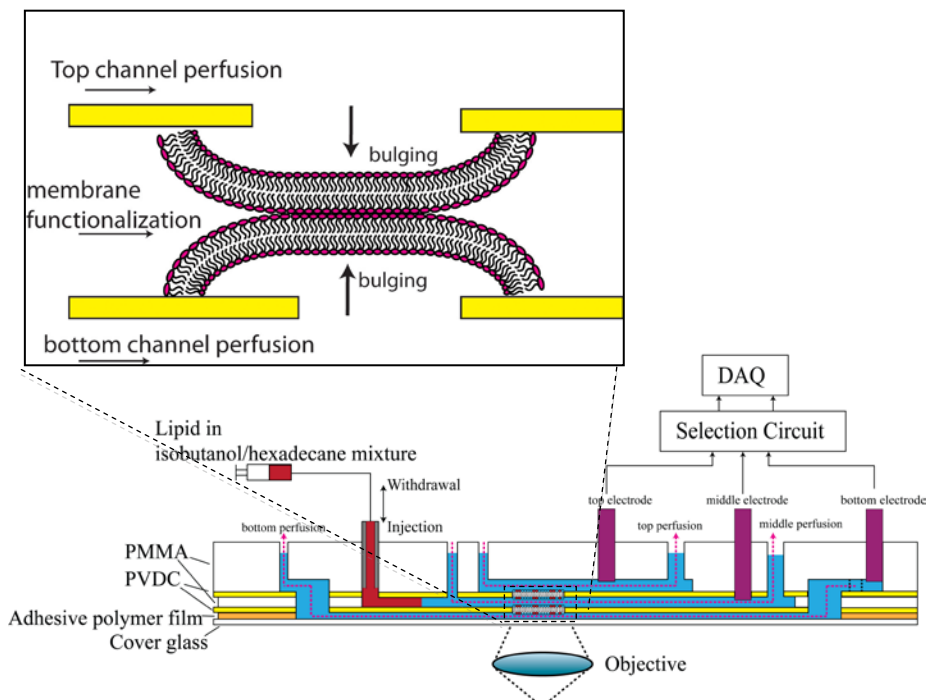
Figure 53 Schematic of dBLM chip.

Three independent Ag/AgCl electrodes are connected to the top, middle and bottom channels, and a custom FET-based membrane selection circuit (Fig. 54) has been developed to support capacitance measurements the lower membrane, upper membrane, or series combination of both membranes in real time. By independently controlling the pressure difference across each membrane, the curvature of each bilayer may be adjusted to bring the membranes into contact (inset in Fig. 53).
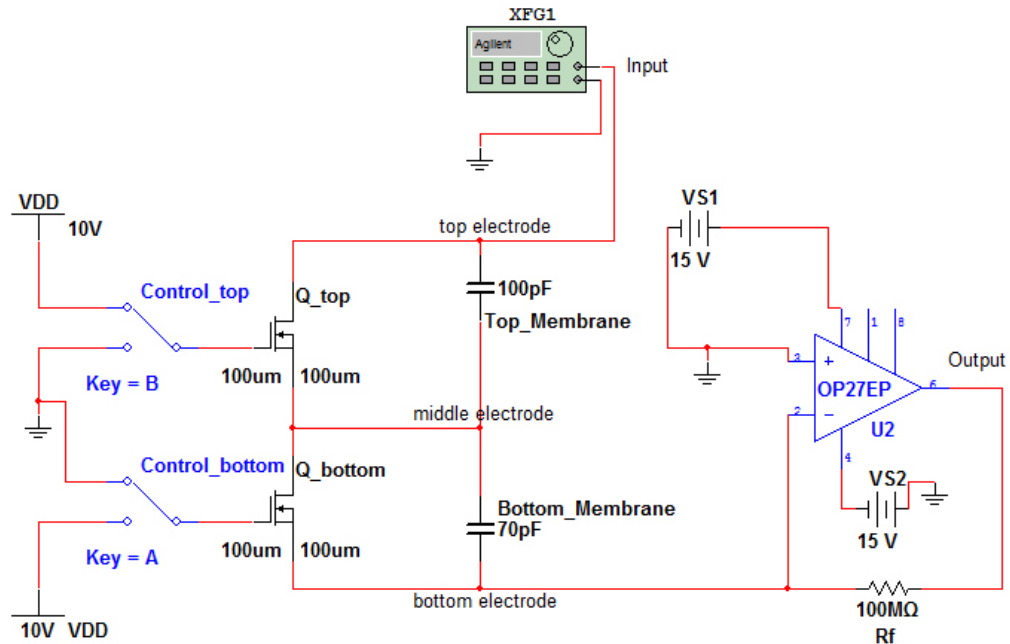
Figure 54 Diagram of membrane impedance monitoring circuit. Top, middle and bottom electrodes are connected to two MOSFETs, which are controlled separated by voltage switches, enabling continuous monitoring of top, bottom and the combination of two membranes, providing essential knowledge to understand the membrane fusion process.

6.3 Preliminary Results

6.3.1 Forming Two Membranes Simultaneously

A unique aspect of this platform is that, with the help of an automatic z-slicing confocal microscope, the interfacing bilayer region remains in the microscope imaging plane (Fig. 55), allowing the sequential process of membrane aggregation, contact, dehydration, defect formation, and finally defect growth and membrane destabilization to be optically observed with high spatial and temporal resolution. Two membranes are formed simultaneously when a "kiss and retreat" method is performed in middle channel.

108

50 μm

Top membrane   Bottom membrane
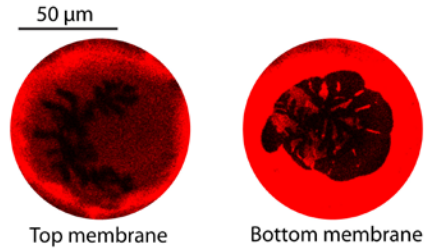
Figure 55 Two membranes are formed simultaneously when a "kiss and retreat" method is performed in middle channel. The membranes were formed by equal molar mixture of DPPC, DPhPC and cholesterol.

6.3.2 Bulge Membrane out of Orifice

As shown in Fig. 56, application of differential perfusion rates through the channels on either side of a membrane leads to membrane formation, forcing the BLM out of the plane of its supporting aperture. Continuous bulging of membranes up to 200 µm has been successfully achieved, enabling two mating membranes to be brought into contact across the 100 µm thick middle perfusion channel separating their respective apertures.

50 μm

z = 0 µm   z = 18.3 µm   z = 36.6 µm

z = 54.9 µm   z = 73.2 µm   z = 91.5 µm   z = 109.8 µm
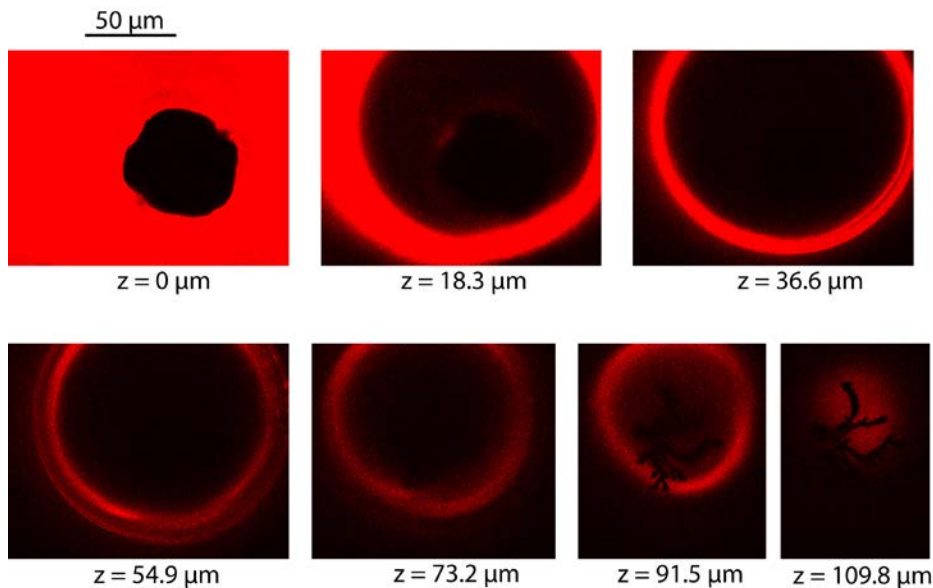
Figure 56 Bulging of membrane under transmembrane pressure. The high of the resulting membrane is ~ 110 µm while the aperture size is only ~70 µm. Images were obtained at 22 ºC to induce gel phase formation in the bilayer, as seen near the top of the deformed membrane.

The dBLM chips offer unique opportunities for biomembrane fusion studies using a combination of both electrical and optical characterization. Coupled measurements of membrane interaction, contact, and fusion are currently ongoing to probe membrane defects prior to fusion, with the goal of shedding light on the debate over the dominant fusion mechanism by the stalk model or defect model[185].

Chapter 7: Micro-PPM System with Rapid Temperature Modulation Capability

7.1 Brief Discussion of Thermodynamics of Ion Channel

7.1.1 Ceramide Channel Thermodynamics

There are a lot of interesting theories and hypothesis to explore about the driving force of ceramide channel formation. Simply put, the driving force in ceramide channel formation can be described in: $\Delta G = \Delta H - T\Delta S$, where ΔG is the Gibbs free energy, whose sign indicate whether channel formation is favored or unflavored. If ΔG is negative, then formation is favored. S is the entropy change associated with the organization degree of the ceramide molecules. Since ceramide channel is surely more organized than ceramide rafts, ΔS is always negative. H is enthalpy which relates to bonding breaking and reforming. To make ceramide channel formation energetically favorable, ΔH need to be negative enough to offset the entropy price. In other words, the number of hydrogen bonding available in ceramide channel should be sufficient to overcome the entropy decrease by being more organized.

In ceramide channel formation critical point, certain external conditions change the sign of ΔG of a raft (or several rafts) of ceramide from positive to negative so that the formation of channel becomes energy favorable. These conditions might relate to enthalpy, temperature or entropy. For example, a collision between ceramide rafts may provide more molecules and more possible inter molecule hydrogen bondings that may promote channel formation. A stress shock in the

membrane may accidently overcome the energy barrier of rotating rafts surface to vertical direction so that channel can be formed. Or a temperature drop can lower the vibration energy that breaks hydrogen bonding so channel can be stabilized, just like water frozen to ice.

Current PPM formation and ceramide channel formation technique doesn't guarantee exact ceramide composition in membrane, thus enthalpy change and entropy change may vary from one ceramide channel to another. Therefore, ΔH or ΔS cannot be held constant in multiple ceramide channels. To this end, temperature is the only variable we can change within a life span of one single ceramide channel, thus an apparatus with ability to manipulate the third variable in this equation: temperature T is highly desirable.

Ideally, at temperature T_0 a ceramide channel would form from a membrane and gradually reach its equilibrium state with stable conductance. We can safely assume in micro-scale the ceramide channel is "isolated" from other floating rafts, which means it will not actively recruit or lose ceramide molecules unless a significant external condition affects it. Then temperature can be modulated from T_0 to T_1, T_2, T_3, and different conductance levels can be detected. By estimating the diameter of the ceramide channel from the conductance, the number of ceramide molecules can be calculated. Finally a group of equations are assembled:

$$G_1 - G_0 = (H_1 - H_0) - T_1(S_1 - S_0);$$

$$G_2 - G_0 = (H_2 - H_0) - T_2(S_2 - S_0);$$

$$G_3 - G_0 = (H_3 - H_0) - T_3(S_3 - S_0) \ldots \text{(Equation Set *)}$$

The experiment will provide a clue how to relate the enthalpy and entropy change to the number of ceramide in one single experiment. Combining the morphology information of ceramide rafts gained from spectroscopy, it might provide more deep understanding of this formation process.

In order to make the equations hold and the whole experiment meaningful, local temperature measurement should be very precise and accurate. Otherwise, if not small enough temperature increments can be resolved, then $S\Delta T + T\Delta S$ is not a good approximation to $\Delta(ST)$. If measurements of T is not accurate, then information gained from equations above might not reflect the real situation. Microfluidic based PPM device naturally becomes the best choice to undertake this task, with its compatibility to a whole set of microfabrication toolbox of high accuracy temperature modulator and temperature sensor.

7.1.2 Thermal Sensitive Ion Channels: ThermoTRP

Temperature controller and sensor embedded in PPM and ion channel system will not only benefit the research involving ceramide channels but also other temperature sensitive ion channels. Among others, cation channels of the transient receptor potential (TRP) superfamily are the most prominent sensing channels to ambient temperature. With distinct sensing range and sensitivities, the group of ion channel covers the temperature ranging from the noxious cold (<8 °C) and noxious heat (>52 °C). Table 4 lists the different activation temperature of known thermal sensitive channels (ThermoTRP) [186]. For a recent review of TRP channels and

temperature sensation, please refere to [187]. A typical experiment to study the thermo response of TRPV channels is shown in Fig.57.

Table 4 Activation temperature of different types of thermal sensitive channels [186]

Activation Type	Channel code	Activation temperature
Heat	TRPV1 [188]	> 43 °C
	TRPV2 [189, 190]	> 52 °C
	TRPV3 [191, 192]	> 31 °C
	TRPV4 [193, 194]	> 25 °C
Cold	TRPM8 [195, 196]	< 28 °C
	TRPA1[197]	< 18 °C
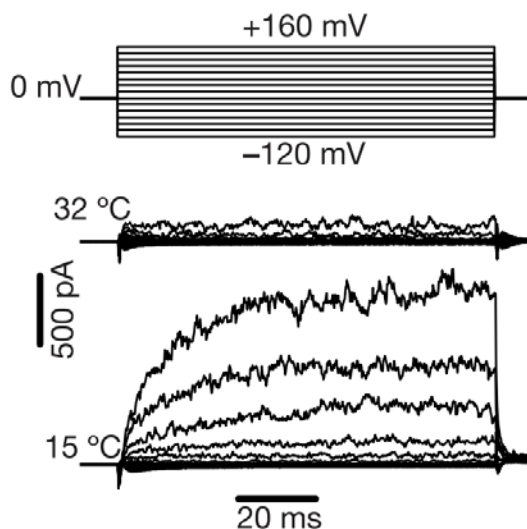
Figure 57 A sample experiment to study thermal activation of TRPM8 channel. [20]

It is believed that temperature measurement with high resolution would shed a light on the sensing mechanism on these ion channels and even quantitative study is possible. Interestingly, TRPV1 has a potent channel activator: capsaicin, active gradient in pepper and other "spicy" food. Other evidences are accumulating that natural compounds causing burning or cooling sensation act actually on these thermo

---

[20] Source of image: 186.   Voets, T., et al., *The principle of temperature-dependent gating in cold- and heat-sensitive TRP channels.* Nature, 2004. **430**(7001): p. 748-754.

sensitive channels [187, 196]. It would be interesting to do multiple perfusion tests with our PPM system.

This chapter will present experiments on a thermal PPM microfluidic platform. A prototype will be presented together with some preliminary data with regard to ceramide channels. A more sophisticated thin metal film based microchip design is presented and the challenges are also discussed.

7.2 First Generation of Thermal PPM Chip

To first validate that ceramide is responsive to changing temperature, a prototype device is designed and tested.

7.2.1 Thermal PPM Chip Design

As shown in Fig. 58, a recess is drilled at the back side of a PPM chip fabricated following description in Chapter 3 except no perfusion channels are integrated. Thermoelectric controller and a thermocouple are fixed to the recess by thermal compound. Black tape is applied to fix the whole assembly.

Membrane and ion channels are incorporated in same protocol described in section 3.1.2. The voltage supplied is then adjusted to create heat source or sink at the bottom surface of the recess, while the temperature can read out in a thermometer.
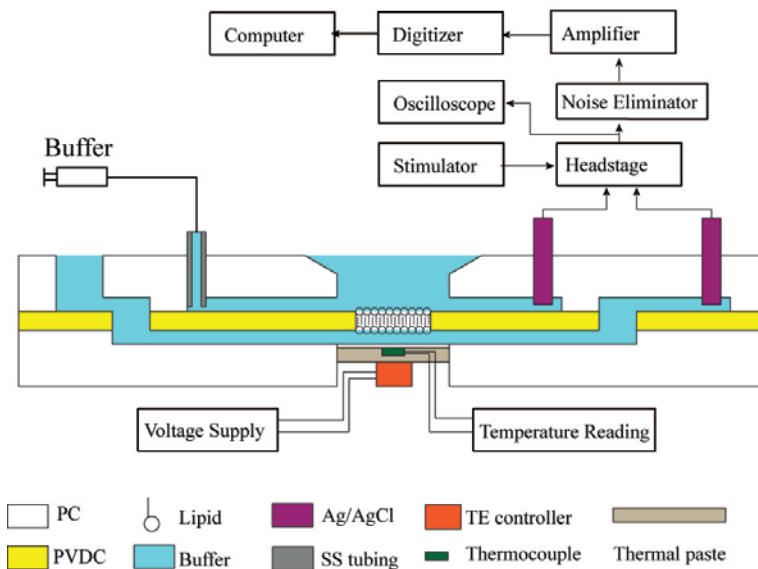
Figure 58 Schematic diagram for 1ˢᵗ generation thermal PPM chip.

It is very important to know the relationship between local temperature at the PPM and the temperature read from thermometer. However, directly dipping another thermometer to the open well is not practical. In fact sometimes, immersing another thermocouple to the open well can rupture membrane, probably by large static voltage. Thus a simple 2-D finite element model is stimulated to acquire some information from which the PPM temperature can be deduced from thermometer readings.
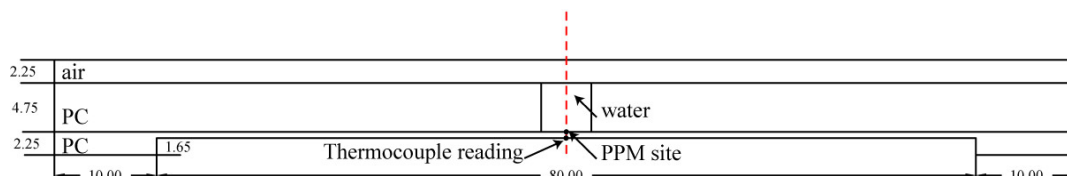
Figure 59 Dimensions for a COMSOL model to simulate the thermal behavior of thermal PPM prototype chip. Numbers are in mm.

As shown in Fig. 59, the model used here in COMSOL 3.5 simplified to PC, water and air system, neglecting the presence of PVDC and membrane. It is legitimate considering the thermal mass of PVDC film and membrane is very

small.The simulation parameters are shown in Table 5. The bottom of the recess is heated from 22 ℃ to 40 ℃ in 18 seconds, and all boundaries are set "insulation/symmetry" except those have contact with air. The heat transfer coefficient for air-contact surfaces are set 50 W/(m^2*K) to reflect the heat dissipation into room temperature air environment. The grid is created using default meshing command and refine command is repeated twice to get better accuracy. Fig. 60 shows the corresponding heating process from t = 0 s to t = 180 s simulated in COMSOL.

Table 5 Parameters for simulating the thermal behavior of model in Figure 45

Parameter		Value
Specific heat of PC	C_p *	1200 J/(K*kg)
Thermal conductivity of PC	k*	0.2 W/(m*K)
Density of PC	ρ*	1200 kg/m^3
Specific heat of water	C_p **	4181.3 J/(K*kg)
Thermal conductivity of water	k**	0.58 W/(m*K)
Density of water	ρ**	1000 kg/m^3
Specific heat of air	C_p**	1003.5 J/(K*kg)
Thermal conductivity of air	k**	0.024 W/(m*K)
Density of air	ρ**	1.2754 kg/m^3
Heating boundary conditions		(295.15+t*1[K/s])*(t<18)+(313.15)*(t>=18)
Air contacting boundaries		50 W/(m^2*K)

* Material properties for polycarbonate is got from goodfellow.com
** Material properties for water and air are from Wikipedia.com. Dry air properties are used.
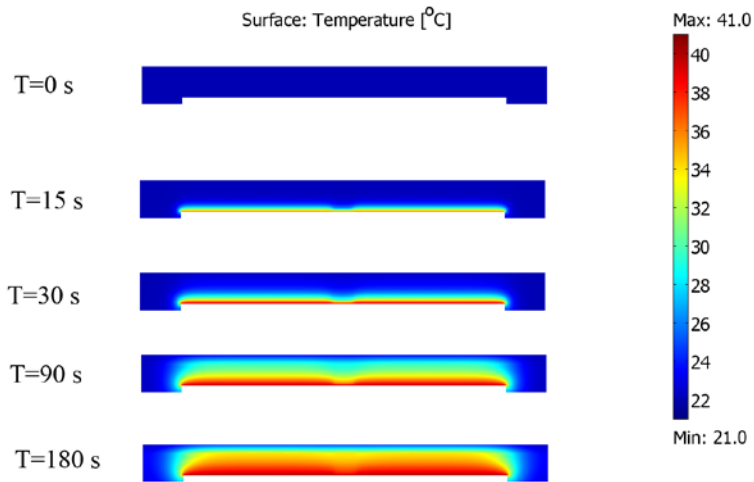
Figure 60 Heating process of the thermal PPM chip, simulated by COMSOL
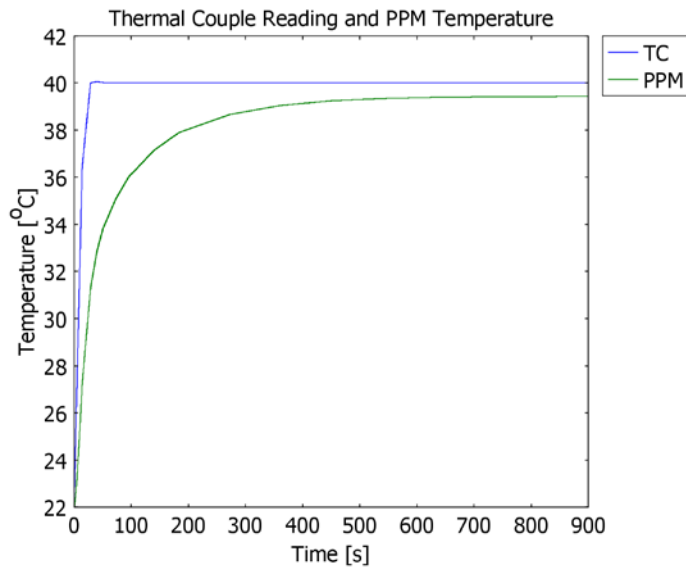
Figure 61 Temperature ramping curve of thermal couple reading site (TC, blue) and PPM site (PPM, green)

Fig. 61 shows the temperature ramping curve of PPM site and thermocouple reading site. It can be used to roughly estimate the temperature of PPM site with thermocouple reading.

7.2.2 Preliminary Results

As discussed in Section 4.1.1, ceramide channel is fundamentally different from protein ion channels. The composition of each channel, namely the number of molecules constituting the channel is different from one to another. The comparison between different experiments is almost meaningless until the formation process can be quantified based on experiment with one channel. Thus following results are all about temperature manipulation of one channel until the membrane burst. Other collective data of different experiments are not as exciting so as to reveal any mechanism of formation process.
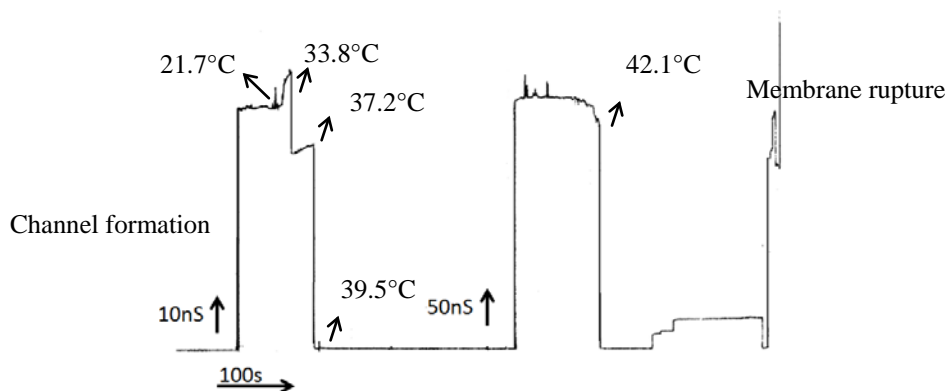
Figure 62 Trans-membrane conductance measurements during heating of the membrane site from room temperature to 42.1°C.

As shown in Fig. 62, the characteristic of ceramide channel conductance is largely different from a typical one (see Fig. 28). A typical ceramide channel usually undergoes continuous conductance growth until equilibrium while the heated ceramide channel display frequent opening and closing events. This is consistent with the expectation that increased thermal energy kT will generate larger vibration to the

hydrogen bondings and thus make the channel easier to jump out of the energy cavity in channel state.
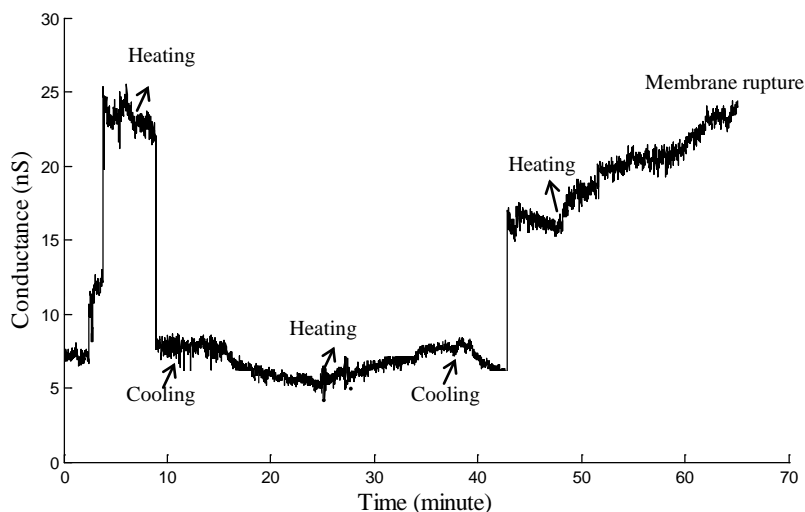
Figure 63 Trans-membrane conductance measurements during repetitive heating and cooling of the membrane site. Heating: 33 ºC, cooling: 25 ºC.

As shown in Fig. 63, another experiment shows that a ceramide channel conductance grows at cooling and decreases at heating. This is also consistent with the expectation that ceramide channel, linked through hydrogen bondings is like a piece of ice that would freeze into channel at low temperature and melt into rafts at higher temperature.

7.2.3 Challenges

Results shown in 7.2.2 are very preliminary, far from any mechanism revelation. Challenges with current design and current methodology can be classified into following categories:

1. Control experiments are not feasible in ceramide channel before any quantitation can be made on single channels.

2. Heated PPM tends to break more easily than PPM in room temperature. Together with 1st challenge, it is very difficult to have sufficient meaningful data in single channel. Otherwise, an extensive temperature manipulation of ceramide channel would largely improve the understanding of the temperature response.

3. Calibration of current thermal PPM devices need a well characterized thermal responsive channel other than ceramide channel. Since this 1st generation of PPM doesn't provide accurate temperature reading at the PPM site, the uncertainty of local PPM temperature and the uncertainty of ceramide channel thermal response tangle together, imposing difficulty to deduce useful information.

7.3 Thin Film Based Thermal PPM Chip

In response to the challenges listed above, here I demonstrate an effort to increase the thermal sensitivity and accuracy of PPM chip which could be pre-calibrated before PPM experiment.

7.3.1 Design

Microfluidics can be naturally integrated with enormous microfabrication methods available in semiconductor industry, such as metal deposition and etching. The method employed here to increase the functionality of PPM chip is to deposit a small resistor heater and resistor thermal detector (RTD) locally adjacent to the PPM.

121

As shown in Fig. 64, a thin layer of aluminum can be deposit on to finished PPM channels, trace from PPM site to the PC surface, through the slope of the tapped open well. To lower the stress introduced by unmatched coefficient of thermal expansion (CTE), a layer of parylene, nickel is deposited before aluminum. Another layer of parylene is deposited to protected aluminum trace from shorting through salty buffer in open well. Table 6 lists relevant material properties for this purpose.
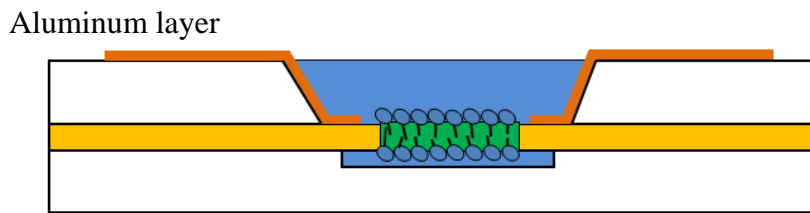
Aluminum layer

Figure 64 Thin film resistor heater and RTD by deposition an aluminum layer adjacent to PPM
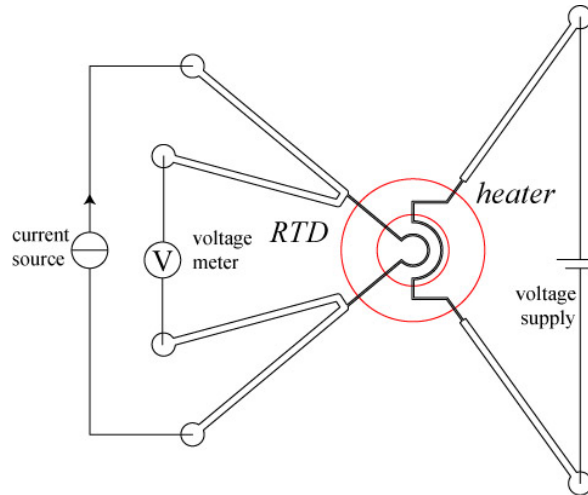
Figure 65 Schematics of thin film RTD and heater.

Shown in Fig. 65 is design of thin film RTD and heater and its connection to calibration electronics. The two red circles are edges of the tapped open well and PPM is right in the middle of the smaller circle. A voltage supply is connected to

122

resistor heater and voltage can be adjusted to output right power. A four-electrodes configuration is setup for resistance measurements for RTD.

Table 6 Properties of different materials.

Material	Resistivity (nΩ*m)	TCR* ($\times 10^{-3}$ /°C)	CTE** ($\times 10^{-6}$ /°C)
Pt	105	3.92	8.8
Ni	69.3	6	13.4
Al	28.2	6	23
Si	NA	NA	3
Parylene	NA	NA	3.5
PVDC	NA	NA	190
PC	NA	NA	66 ~ 70

* TCR: thermal coefficient of resistance
** CTE: coefficient of thermal expansion

5.3.2 Challenges

Unfortunately, the design presented in 4.3.1 didn't generate satisfactory results since the metal trace on PVDC layer always experience excessive stress which lead to crack or delamination of aluminum trace. Fig. 66 shows typical cracking failure.
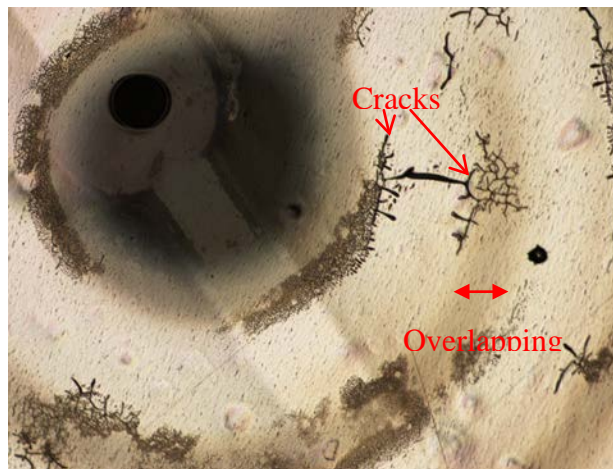
Figure 66 Failure of thin film metal trace on PVDC

First of all, the addition parylene layer between PVDC and Ni/Al helps stabilize the electrode trace a lot. It is probably due to eliminating stress introduced

by inherent atom or molecule mismatch. However, the cracks started to grow after stored in room temperature for several days. It is possibly mismatch of CTEs happening that leads to thermal residue stress and finally cracks. It is promising to using intermediate PVDC layer to mitigate this issue (show in Fig.67).
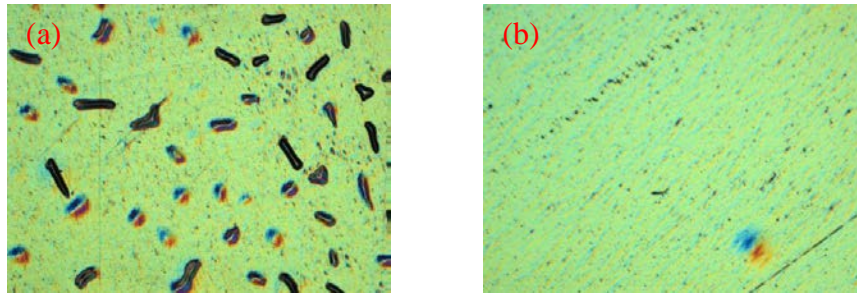
Figure 67 26 hours after deposition of aluminum film without (a) and with (b) parylene between PVDC

7.4 Future Work

See 8.2 and 8.4 in Chapter 8.

Chapter 8: Conclusion

Microfluidic PPM systems have promised unique contributions to characterization and quantification of ion channels. These systems can play an important role in improving our understanding of ion channel functions *in vivo*. As a bridge between micro-scale device to nano scale ion channels, microfluidic devices integrate different levels of elements, enabling studies that would not be possible in macro-scale devices. This dissertation focuses on the effort to integrate planar phospholipid membrane into microfludics and their utility to study dynamic aspects of ceramide channel and lipid microdomains. Through integration of membrane formation and buffer perfusion capability into microfluidics, both dynamic aspects of ceramide lipid ion channel and lipid microdomains are investigated for the first time. The technology advancement and biophysical studies presented here represent a steady step towards a fully functional PPM device that supports a broader scope of studies performed with *in vitro* reconstituted bilayers.

8.1 Summary of Intellectual Contributions

Since the birth of microfluidics, the community has long been searching for applications that are truly superior to traditional devices. In my opinion, the microfluidic PPM system is an excellent example that one can take advantage of the intrinsic properties of microfludics to probe properties of a subject of interest that are inaccessible otherwise. In particular, this dissertation focuses on the following three motivations of annulus-supported micro-PPM (AS-µPPM): 1) small fluidic volume in PPM chambers for dynamic studies based on rapid perfusion; 2) small thermal mass

for thermodynamic studies based on in-chip temperature controller and sensor; 3) horizontal configuration of PPM for electro-optical chip based on the compatibility to confocal microscope. As shown in Figure 68. These three motivations generated six conference papers as proof of concept, and two engineering papers, each for the dynamic aspect and the electro-optical aspect. Perfusion chip were used for studies of ceramide channels and one paper was submitted to PLoS One. In addition, Dr. Eric L Kendall and I developed a solvent free micro-PPM system (SF-µPPM) to realize the first asymmetric solvent free PPM in microfluidics. A conference paper for proof of concept and an engineering paper have been published.
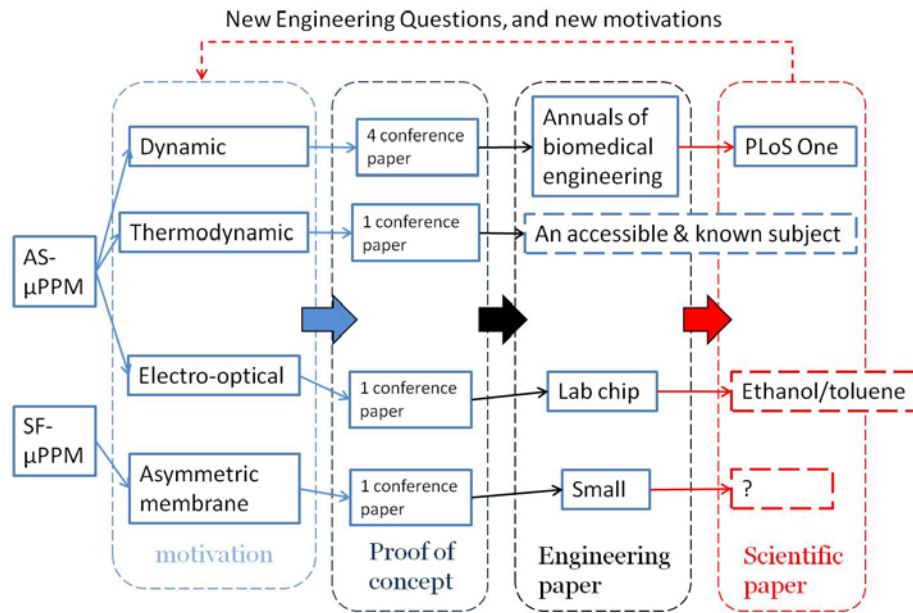
Figure 68 Technology roadmap and future directions of µPPM. See texts for details.

Perfusion Chip. Buffer exchange in a traditional bilayer system is possible but extra care is needed to avoid pressure induced membrane failure. Small volume in a microfluidic channel allows an easy and safe buffer exchange adjacent to the bilayer. Such capability is explored in this dissertation with a demonstration of ceramide ion

126

channel. Since the buffer condition and back pressure in microfluidic perfusion can be accurately predicted, quantitative studies are possible. Modulated opening and closing of ceramide channel was achieved through cyclic application of channel inhibitor La^{3+} and chelator EDTA. Based on the changes La^{3+} brought to membrane lateral pressure in an independent experiment, the gating of ceramide channel was interpreted as an elastic distortion response. Accordingly, a novel biconcave distortion model was proposed to explain such behavior, leading to a conductance ratio of the opening and closing state of ceramide channel that is consistent with experimental observations. Importantly, this perfusion scheme is virtually compatible to any micro-PPM systems.

Thermodynamic chip. While still in a preliminary stage, a microfluidic thermal PPM system was designed aiming to study the thermodynamic properties of lipid membrane and membrane proteins. The working principle of the device is demonstrated with thermal response of ceramide channels. With future development, this type of device can be really useful for revealing thermodynamic properties of ion channels with a much greater resolution than traditional PPM devices.

Electro-optical chip. In addition to electrophysiological recordings, Fluorescence observation of membrane and membrane proteins is another important probing method. A microfluidic PPM system is a perfect match for this purpose because the membrane in the microchip is horizontal, and thus compatible with microscopes. A plastic-glass hybrid chip was designed to enable confocal imaging of the membrane and the differential florescence properties of ordered and disordered lipid microdomains. With well-defined transmembrane pressure gradient by perfusion,

127

the response to pressure of a membrane with two liquid phases in co-existence is probed in real-time. The composition equilibrium between bilayer and supporting annulus is captured as lipid domain generation in early stages of membrane stabilization. The domain growth in response to moderate pressure shows lipid migration from annulus to bilayer. The following domain dissolution reveals that the line tension between domains becomes less significant as a larger transmembrane pressure increases the membrane tension. The system provided important tool to study ion channels with both electrical measurements and optical observations.

In situ **bilayer formation technique.** Along with the efforts mentioned above, this dissertation also covers a new *in situ* bilayer formation technique called "kiss and retreat" method. This method was meant to facilitate the membrane formation by eliminating the manual painting stage in original version of PPM chip developed by Dr. L. P. Hromada. The success rate with this method is significantly improved because the effect of human error is minimized. Since this is highly reproducible, it was then further employed to produce two parallel bilayers at one time, which could be very useful to study the mechanical and chemical interaction between two bilayers.

8.2 Future Development: Thermal PPM Chip

As discussed earlier, a high resolution of temperature controller and high accuracy is essential to study the thermal response of ion channels quantitatively. Thermal PPM chips will be redesigned to solve some critical drawbacks discussed in previous chapter. Thin film resistor heater and thermistor would be a big challenge to fabricate on plastic, particularly on thin film PVDC. The inherent and thermal stress introduced would significantly lower the performance and life time of the electrical

elements. Alternative approaches are necessary to address this problem. One promising approach is to integrate silicon based sensor into PPM chip.
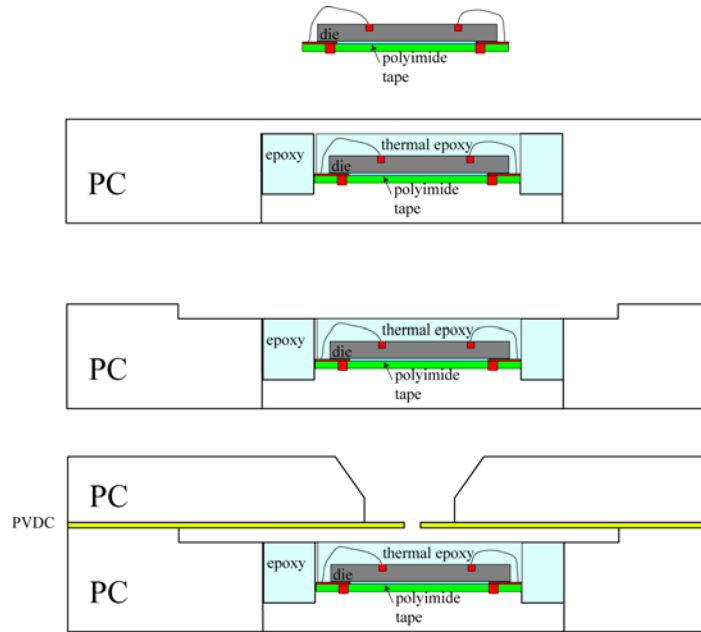
Figure 69 Si-in-Plastic design of thermal PPM Chip

As shown in Fig. 69, a polyimide tape patterned with metal trace is applied onto the back side of a silicon die where a resistive heater and diode temperature sensor are pre-fabricated. Gold wire connects the bond pads on silicon to the metal traces which lead to the soldering bump at the bottom. Then it can be fixed into a recess milled at the bottom of polycarbonate by thermal epoxy. A bottom channel at the top side of this PC can be milled such that the channel has direct contact with the thermal epoxy. PVDC patterning and thermal bonding can be performed as usual and final electrical connections can be made from the bump to electrical devices such as voltage supply and current meter (not shown).

The challenge in this design mainly lies on the packaging of bare die into PPM chip without compromising the chip integrity. However, it is outweighed by its

advantages. Firstly, it eliminates the need to fabricate metal traces on polymer, which has been a major challenge in this project. Second, the silicon microheater and temperature sensor can be well characterized or even bought from commercial vendor so the accuracy of the thermal control and measurement will be much better. Lastly, the bumping method used here conveniently connects the silicon chip to outer world electronics with only one photolithography step necessary to pattern the metal trace on polyimide tape.

As shown in Figure 68, it is important to utilize a well-known thermosensitive ion channel to calibrate the thermodynamic chip before we can apply it to study ceramide channels. These channels should have biological relevance and also readily accessible from vendors or through collaboration with a biology lab. TRP channels mentioned in Chapter 7 would be a good candidate, if purified TRP channels become commercially available.

8.3 Future Development: PPM With Pressure Calibration

It is observed that transmembrane pressure is a very important factor affecting the state of membrane or membrane proteins. Current transmembrane pressure is calculated as a product of perfusion volumetric flow rate and the hydraulic resistance of microfluidic channels. While it provides a fairly good estimation, a more precise and direct method based on an electronic sensor would greatly improve the accuracy and render a more useful tool for quantitative studies of membrane physics. Fortunately, the Si-in-Plastic design discussed in previous section can be applied to other silicon sensors as well. A pressure sensor can be integrated into the PPM chip with some modifications shown in Fig. 70. A commercialized pressure sensor with

backside open to bottom channel is fixed to the bottom of PPM chip. Electrical connection can be made directly from bond pad to electronics. Pressure sensing capability might help us to understand the relationship between stress state of membrane to ceramide channel gating, addressing the mechanism of La^{3+} ion disassembling ceramide channel.
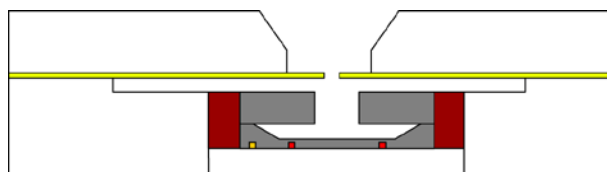
Figure 70 Design of Si-in-Polymer PPM design with pressure sensing capability.

8.3 Future Development and applications: Solvent-free Bilayers in Microchip

An important observation along this work is that ceramide channel in annulus supported membrane responds to mechanical stimulus introduced by La^{3+} differently compared to in solvent free PPM. To understand this difference and further shed light on the structure of ceramide channel, a practical microfluidic solvent-free membrane system needs to be developed. Dr. Eric Kendall in MML and I worked to developed a prototype of such system (Fig. 71) and observed lipid microdomains during the monolayer folding process. [21] This process can be also useful for creation of membranes that have different lipid compositions in each leaflet. Future directions of this work include optimization of the monolayer folding to achieve higher success rate and application to studies of asymmetric PPMs to mimic neuron cell membranes.

---

[21] This work has been composed to a manuscript "Visualizing the growth and dynamics of liquid-ordered domains during lipid bilayer folding in a microfluidic chip" and submitted to Small for review.
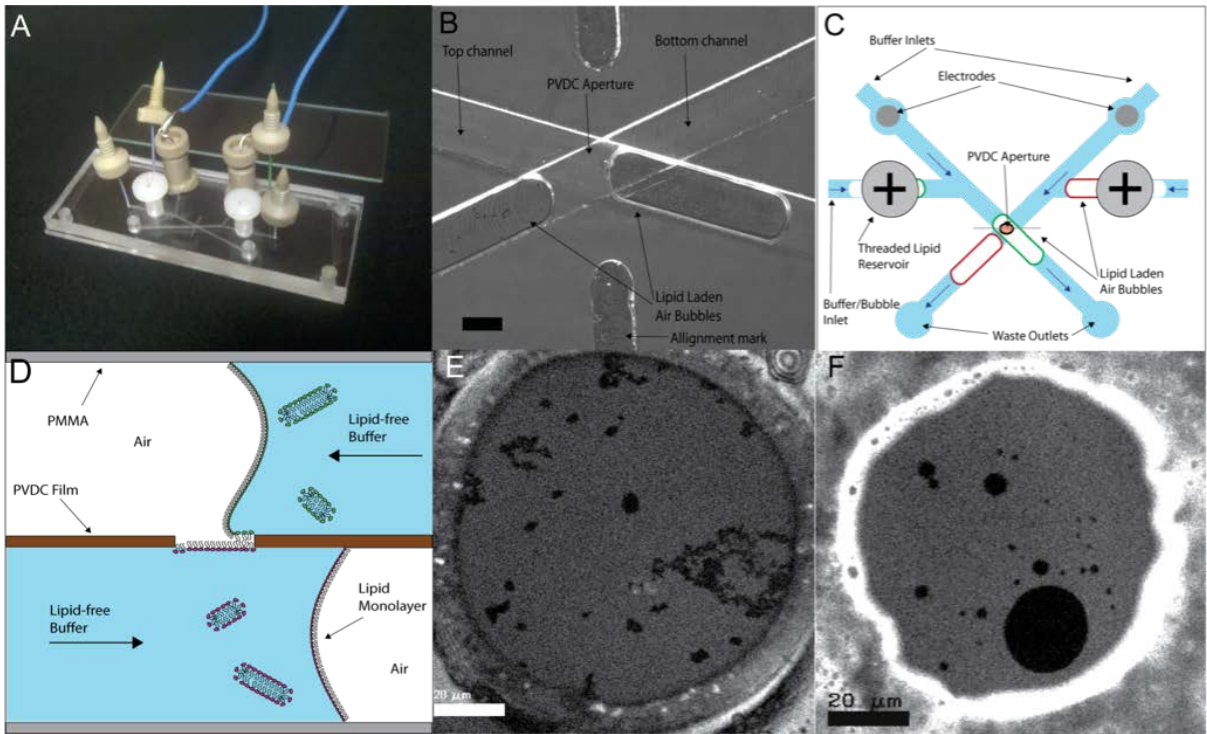
Figure 71 a) A fabricated thermoplastic microfluidic SF-Bilayer chip, next to a standard 75x25 mm microscope slide for scale. (b) Brightfield image of discrete lipid-laden air bubbles approaching the membrane formation site. (c) Chip layout schematic. (d) Side view diagram of the asymmetric monolayer folding process. (e) Confocal fluorescence image of a DPPC/PEG-40-stearate monolayer with gel-phase domains rich in DPPC. (f) Confocal fluorescence image of a bilayer composed of a 1:1:1 mixture of DPPC:DPhPC:cholesterol, where dark regions indicate liquid ordered domains rich in DPPC/cholesterol. Scale bars in (e) and (f) are both 20 μm.

8.4 Future Application: Ceramide Thermodynamic Studies

Thermodynamic studies of ceramide channel will further advance our understanding. Following steps are essential to a successful investigation.

1. The fragility of PPM at elevated temperature will be thoroughly investigated. Necessary measures will be taken to maintain high stability and long life-time of the membrane.

2. Well characterized thermal responsive ion channels will be used to validate the performance of new PPM devices before ceramide channel is studied. A good

132

model ion channel is gramicidin A. The temperature dependence of activation energies of proton transfer in gramicidin A channel has been well characterized between 4 ℃ and 40 ℃ [198]. The effort will be made to replicate the data in gramicidin A.

3. Longer life time of PPM at high temperature and more accurate temperature controlling and sensing should allow us to do better job collecting data with one single ion channel. Single channel quantification of such a ceramide channel should be pursued before the knowledge can be applied to ceramide channels with wider conductance range.

4. A simpler quantitative thermodynamic model than equation set (*) in 7.1.1 needs to be developed for ceramide channel. Details for the following formulation can be found in reference [150].Assuming the ceramide channel assembly and disassembly can be described in following process:

$$C_m \underset{k_{-1}}{\overset{k_1}{\rightleftharpoons}} C_{i1} \underset{k_{-2}}{\overset{k_2}{\rightleftharpoons}} C_{i2}... \underset{k_{-n}}{\overset{k_n}{\rightleftharpoons}} C_{in} \underset{k_{-n-1}}{\overset{k_{n+1}}{\rightleftharpoons}} C_c$$
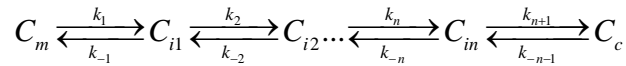
Where C_m represents ceramide molecules, C_{in} represents ceramide in nth intermediate state, and C_c represents ceramide channel. To further simplify the model, we can assume that k_1 is the activation step for forward reaction, which limits rate of the channel formation, and k_{-n-1} is the activation step for backward reaction, which limits rate of the channel disassembly. It is guessed that k_1 may describe the energy barrier of ceramide rafts rotation initially to form an aqueous pore spanning across the membrane, and k_{-n-1} may describe the energy needed to break hydrogen

bondings in ceramide channel to promote channel collapse. This will further assume that once ceramide enters the C_{i1} state, it will quickly form a channel; and once a ceramide channel enters the C_{in} state, it will quickly collapse.

For a given ceramide concentration in a lipid membrane at initial temperature T_0, we can adjust the temperature target $T_1 > T_0$ and ceramide channel is expected to form since higher temperature will provide more energy to overcome E_a. The relationship between percentage of ceramide channel opening to dwell time (which is the time period between temperature switching and channel formation) in multiple tests can be plotted. Depending on the shape of the curve, the order of reaction can be decided and k_1 for temperature T_1 can be calculated. k_1 at other temperature can be determined in a similar manner. k_{-n-1} for different temperatures can be determined by examining the relationship between percentage of ceramide channel closing to dwell time upon temperature increase given an existing ceramide channel is the initial condition.

Using Arrhenious plot: $\ln k_1 = -\left(\dfrac{E_a}{RT}\right) + \ln A_+$ and $\ln k_{-n-1} = -\left(\dfrac{E_{-a}}{RT}\right) + \ln A_-$, where E_a and E_{-a} is activation energy for k_1 and k_{-n-1} processs, R is nature gas constant, T is temperature in K, and A_+ and A_- are pre-exponential factor, the activation energy E_a and E_{-a} can be determined. Then the enthalpy and entropy change of k_1 process can be estimated as $\Delta H_1 \approx E_a$ and $\Delta S_1 \approx R \ln(\dfrac{A_+ h}{k_B T})$. The free energy for this step can be determined as $\Delta G_1 = \Delta H_1 - T\Delta S_1$. Similarly those of k_{-n-1}

process can be estimated as $\Delta H_{-n-1} \approx E_{-a}$, $\Delta S_{-n-1} \approx R \ln(\frac{A\_h}{k_B T})$ and

$\Delta G_{-n-1} = \Delta H_{-n-1} - T \Delta S_{-n-1}$, where h is Planck's constant and k_B is the Boltzmann's

constant.

Assuming there is only one intermediate state C_i, i.e. the process can be

simplified as $C_m \underset{k_{-1}}{\overset{k_1}{\rightleftarrows}} C_i \underset{k_{-2}}{\overset{k_2}{\rightleftarrows}} C_c$, then overall free energy can be determined

$\Delta G = \Delta G_1 - \Delta G_{-1}$ shown in Figure 72.
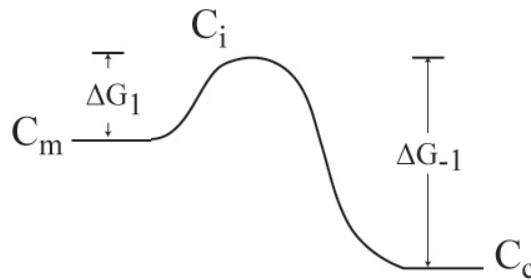
Figure 72 Progress of ceramide channel formation according to transition state theory.

8.5 Future Application: Electro-optical Studies of Membrane

The combination of confocal imaging and the perfusion capability in PPM

chips is a powerful tool for the study of membranes and membrane proteins. It

supports sequential injection or removal of (bio)chemicals and well defined

transmembrane pressure. Interesting applications include studies of protein

localizations to different domains and their optical and electrical responses to

different (bio)chemical and mechanical stimuli.

Glossary

α-HL: Alpha-hemolysin
BLM: Bilayer lipid membrane or Black lipid membrane
C_2-ceramide: N-acetoyl-D-erythro-sphingosine
C_{16}-ceramide: N-palmitoyl-D-erythro-sphingosine
COC: Cyclic olefin copolymer
COP: Cyclic olefin polymer
CTE: Coefficient of Thermal Expansion
DiPhyPC: 1,2-diphytanoyl-sn-glycero-3-phosphocholine
DPPC: 1,2-dipalmitoyl-sn-glycero-3-phosphocholine
POPC: 1-palmitoyl-2-oleoyl-sn-glycero-3-phosphocholine
PSM: N-palmitoyl-D-*erythro*-sphingosylphosphorylcholine
TR-DHPE:Texas Red labeled 1,2-dihexadecanoyl-sn-glycero-3-phosphoethanolamine
DRIE: Deep reaction ion etching
FEP: fluorinated ethylene propylene copolymer
PC: Polycarbonate
PET: Polyethylene terephthalate
PMMA: Poly(methyl methacrylate)
PTFE: polytetrafluoroethylene
PVDC: Polyvinylidene chloride
PPM: Planar phospholipid membrane
RTD: Resistor Thermal Detector
TCR: Thermal Coefficient of Resistivity

Bibliography

1. Gurr, M.I., K.N. Frayn, and J.L. Harwood, *Lipid biochemistry*. 5th ed2002, Malden, MA: Blackwell Science. xv, 320 p.
2. Silverstein, T.P., *The real reason why oil and water don't mix.* Journal of Chemical Education, 1998. **75**(1): p. 116-118.
3. Vance, D.E. and J.E. Vance, *Biochemistry of lipids, lipoproteins and membranes*. 5th ed2008, Amsterdam ; Boston: Elsevier. xii, 631, 8 p. of col. plates.
4. Hille, B., *Ion channels of excitable membranes*. 3rd ed2001, Sunderland, Mass.: Sinauer. xviii, 814 p.
5. Kew, J.N.C. and C.H. Davies, *Ion channels : from structure to function*. 2nd ed2010, Oxford: Oxford University Press. xiii, 562 p.
6. Siskind, L.J., et al., *Enlargement and contracture of C-2-ceramide channels.* Biophysical Journal, 2003. **85**(3): p. 1560-1575.
7. Siskind, L.J. and M. Colombini, *The lipids C-2- and C-16-ceramide form large stable channels - Implications for apoptosis.* Journal of Biological Chemistry, 2000. **275**(49): p. 38640-38644.
8. Siskind, L.J., R.N. Kolesnick, and M. Colombini, *Ceramide channels increase the permeability of the mitochondrial outer membrane to small proteins.* Journal of Biological Chemistry, 2002. **277**(30): p. 26796-26803.
9. Siskind, L.J., et al., *Anti-apoptotic Bcl-2 family proteins disassemble ceramide channels.* Journal of Biological Chemistry, 2008. **283**(11): p. 6622-6630.
10. Ganesan, V., et al., *Ceramide and activated Bax act synergistically to permeabilize the mitochondrial outer membrane.* Apoptosis, 2010. **15**(5): p. 553-562.
11. Siskind, L.J., R.N. Kolesnick, and M. Colombini, *Ceramide forms channels in mitochondrial outer membranes at physiologically relevant concentrations.* Mitochondrion, 2006. **6**(3): p. 118-125.
12. Anishkin, A., S. Sukharev, and M. Colombini, *Searching for the molecular arrangement of transmembrane ceramide channels.* Biophysical Journal, 2006. **90**(7): p. 2414-2426.
13. Siskind, L.J., et al., *Sphingosine forms channels in membranes that differ greatly from those formed by ceramide.* Journal of Bioenergetics and Biomembranes, 2005. **37**(4): p. 227-236.
14. Stiban, J., D. Fistere, and M. Colombini, *Dihydroceramide hinders ceramide channel formation: Implications on apoptosis.* Apoptosis, 2006. **11**(5): p. 773-780.
15. Colombini, M., *Ceramide channels and their role in mitochondria-mediated apoptosis.* Biochimica Et Biophysica Acta-Bioenergetics, 2010. **1797**(6-7): p. 1239-1244.
16. Neher, E., B. Sakmann, and J.H. Steinbach, *Extracellular Patch Clamp - Method for Resolving Currents through Individual Open Channels in Biological-Membranes.* Pflugers Archiv-European Journal of Physiology, 1978. **375**(2): p. 219-228.

17. Neher, E. and B. Sakmann, *Single-Channel Currents Recorded from Membrane of Denervated Frog Muscle-Fibers.* Nature, 1976. **260**(5554): p. 799-802.

18. Sakmann, B., E. Neher, and SpringerLink (Online service), *Single-Channel Recording*, 2009, Springer Science+Business Media, LLC: Boston, MA.

19. Miller, C., *Ion channel reconstitution* 1986, New York: Plenum Press. xxi, 577 p.

20. Mueller, P., et al., *Reconstitution of Excitable Cell Membrane Structure in Vitro.* Circulation, 1962. **26**(5): p. 1167-1171.

21. Mueller, P., et al., *Reconstitution of Cell Membrane Structure in Vitro and Its Transformation into an Excitable System.* Nature, 1962. **194**(4832): p. 979-980.

22. Mueller, P., et al., *Methods for Formation of Single Bimolecular Lipid Membranes in Aqueous Solution.* Journal of Physical Chemistry, 1963. **67**(2): p. 534-535.

23. Ide, T. and T. Yanagida, *An artificial lipid bilayer formed on an agarose-coated glass for simultaneous electrical and optical measurement of single ion channels.* Biochemical and Biophysical Research Communications, 1999. **265**(2): p. 595-599.

24. Malmstadt, N., et al., *Automated formation of lipid-bilayer membranes in a microfluidic device.* Nano Letters, 2006. **6**(9): p. 1961-1965.

25. Funakoshi, K., H. Suzuki, and S. Takeuchi, *Lipid bilayer formation by contacting monolayers in a microfluidic device for membrane protein analysis.* Analytical Chemistry, 2006. **78**(24): p. 8169-8174.

26. Castellana, E.T. and P.S. Cremer, *Solid supported lipid bilayers: From biophysical studies to sensor design.* Surface Science Reports, 2006. **61**(10): p. 429-444.

27. Tamm, L.K. and H.M. McConnell, *Supported phospholipid bilayers.* Biophysical Journal, 1985. **47**(1): p. 105-13.

28. Gufler, P.C., et al., *Highly robust lipid membranes on crystalline S-layer supports investigated by electrochemical impedance spectroscopy.* Biochimica Et Biophysica Acta-Biomembranes, 2004. **1661**(2): p. 154-165.

29. Sackmann, E., *Supported membranes: Scientific and practical applications.* Science, 1996. **271**(5245): p. 43-48.

30. Sackmann, E. and M. Tanaka, *Supported membranes on soft polymer cushions: fabrication, characterization and applications.* Trends in Biotechnology, 2000. **18**(2): p. 58-64.

31. Plant, A.L., M. Gueguetchkeri, and W. Yap, *Supported phospholipid/alkanethiol biomimetic membranes: insulating properties.* Biophysical Journal, 1994. **67**(3): p. 1126-33.

32. Florin, E.L. and H.E. Gaub, *Painted supported lipid membranes.* Biophysical Journal, 1993. **64**(2): p. 375-83.

33. Cornell, B.A., et al., *A biosensor that uses ion-channel switches.* Nature, 1997. **387**(6633): p. 580-583.

34. Terrettaz, S., et al., *Immunosensing by a synthetic ligand-gated ion channel.* Angewandte Chemie-International Edition, 2001. **40**(9): p. 1740-1743.

35. Nikolelis, D.P. and C.G. Siontorou, *Bilayer-Lipid Membranes for Flow-Injection Monitoring of Acetylcholine, Urea, and Penicillin.* Analytical Chemistry, 1995. **67**(5): p. 936-944.

36. Hennesthal, C. and C. Steinem, *Pore-spanning lipid bilayers visualized by scanning force microscopy.* Journal of the American Chemical Society, 2000. **122**(33): p. 8085-8086.

37. Favero, G., et al., *Membrane supported bilayer lipid membranes array: preparation, stability and ion-channel insertion.* Analytica Chimica Acta, 2002. **460**(1): p. 23-34.

38. Matsuno, Y., et al., *Single-channel recordings of gramicidin at agarose-supported bilayer lipid membranes formed by the tip-dip and painting methods.* Analytical Sciences, 2004. **20**(8): p. 1217-1221.

39. Atanasov, V., et al., *Membrane on a chip: A functional tethered lipid bilayer membrane on silicon oxide surfaces.* Biophysical Journal, 2005. **89**(3): p. 1780-1788.

40. Reimhult, E. and K. Kumar, *Membrane biosensor platforms using nano- and microporous supports.* Trends in Biotechnology, 2008. **26**(2): p. 82-89.

41. Schuster, B., et al., *New method for generating tetraether lipid membranes on porous supports.* Langmuir, 2003. **19**(6): p. 2392-2397.

42. Schiller, S.M., et al., *Archaea analogue thiolipids for tethered bilayer lipid membranes on ultrasmooth gold surfaces.* Angewandte Chemie-International Edition, 2003. **42**(2): p. 208-211.

43. Terrettaz, S., M. Mayer, and H. Vogel, *Highly electrically insulating tethered lipid bilayers for probing the function of ion channel proteins.* Langmuir, 2003. **19**(14): p. 5567-5569.

44. Schuster, B., et al., *S-layer ultrafiltration membranes: A new support for stabilizing functionalized lipid membranes.* Langmuir, 2001. **17**(2): p. 499-503.

45. Fujiwara, H., M. Fujihara, and T. Ishiwata, *Dynamics of the spontaneous formation of a planar phospholipid bilayer: A new approach by simultaneous electrical and optical measurements.* Journal of Chemical Physics, 2003. **119**(13): p. 6768-6775.

46. Niles, W.D., R.A. Levis, and F.S. Cohen, *Planar Bilayer-Membranes Made from Phospholipid Monolayers Form by a Thinning Process.* Biophysical Journal, 1988. **53**(3): p. 327-335.

47. Colombini, M., *Voltage gating in the mitochondrial channel, VDAC.* J Membr Biol, 1989. **111**(2): p. 103-11.

48. Montal, M. and P. Mueller, *Formation of Bimolecular Membranes from Lipid Monolayers and a Study of Their Electrical Properties.* Proceedings of the National Academy of Sciences of the United States of America, 1972. **69**(12): p. 3561-3566.

49. Requena, J. and D.A. Haydon, *Van der Waals forces in oil-water systems from the study of thin lipid film II. The dependence of the van der Waals free energy of thinning on film composition and structure.* Proc. R. Soc. Lond. A., 1975. **347**: p. 17.

50.   White, S.H., *Analysis of Torus Surrounding Planar Lipid Bilayer Membranes.* Biophysical Journal, 1972. **12**(4): p. 432-&.

51.   Hromada, L., *Bilayer Lipid Membrane (BLM) Integration Into Microfludic Platforms With Application Toward BLM-Based Biosensors*, in *Department of Mechanical Engineering*2007, University of Maryland: College Park.

52.   Ross, E.E., et al., *Planar supported lipid bilayer polymers formed by vesicle fusion. 1. Influence of diene monomer structure and polymerization method on film properties.* Langmuir, 2003. **19**(5): p. 1752-1765.

53.   Nikolelis, D.P. and M. Mitrokotsa, *Stabilized lipid film based biosensor for atenolol.* Biosensors & Bioelectronics, 2002. **17**(6-7): p. 565-572.

54.   Shenoy, D.K., et al., *Functional reconstitution of protein ion channels into planar polymerizable phospholipid membranes.* Nano Letters, 2005. **5**(6): p. 1181-1185.

55.   Heitz, B.A., et al., *Enhanced long-term stability for single ion channel recordings using suspended poly(lipid) bilayers.* J Am Chem Soc, 2009. **131**(19): p. 6662-3.

56.   Jeon, T.J., J.L. Poulos, and J.J. Schmidt, *Long-term storable and shippable lipid bilayer membrane platform.* Lab on a Chip, 2008. **8**(10): p. 1742-1744.

57.   Kang, X.F., et al., *A storable encapsulated bilayer chip containing a single protein nanopore.* Journal of the American Chemical Society, 2007. **129**(15): p. 4701-4705.

58.   Jeon, T.J., N. Malmstadt, and J.J. Schmidt, *Hydrogel-encapsulated lipid membranes.* Journal of the American Chemical Society, 2006. **128**(1): p. 42-3.

59.   Beddow, J.A., et al., *Reconstitution of nicotinic acetylcholine receptors into gel-protected lipid membranes.* Analytical Chemistry, 2004. **76**(8): p. 2261-5.

60.   Shim, J.W. and L.Q. Gu, *Stochastic sensing on a modular chip containing a single-ion channel.* Analytical Chemistry, 2007. **79**(6): p. 2207-13.

61.   Koulen, P., et al., *Polycystin-2 is an intracellular calcium release channel.* Nature Cell Biology, 2002. **4**(3): p. 191-197.

62.   Schmidt, C., M. Mayer, and H. Vogel, *A chip-based biosensor for the functional analysis of single ion channels.* Angewandte Chemie-International Edition, 2000. **39**(17): p. 3137-3140.

63.   Ogier, S.D., et al., *Suspended planar phospholipid bilayers on micromachined supports.* Langmuir, 2000. **16**(13): p. 5696-5701.

64.   Cheng, Y.L., et al., *Single ion channel sensitivity in suspended bilayers on micromachined supports.* Langmuir, 2001. **17**(4): p. 1240-1242.

65.   Pantoja, R., et al., *Bilayer reconstitution of voltage-dependent ion channels using a microfabricated silicon chip.* Biophysical Journal, 2001. **81**(4): p. 2389-2394.

66.   Fertig, N., et al., *Microstructured glass chip for ion-channel electrophysiology.* Physical Review E, 2001. **64**(4): p. 040901.

67.   Fertig, N., et al., *Microstructured apertures in planar glass substrates for ion channel research.* Receptors & Channels, 2003. **9**(1): p. 29-40.

68.   Suzuki, H., et al., *Planar lipid bilayer reconstitution with a micro-fluidic system.* Lab on a Chip, 2004. **4**(5): p. 502-505.

69.   Suzuki, H., et al., *Highly reproducible method of planar lipid bilayer reconstitution in polymethyl methacrylate microfluidic chip.* Langmuir, 2006. **22**(4): p. 1937-1942.

70.   Holden, M.A., D. Needham, and H. Bayley, *Functional bionetworks from nanoliter water droplets.* Journal of the American Chemical Society, 2007. **129**(27): p. 8650-8655.

71.   Hwang, W.L., et al., *Electrical behavior of droplet interface bilayer networks: Experimental analysis and Modeling.* Journal of the American Chemical Society, 2007. **129**(38): p. 11854-11864.

72.   Hwang, W.L., et al., *Asymmetric droplet interface bilayers.* Journal of the American Chemical Society, 2008. **130**(18): p. 5878-+.

73.   Bayley, H., et al., *Droplet interface bilayers.* Molecular Biosystems, 2008. **4**(12): p. 1191-1208.

74.   Sandison, M.E. and H. Morgan, *Rapid fabrication of polymer microfluidic systems for the production of artificial lipid bilayers.* Journal of Micromechanics and Microengineering, 2005. **15**(7): p. S139-S144.

75.   Sandison, M.E., et al., *Micromachined glass apertures for artificial lipid bilayer formation in a microfluidic system.* Journal of Micromechanics and Microengineering, 2007. **17**(7): p. S189-S196.

76.   Hromada, L.P., et al., *Single molecule measurements within individual membrane-bound ion channels using a polymer-based bilayer lipid membrane chip.* Lab on a Chip, 2008. **8**(4): p. 602-608.

77.   Suzuki, H., B. Le Pioufle, and S. Takeuhci, *Ninety-six-well planar lipid bilayer chip for ion channel recording Fabricated by hybrid stereolithography.* Biomedical Microdevices, 2009. **11**(1): p. 17-22.

78.   Zagnoni, M., M.E. Sandison, and H. Morgan, *Microfluidic array platform for simultaneous lipid bilayer membrane formation.* Biosensors & Bioelectronics, 2009. **24**(5): p. 1235-1240.

79.   Le Pioufle, B., et al., *Lipid bilayer microarray for parallel recording of transmembrane ion currents.* Analytical Chemistry, 2008. **80**(1): p. 328-332.

80.   Duffy, D.C., et al., *Rapid prototyping of microfluidic systems in poly(dimethylsiloxane).* Analytical Chemistry, 1998. **70**(23): p. 4974-4984.

81.   McCormick, R.M., et al., *Microchannel electrophoretic separations of DNA in injection-molded plastic substrates.* Analytical Chemistry, 1997. **69**(14): p. 2626-2630.

82.   Roberts, M.A., et al., *UV laser machined polymer substrates for the development of microdiagnostic systems.* Analytical Chemistry, 1997. **69**(11): p. 2035-2042.

83.   Martynova, L., et al., *Fabrication of plastic microfluid channels by imprinting methods.* Analytical Chemistry, 1997. **69**(23): p. 4783-4789.

84.   Harrison, D.J., et al., *Micromachining a Miniaturized Capillary Electrophoresis-Based Chemical-Analysis System on a Chip.* Science, 1993. **261**(5123): p. 895-897.

85.   Boone, T., et al., *Plastic advances microfluidic devices.* Analytical Chemistry, 2002. **74**(3): p. 78a-86a.

86.   Chen, C.F., et al., *High-pressure needle interface for thermoplastic microfluidics.* Lab on a Chip, 2009. **9**(1): p. 50-55.

87.   Zagnoni, M., et al., *Controlled delivery of proteins into bilayer lipid membranes on chip.* Lab on a Chip, 2007. **7**(9): p. 1176-83.

88.   Sandison, M.E., M. Zagnoni, and H. Morgan, *Air-exposure technique for the formation of artificial lipid bilayers in microsystems.* Langmuir, 2007. **23**(15): p. 8277-8284.

89.   Suzuki, H., et al., *Electrophysiological recordings of single ion channels in planar lipid bilayers using a polymethyl methacrylate microfluidic chip.* Biosensors & Bioelectronics, 2007. **22**(6): p. 1111-1115.

90.   Oconnell, A.M., R.E. Koeppe, and O.S. Andersen, *Kinetics of Gramicidin Channel Formation in Lipid Bilayers - Transmembrane Monomer Association.* Science, 1990. **250**(4985): p. 1256-1259.

91.   Woolley, G.A. and B.A. Wallace, *Model Ion Channels - Gramicidin and Alamethicin.* Journal of Membrane Biology, 1992. **129**(2): p. 109-136.

92.   Chiantia, S., et al., *Role of ceramide in membrane protein organization investigated by combined AFM and FCS.* Biochimica Et Biophysica Acta-Biomembranes, 2008. **1778**(5): p. 1356-1364.

93.   Reed, K.C. and F.L. Bygrave, *The inhibition of mitochondrial calcium transport by lanthanides and ruthenium red.* Biochemical Journal, 1974. **140**(2): p. 143-55.

94.   Hammoudah, M.M., et al., *Interactions of La3+ with phosphatidylserine vesicles. Binding, phase transition, leakage and fusion.* Biochimica Et Biophysica Acta, 1979. **558**(3): p. 338-43.

95.   Akutsu, H. and J. Seelig, *Interaction of metal ions with phosphatidylcholine bilayer membranes.* Biochemistry, 1981. **20**(26): p. 7366-73.

96.   Seelig, J., P.M. Macdonald, and P.G. Scherer, *Phospholipid head groups as sensors of electric charge in membranes.* Biochemistry, 1987. **26**(24): p. 7535-41.

97.   Bentz, J., et al., *La3+-induced fusion of phosphatidylserine liposomes. Close approach, intermembrane intermediates, and the electrostatic surface potential.* Biophysical Journal, 1988. **53**(4): p. 593-607.

98.   Petersheim, M. and J. Sun, *On the coordination of La3+ by phosphatidylserine.* Biophysical Journal, 1989. **55**(4): p. 631-6.

99.   Tanaka, T., et al., *La(3+) stabilizes the hexagonal II (H(II)) phase in phosphatidylethanolamine membranes.* Biochimica Et Biophysica Acta, 2001. **1515**(2): p. 189-201.

100.   Hsu, Y.T., K.G. Wolter, and R.J. Youle, *Cytosol-to-membrane redistribution of Bax and Bcl-X(L) during apoptosis.* Proc Natl Acad Sci U S A, 1997. **94**(8): p. 3668-72.

101.   Hausmann, G., et al., *Pro-apoptotic apoptosis protease-activating factor 1 (Apaf-1) has a cytoplasmic localization distinct from Bcl-2 or Bcl-x(L).* J Cell Biol, 2000. **149**(3): p. 623-34.

102.   Wiesner, D.A., et al., *Anti-immunoglobulin-induced apoptosis in WEHI 231 cells involves the slow formation of ceramide from sphingomyelin and is blocked by bcl-XL.* J Biol Chem, 1997. **272**(15): p. 9868-76.

103. Yethon, J.A., et al., *Interaction with a membrane surface triggers a reversible conformational change in Bax normally associated with induction of apoptosis.* J Biol Chem, 2003. **278**(49): p. 48935-41.

104. Billen, L.P., et al., *Bcl-XL inhibits membrane permeabilization by competing with Bax.* PLoS Biol, 2008. **6**(6): p. e147.

105. Jeong, S.Y., et al., *Bcl-x(L) sequesters its C-terminal membrane anchor in soluble, cytosolic homodimers.* EMBO J, 2004. **23**(10): p. 2146-55.

106. Taylor, G., *Dispersion of Soluble Matter in Solvent Flowing Slowly Through a Tube.* Proceedings of the Royal Society of London. Series A, Mathematical and Physical Science, 1953. **219**: p. 8.

107. Ganesan, V. and M. Colombini, *Regulation of ceramide channels by Bcl-2 family proteins.* Febs Letters, 2010. **584**(10): p. 2128-2134.

108. Samanta, S., et al., *Visualization of ceramide channels by transmission electron microscopy.* Biochimica Et Biophysica Acta-Biomembranes, 2011. **1808**(4): p. 1196-1201.

109. Ermakov, Y.A., et al., *Gadolinium Ions Block Mechanosensitive Channels by Altering the Packing and Lateral Pressure of Anionic Lipids.* Biophysical Journal, 2010. **98**(6): p. 1018-1027.

110. Heimburg, T., *Lipid ion channels.* Biophysical Chemistry, 2010. **150**(1-3): p. 2-22.

111. Heimburg, T. and A.D. Jackson, *The thermodynamics of general anesthesia.* Biophysical Journal, 2007. **92**(9): p. 3159-3165.

112. Basanez, G., et al., *Bax, but not Bcl-x(L), decreases the lifetime of planar phospholipid bilayer membranes at subnanomolar concentrations.* Proceedings of the National Academy of Sciences of the United States of America, 1999. **96**(10): p. 5492-5497.

113. Shao, C.R., et al., *Rapid Microfluidic Perfusion Enabling Kinetic Studies of Lipid Ion Channels in a Bilayer Lipid Membrane Chip.* Annals of Biomedical Engineering, 2011. **39**(8): p. 2242-2251.

114. Cantor, R.S., *The influence of membrane lateral pressures on simple geometric models of protein conformational equilibria.* Chemistry and Physics of Lipids, 1999. **101**(1): p. 45-56.

115. Gullingsrud, J. and K. Schulten, *Lipid bilayer pressure profiles and mechanosensitive channel gating.* Biophys J, 2004. **86**(6): p. 3496-509.

116. Linke, W.A., *Stretching molecular springs: elasticity of titin filaments in vertebrate striated muscle.* Histol Histopathol, 2000. **15**(3): p. 799-811.

117. van Meer, G., *Lipid traffic in animal cells.* Annu Rev Cell Biol, 1989. **5**: p. 247-75.

118. Bretscher, M.S., *Membrane Structure - Some General Principles.* Science, 1973. **181**(4100): p. 622-629.

119. Parton, R.G., *Caveolae and caveolins.* Curr Opin Cell Biol, 1996. **8**(4): p. 542-8.

120. Anderson, R.G.W., *The caveolae membrane system.* Annual Review of Biochemistry, 1998. **67**: p. 199-225.

121. Parton, R.G. and K. Simons, *The multiple faces of caveolae.* Nat Rev Mol Cell Biol, 2007. **8**(3): p. 185-94.

122. Chidlow, J.H., Jr. and W.C. Sessa, *Caveolae, caveolins, and cavins: complex control of cellular signalling and inflammation.* Cardiovasc Res, 2010. **86**(2): p. 219-25.

123. Simons, K. and E. Ikonen, *Functional rafts in cell membranes.* Nature, 1997. **387**(6633): p. 569-72.

124. Brown, D.A. and E. London, *Functions of lipid rafts in biological membranes.* Annual Review of Cell and Developmental Biology, 1998. **14**: p. 111-136.

125. Rietveld, A. and K. Simons, *The differential miscibility of lipids as the basis for the formation of functional membrane rafts.* Biochimica Et Biophysica Acta-Reviews on Biomembranes, 1998. **1376**(3): p. 467-479.

126. Eggeling, C., et al., *Direct observation of the nanoscale dynamics of membrane lipids in a living cell.* Nature, 2009. **457**(7233): p. 1159-62.

127. Mellman, I. and W.J. Nelson, *Coordinated protein sorting, targeting and distribution in polarized cells.* Nature Reviews Molecular Cell Biology, 2008. **9**(11): p. 833-845.

128. Simons, K. and D. Lingwood, *Lipid Rafts As a Membrane-Organizing Principle.* Science, 2010. **327**(5961): p. 46-50.

129. Stockl, M., J. Nikolaus, and A. Herrmann, *Visualization of lipid domain-specific protein sorting in giant unilamellar vesicles.* Methods Mol Biol, 2010. **606**: p. 115-26.

130. Dart, C., *Lipid microdomains and the regulation of ion channel function.* J Physiol, 2010. **588**(Pt 17): p. 3169-78.

131. Hanzal-Bayer, M.F. and J.F. Hancock, *Lipid rafts and membrane traffic.* FEBS Lett, 2007. **581**(11): p. 2098-104.

132. Anderson, R.G.W., *Caveolae - Where Incoming and Outgoing Messengers Meet.* Proceedings of the National Academy of Sciences of the United States of America, 1993. **90**(23): p. 10909-10913.

133. Simons, K. and D. Toomre, *Lipid rafts and signal transduction.* Nature Reviews Molecular Cell Biology, 2000. **1**(1): p. 31-39.

134. Quest, A.F.G., J.L. Gutierrez-Pajares, and V.A. Torres, *Caveolin-1: an ambiguous partner in cell signalling and cancer.* Journal of Cellular and Molecular Medicine, 2008. **12**(4): p. 1130-1150.

135. Patel, H.H., F. Murray, and P.A. Insel, *Caveolae as organizers of pharmacologically relevant signal transduction molecules.* Annual Review of Pharmacology and Toxicology, 2008. **48**: p. 359-391.

136. Simons, K. and R. Ehehalt, *Cholesterol, lipid rafts, and disease.* Journal of Clinical Investigation, 2002. **110**(5): p. 597-603.

137. Fittipaldi, A., et al., *Cell membrane lipid rafts mediate caveolar endocytosis of HIV-1 Tat fusion proteins.* Journal of Biological Chemistry, 2003. **278**(36): p. 34141-34149.

138. Toborek, M., Y. Zhong, and B. Hennig, *Intact lipid rafts regulate HIV-1 Tat protein-induced activation of the Rho signaling and upregulation of P-glycoprotein in brain endothelial cells.* Journal of Cerebral Blood Flow and Metabolism, 2010. **30**(3): p. 522-533.

139. Nakai, Y. and H. Kamiguchi, *Migration of nerve growth cones requires detergent-resistant membranes in a spatially defined and substrate-dependent manner.* Journal of Cell Biology, 2002. **159**(6): p. 1097-1108.

140. Yeaney, N.K., et al., *Ethanol inhibits L1 cell adhesion molecule tyrosine phosphorylation and dephosphorylation and activation of pp60(src).* Journal of Neurochemistry, 2009. **110**(3): p. 779-790.

141. Kawarabayashi, T., et al., *Dimeric amyloid beta protein rapidly accumulates in lipid rafts followed by apolipoprotein E and phosphorylated tau accumulation in the Tg2576 mouse model of Alzheimer's disease.* Journal of Neuroscience, 2004. **24**(15): p. 3801-3809.

142. Rushworth, J.V. and N.M. Hooper, *Lipid Rafts: Linking Alzheimer's Amyloid-β Production, Aggregation, and Toxicity at Neuronal Membranes.* International Journal of Alzheimer's Disease, 2011. **2011**: p. 14.

143. Brown, D.A. and H. Shogomori, *Use of detergents to study membrane rafts: The good, the bad, and the ugly.* Biological Chemistry, 2003. **384**(9): p. 1259-1263.

144. Angelova, M.I. and D.S. Dimitrov, *Liposome Electroformation.* Faraday Discussions, 1986. **81**: p. 303-+.

145. Meleard, P., L.A. Bagatolli, and T. Pott, *Giant Unilamellar Vesicle Electroformation: From Lipid Mixtures to Native Membranes under Physiological Conditions.* Methods in Enzymology Liposomes, Pt G, 2009. **465**: p. 161-176.

146. Dietrich, C., et al., *Lipid rafts reconstituted in model membranes.* Biophysical Journal, 2001. **80**(3): p. 1417-28.

147. Haverstick, D.M. and M. Glaser, *Visualization of Ca-2+-Induced Phospholipid Domains.* Proceedings of the National Academy of Sciences of the United States of America, 1987. **84**(13): p. 4475-4479.

148. Veatch, S.L. and S.L. Keller, *Organization in lipid membranes containing cholesterol.* Phys Rev Lett, 2002. **89**(26): p. 268101.

149. Nag, K., et al., *Segregation of saturated chain lipids in pulmonary surfactant films and bilayers.* Biophysical Journal, 2002. **82**(4): p. 2041-51.

150. Tinoco, I., *Physical chemistry : principles and applications in biological sciences.* 4th ed2002, Upper Saddle River, N.J. ; London: Prentice Hall. xix, 740 p.

151. Veatch, S.L. and S.L. Keller, *Separation of liquid phases in giant vesicles of ternary mixtures of phospholipids and cholesterol.* Biophysical Journal, 2003. **85**(5): p. 3074-83.

152. Kahya, N., et al., *Probing lipid mobility of raft-exhibiting model membranes by fluorescence correlation spectroscopy.* Journal of Biological Chemistry, 2003. **278**(30): p. 28109-15.

153. Bernardino de la Serna, J., et al., *Cholesterol rules: direct observation of the coexistence of two fluid phases in native pulmonary surfactant membranes at physiological temperatures.* Journal of Biological Chemistry, 2004. **279**(39): p. 40715-22.

154. Veatch, S.L. and S.L. Keller, *Miscibility phase diagrams of giant vesicles containing sphingomyelin.* Phys Rev Lett, 2005. **94**(14): p. 148101.

155. Klose, C., et al., *Yeast Lipids Can Phase-separate into Micrometer-scale Membrane Domains.* Journal of Biological Chemistry, 2010. **285**(39): p. 30224-30232.

156. Samsonoc, A.V., I. Mihakyav, and F.S. Cohen, *Characterization of cholesterol-sphingomyelin dimaons and their dynamics in bilayer membranes.* Biophysics Journal, 2001. **81**: p. 1486-1500.

157. Tokumasu, F., et al., *Nanoscopic lipid domain dynamics revealed by atomic force microscopy.* Biophysical Journal, 2003. **84**(4): p. 2609-2618.

158. Lin, W.C., et al., *Lipid asymmetry in DLPC/DSPC-supported lipid bilayers: A combined AFM and fluorescence microscopy study.* Biophysical Journal, 2006. **90**(1): p. 228-237.

159. Sonnleitner, A., G.J. Schutz, and T. Schmidt, *Free brownian motion of individual lipid molecules in biomembranes.* Biophys. J., 1999. **77**: p. 2638-2642.

160. Baaken, G., et al., *Planar microelectrode-cavity array for high-resolution and parallel electrical recording of membrane ionic currents.* Lab on a Chip, 2008. **8**(6): p. 938-944.

161. Honigmann, A., et al., *Characterization of Horizontal Lipid Bilayers as a Model System to Study Lipid Phase Separation.* Biophysical Journal, 2010. **98**(12): p. 2886-2894.

162. Picard, G., N. Denicourt, and J.H. Fendler, *Simultaneous Electrical and Optical Interferometric Measurements of Pressure-Potential-Induced and Applied-Potential-Induced Bilayer Lipid-Membrane Deformation.* Journal of Physical Chemistry, 1991. **95**(9): p. 3705-3715.

163. Ichikawa, T., et al., *Immobilizing single lipid and channel molecules in artificial lipid bilayers with annexin A5.* Langmuir, 2006. **22**(14): p. 6302-6307.

164. Borisenko, V., et al., *Simultaneous optical and electrical recording of single gramicidin channels.* Biophysical Journal, 2003. **84**(1): p. 612-622.

165. Harms, G., G. Orr, and H.P. Lu, *Probing ion channel conformational dynamics using simultaneous single-molecule ultrafast spectroscopy and patch-clamp electric recording.* Applied Physics Letters, 2004. **84**(10): p. 1792-1794.

166. Samsonov, A.V., I. Mihalyov, and F.S. Cohen, *Characterization of cholesterol-sphingomyelin domains and their dynamics in bilayer membranes.* Biophysical Journal, 2001. **81**(3): p. 1486-1500.

167. Collins, M.D. and S.L. Keller, *Tuning lipid mixtures to induce or suppress domain formation across leaflets of unsupported asymmetric bilayers.* Proceedings of the National Academy of Sciences of the United States of America, 2008. **105**(1): p. 124-128.

168. Fidorra, M., et al. *Do GUVs composed of binary lipid mixtures obey the lever rule? A quantitative microscopy imaging approach* in *Biophyscial Society Annual Meeting*. 2008.

169. Meleard, P., et al., *Bending elasticities of model membranes: Influences of temperature and sterol content.* Biophysical Journal, 1997. **72**(6): p. 2616-2629.

170. Pagano, R.E., Ruysscha.Jm, and I.R. Miller, *Molecular Composition of Some Lipid Bilayer Membranes in Aqueous-Solution.* Journal of Membrane Biology, 1972. **10**(1): p. 11-30.

171. Bunce, A.S. and R.C. Hider, *Composition of Black Lipid-Membranes Formed from Egg-Yolk Lecithin, Cholesterol and Normal-Decane.* Biochimica Et Biophysica Acta, 1974. **363**(3): p. 423-427.

172. Bagatolli, L.A., *To see or not to see: Lateral organization of biological membranes and fluorescence microscopy.* Biochimica Et Biophysica Acta-Biomembranes, 2006. **1758**(10): p. 1541-1556.

173. Baumgart, T., et al., *Fluorescence probe partitioning between L-o/L-d phases in lipid membranes.* Biochimica Et Biophysica Acta-Biomembranes, 2007. **1768**(9): p. 2182-2194.

174. Bagatolli, L.A. and E. Gratton, *A correlation between lipid domain shape and binary phospholipid mixture composition in free standing bilayers: A two-photon fluorescence microscopy study.* Biophysical Journal, 2000. **79**(1): p. 434-447.

175. Cicuta, P., S.L. Keller, and S.L. Veatch, *Diffusion of liquid domains in lipid bilayer membranes.* J Phys Chem B, 2007. **111**(13): p. 3328-31.

176. de Almeida, R.F., A. Fedorov, and M. Prieto, *Sphingomyelin/phosphatidylcholine/cholesterol phase diagram: boundaries and composition of lipid rafts.* Biophysical Journal, 2003. **85**(4): p. 2406-16.

177. Hromada, L., et al., *Integrated Microfluidic Bilayer Lipid Membrane (BLM) Arrays*, in *Miniaturized Systems for Chemistry and Life Sciences*2006: Tokyo, Japan.

178. Veatch, S.L., K. Gawrisch, and S.L. Keller, *Closed-loop miscibility gap and quantitative tie-lines in ternary membranes containing diphytanoyl PC.* Biophysical Journal, 2006. **90**(12): p. 4428-4436.

179. Veatch, S.L. and S.L. Keller, *Seeing spots: complex phase behavior in simple membranes.* Biochim Biophys Acta, 2005. **1746**(3): p. 172-85.

180. Zachowski, A., *Phospholipids in Animal Eukaryotic Membranes - Transverse Asymmetry and Movement.* Biochemical Journal, 1993. **294**: p. 1-14.

181. Ayuyan, A.G. and F.S. Cohen, *Raft composition at physiological temperature and pH in the absence of detergents.* Biophysical Journal, 2008. **94**(7): p. 2654-2666.

182. Baumgart, T., S.T. Hess, and W.W. Webb, *Imaging coexisting fluid domains in biomembrane models coupling curvature and line tension.* Nature, 2003. **425**(6960): p. 821-824.

183. Tien, H.T., *Black Lipid Membranes in Aqueous Media - Interfacial Free Energy Measurements and Effect of Surfactants on Film Formation and Stability.* Journal of Physical Chemistry, 1967. **71**(11): p. 3395-&.

184. Kaganer, V.M., H. Mohwald, and P. Dutta, *Structure and phase transitions in Langmuir monolayers.* Reviews of Modern Physics, 1999. **71**(3): p. 779-819.

185. Tanaka, T. and M. Yamazaki, *Membrane fusion of giant unilamellar vesicles of neutral phospholipid membranes induced by La3+.* Langmuir, 2004. **20**(13): p. 5160-5164.

186. Voets, T., et al., *The principle of temperature-dependent gating in cold- and heat-sensitive TRP channels.* Nature, 2004. **430**(7001): p. 748-754.

187. Dhaka, A., V. Viswanath, and A. Patapoutian, *TRP ion channels and temperature sensation.* Annual Review of Neuroscience, 2006. **29**: p. 135-161.

188. Caterina, M.J., et al., *The capsaicin receptor: a heat-activated ion channel in the pain pathway.* Nature, 1997. **389**(6653): p. 816-824.

189. Caterina, M.J., et al., *A capsaicin-receptor homologue with a high threshold for noxious heat.* Nature, 1999. **398**(6726): p. 436-441.

190. Togashi, K., et al., *Heat-evoked activation of ion channel, TRPM2.* Faseb Journal, 2005. **19**(5): p. A1164-A1164.

191. Xu, H.X., et al., *TRPV3 is a calcium-permeable temperature-sensitive cation channel.* Nature, 2002. **418**(6894): p. 181-186.

192. Smith, G.D., et al., *TRPV3 is a temperature-sensitive vanilloid receptor-like protein.* Nature, 2002. **418**(6894): p. 186-190.

193. Watanabe, H., et al., *Heat-evoked activation of TRPV4 channels in a HEK293 cell expression system and in native mouse aorta endothelial cells.* Journal of Biological Chemistry, 2002. **277**(49): p. 47044-47051.

194. Guler, A.D., et al., *Heat-evoked activation of the ion channel, TRPV4.* Journal of Neuroscience, 2002. **22**(15): p. 6408-6414.

195. McKemy, D.D., W.M. Neuhausser, and D. Julius, *Identification of a cold receptor reveals a general role for TRP channels in thermosensation.* Nature, 2002. **416**(6876): p. 52-58.

196. Peier, A.M., et al., *A TRP channel that senses cold stimuli and menthol.* Cell, 2002. **108**(5): p. 705-715.

197. Story, G.M., et al., *ANKTM1, a TRP-like channel expressed in nociceptive neurons, is activated by cold temperatures.* Cell, 2003. **112**(6): p. 819-829.

198. Chernyshev, A. and S. Cukierman, *Thermodynamic view of activation energies of proton transfer in various gramicidin A channels.* Biophysical Journal, 2002. **82**(1): p. 182-192.